

# Micromanipulation - Force Feedback Pushing

Shahzad Khan

A Thesis presented for the degree of  
Doctor of Philosophy

Mechatronics Program  
Electronics Engineering and Computer Science  
Faculty of Engineering and Natural Science  
Sabanci University  
Turkey

December 2007

## Micromanipulation – Force Feedback Pushing

Approved By:


Prof. Dr. Asif Sabanovic  
(Thesis Advisor)



Asst. Prof. Dr. Volkan Patoglu  
(Thesis Co-Advisor)



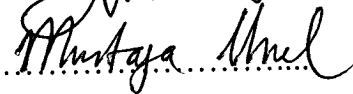
Assoc. Prof. Dr. Ayhan Bozkurt



Assoc. Prof. Dr. Mahmut Aksit



Assoc. Prof. Dr. Mustafa Unel



Date of Approval:.....

*Dedicated to*

My Beloved Wife Shazia Ahmed Khan

# Micromanipulation - Force Feedback Pushing

Shahzad Khan

Submitted for the degree of Doctor of Philosophy

December 2007

## Abstract

In micromanipulation applications, it is often desirable to position and orient polygonal micro-objects lying on a planar surface. Pushing micro-objects using point contact provides more flexibility and less complexity compared to pick and place operation. Due to the fact that in micro-world surface forces are much more dominant than inertial forces and these forces are distributed unevenly, pushing through the center of mass of the micro-object will not yield a pure translational motion. In order to translate a micro-object, the line of pushing should pass through the center of friction. Moreover, due to unexpected nature of the frictional forces between the micro-object and substrate, the maximum force applied to the micro-object needs to be limited to prevent any damage either to the probe or micro-object. In this dissertation, a semi-autonomous manipulation scheme is proposed to push micro-objects with human assistance using a custom built tele-micromanipulation setup to achieve pure translational motion. The pushing operation can be divided into two concurrent processes: In one process human operator who acts as an impedance controller to switch between force-position controllers and alters the velocity of the pusher while in contact with the micro-object through scaled bilateral teleoperation with force feedback. In the other process, the desired line of pushing for the micro-object is determined continuously so that it always passes through the varying center of friction. Visual feedback procedures are adopted to align the resultant velocity vector at the contact point to pass through the center of friction in order to achieve pure translational motion of the micro-object. Experimental results are demonstrated to prove the effectiveness of the proposed controller along with nanometer scale position control, nano-Newton range force sensing, scaled bilateral teleoperation with force feedback.

## Mikromanipülasyon – Güç Geribeslemeli İtme

### Özet

Mikro-manipülasyon uygulamalarında sıklıkla çok köşeli nesnelerin düzlemsel bir yüzey üzerinde konumlanması ve yöneltilmesi amaçlanmaktadır. Mikro nesnelere nokta teması sağlayarak itmek tutup sonra yerleştirme operasyonuna göre daha esnek ve daha az karmaşık bir yöntemdir. Mikro dünyada yüzey kuvvetlerinin atalet kuvvetlerine göre daha baskın olmasından ve bu kuvvetlerin düzensiz dağılımından dolayı, bir mikro nesneyi ağırlık merkezi doğrultusunda itme yöntemi sadece doğrusal bir harekete sebep olmamaktadır. Bir mikro nesneyi sadece doğrusal yönde hareket ettirebilmek için, itme yönü sürtünme merkezinden geçmelidir. Ayrıca, mikro nesne ve taban arasındaki sürtünme kuvvetlerinin beklemeyen mizacından dolayı, itici milde ya da mikro nesnede oluşabilecek zararları engellemek için, mikro nesneye uygulanan maksimum kuvvet değeri sınırlanmalıdır. Bu tezde, özel üretilmiş bir uzaktan mikro manipülasyon düzeneğini kullanarak, insan yardımı ile mikro nesnelere sadece doğrusal yönde hareket ettirmeyi başaran bir yarı-otomatik manipülasyon tasarısı önerilmektedir. İtme operasyonu eş zamanlı gerçekleşen iki adet sürece ayrılabilir. İlkinde, kuvvet ve konum kontrolleri arasında geçiş yapmak için empedans denetleyicisi gibi davranan operatör, kuvvet geri beslemeli, ölçekli ve iki yönlü uzaktan kumanda etme yöntemi ile mikro nesnenin hızını değiştirir. Diğer süreçte ise, mikro nesnenin istenen itilme yönü, her zaman değişken olan sürtünme merkezinden geçecek şekilde belirlenir. Mikro nesnenin sadece doğrusal bir hareket yapmasını sağlamak için, temas noktasındaki bileşke hız vektörünün sürtünme merkezinden geçmesini sağlayan görsel geri besleme prosedürleri benimsenmiştir. Önerilen denetleyicinin etkinliğini ispatlamak için deneysel sonuçlarla birlikte nanometre ölçüsünde konum kontrolü, nano Newton ölçeğinde kuvvet algısı ve kuvvet geri beslemeli, ölçekli ve iki yönlü uzaktan kumanda etme yöntemi gösterilmiştir.

# Declaration

The work in this thesis is based on research carried out at the Mechatronics Research Group, Electronics Engineering and Computer Science, Faculty of Engineering and Natural Science, Sabanci University, Turkey. No part of this thesis has been submitted elsewhere for any other degree or qualification and it all my own work unless referenced to the contrary in the text.

**Copyright © 2007 by Shahzad Khan.**

“The copyright of this thesis rests with the author. No quotations from it should be published without the author’s prior written consent and information derived from it should be acknowledged”.

# Acknowledgements

I would like to express my deep gratitude for everyone who has assisted me directly or indirectly for the completion of this thesis. The most prominent person among them is my thesis advisor, Prof. Dr.Asif Sabanovic who has been always beside me since the day I put my feet in the university. He has always been a constant supporter not only in my research but also in all spheres of my life. Without his guidance, cooperation, understanding and friendly nature, it would have been impossible to complete the thesis. I would also like to convey immense thanks my thesis co-advisor, Asst. Prof. Dr.Volkan Patoglu who has provided me with all his valuable suggestions and helped my latent potentialities to come out for successfully completing the thesis. One of the most wonderful person I have come across is Assoc. Prof. Dr.Mustafa Unel, who has always directed me towards the right path since three years of my graduate education in Sabanci University. Apart from them, I would also like to mention about Assoc. Prof. Dr.Mahmut Aksit, Assoc. Prof. Dr.Kemalettin Erbatur, Asst. Prof. Dr.Gullu Kiziltas and Asst. Prof. Dr.Ahmet Onat for providing me moral support throughout my graduate studies.

The work would never have been completed properly without the contributions from my colleagues especially Ahmet Ozcan Nergiz who gave me a strong hand to complete the experimental setup. I would like to thank Emrah Parlakay who has been very courteous housemate for a long time and helped me out many 'usual' problems faced by a foreigners. Additionally, I am very thankful to Yasser El-Kahlout, Meltem Elitas, Asanterbi Malima, Erdem Ozturk, Selim Yannier, Nusrettin Gulec, Merve Acer, Ertugral Cetinsoy, Elif Hocaoglu, Erhan Demirok, Erol Ozgur, Hakan Bilen, Muhammet Ali Hocaoglu, Khalid Abidi and Okan Kurt for providing me with friendly support. I am indebted to Yalcin Yamaner and Sreenivasa Saravan

Kallempudi for helping me to get various work done from Sabanci University Microelectronics clean room facilities.

I would also like to thank Prof. Metin Sitti and Cagdas Onal from Nanorobotics Laboratory, CMU (Carnegie Mellon University) for providing me with AFM probes to perform the experiments. I wish to express my sincere thanks for Yousef Jameel Scholarship Foundation, Berlin and TUBITAK, Ankara for providing me the financial assistance for the research as well as scholarships for PhD studies. I would also like to thank Anas Abidi for helping with the software developmental part.

Finally, I would not be able to forget the sacrifices made by my mother Mrs. Shamim Akhtar, who left this world after providing me lot of inspiration to pursue a high academic degree and to be a righteous person. Moreover, the effort made by my father Mr. Shaukat Ali Khan to financially support me throughout my academic career cannot be forgotten. I would also like to pinpoint my uncles Mr. Abdul Guffar Khan, Mr. Abdul Rashid Khan and Mr. Liakat Ali Khan who inspired me to continue with higher studies. At the end, I would like to say uncountable thanks to my beloved wife who was always been with me and supported by whatever means during the course of my thesis.



# Contents

<b>Abstract</b>	<b>iii</b>
<b>Declaration</b>	<b>iv</b>
<b>Acknowledgements</b>	<b>v</b>
<b>1 Introduction</b>	<b>1</b>
1.1 Overview . . . . .	1
1.2 Problem Definition and Approach . . . . .	3
1.3 Contribution . . . . .	4
1.4 Outline of the Thesis . . . . .	5
<b>2 State of the Art</b>	<b>6</b>
2.1 What is a Microsystem? . . . . .	6
2.1.1 Introduction . . . . .	6
2.1.2 Several issues for “Micro” World . . . . .	7
2.2 Trend from Macro to Microassembly . . . . .	7
2.2.1 Microassembly Systems . . . . .	9
2.2.2 Serial and Parallel Microassembly . . . . .	10
2.2.3 Existing Microassembly Systems - Microfactory . . . . .	10
2.3 Manipulation of Micro Object and Approaches . . . . .	11
2.3.1 Starting Point Based . . . . .	11
2.3.2 Process Based . . . . .	12
2.3.3 Interaction Type Based . . . . .	12
2.3.4 Operation Based . . . . .	13

---

2.4	Forces in the Manipulation Process . . . . .	14
2.4.1	Classification Scheme of the Forces . . . . .	15
2.4.2	Surface Forces Acting in the Micro World . . . . .	16
2.4.3	Force Sensing in the Micro World . . . . .	16
2.5	Bilateral Control . . . . .	18
2.5.1	Teleoperation vs Bilateral Control . . . . .	19
2.5.2	Ideal Characteristics of Bilateral Control . . . . .	19
2.5.3	Two Channel Bilateral Control Architecture . . . . .	22
2.6	Manipulation by Pushing . . . . .	23
2.6.1	Models of Contact Mechanics . . . . .	24
2.6.2	Mechanism of Pushing . . . . .	25
2.6.3	Requirements for Reliable Pushing . . . . .	27
2.7	Conclusion . . . . .	28
<b>3</b>	<b>Tele-Micromanipulation Setup</b>	<b>30</b>
3.1	Description of the Setup . . . . .	30
3.2	Conclusion . . . . .	31
<b>4</b>	<b>High Precision Motion Control</b>	<b>33</b>
4.1	Modeling and Control of Open Loop PZT Actuator . . . . .	34
4.1.1	Modeling of PZT Actuator . . . . .	35
4.1.2	Introduction to Hysteresis in PZT . . . . .	36
4.1.3	Model for Hysteresis . . . . .	38
4.1.4	Description of Experimental Setup . . . . .	40
4.1.5	Experimental Validation . . . . .	41
4.2	Closed Loop Control of PZT Actuator . . . . .	43
4.2.1	Sliding Mode in Variable Structure System . . . . .	45
4.2.2	Design of Sliding Mode Controller and Realization in Discrete Form . . . . .	47
4.2.3	Estimation of Boundary layer in Discrete Sliding-Mode Control	50
4.2.4	Design of Disturbance Observer based on Sliding-Mode Control	51
4.2.5	Experimental Validation of Position Control . . . . .	54

4.3	Motion Control of Linear drives . . . . .	55
4.3.1	Canudas Frictional Model . . . . .	57
4.3.2	Experimental Description . . . . .	60
4.4	Conclusion . . . . .	62
<b>5</b>	<b>Bilateral Control in Micromanipulation</b>	<b>65</b>
5.1	Force Sensing Using Piezoresistive AFM Cantilever . . . . .	65
5.1.1	Modeling of the AFM Cantilever . . . . .	67
5.1.2	Experimental Validation of Force Sensing . . . . .	68
5.2	Implementation of Scaled Bilateral Teleoperation . . . . .	69
5.2.1	Schematic of Bilateral Control Structure . . . . .	70
5.2.2	Scaling of the Position and Force Information . . . . .	72
5.2.3	Experimental Validation of Position Tracking . . . . .	72
5.2.4	Experimental Validation of Force Tracking . . . . .	73
5.3	Conclusion . . . . .	73
<b>6</b>	<b>Semi-Automated Pushing of Micro Object</b>	<b>78</b>
6.0.1	Introduction . . . . .	78
6.0.2	Problem Definition . . . . .	79
6.0.3	Proposed Approach - Hybrid Force-Position Control . . . . .	80
6.0.4	Pushing Mechanism . . . . .	81
6.0.5	Sliding of Micro-Objects . . . . .	83
6.0.6	Trajectory Control for Known Center of Friction . . . . .	84
6.0.7	Center of Friction . . . . .	86
6.0.8	Method for Online Estimation of the Center of Friction . . . . .	92
6.0.9	Image Processing Procedures . . . . .	93
6.0.10	Pushing Algorithm . . . . .	94
6.0.11	Experimental Validation of Pushing Operation . . . . .	96
6.1	Conclusion . . . . .	98
<b>7</b>	<b>Conclusions</b>	<b>101</b>
7.1	Summary of the Thesis . . . . .	101

---

7.2 Future Works . . . . .	102
<b>Appendix</b>	<b>111</b>
<b>A Bilateral Control Micromanipulation</b>	<b>111</b>
A.1 PI P-854 PiezoMike: Piezoelectric Micrometer Drive . . . . .	111
A.2 PI P-611 NanoCube XYZ Piezo Nanopositioning Systems . . . . .	112
A.3 PI E664 NanoCube Piezo Controller . . . . .	112
A.4 Maxon RE-40 DC Servo Motor . . . . .	112
A.5 Maxon 4-Q-DC Servoamplifier ADS in Module Housing . . . . .	113

# List of Figures

1.1	The Scale of Things . . . . .	2
2.1	Microassembly Functions according to, adapted from [1] . . . . .	11
2.2	Micro/nano scale manipulation approaches, adapted from [2] . . . . .	12
2.3	Classification of microassembly operation-based techniques . . . . .	13
2.4	Comparison of surfaces forces effect, adapted from [3] . . . . .	15
2.5	General force reflecting teleoperation systems/bilateral systems, adapted from [4] . . . . .	18
2.6	Rigid coupled ideal bilateral teleoperation system, adapted from [5] . . . . .	20
2.7	Position-Force Direct Force Feedback scheme . . . . .	22
2.8	The object is stable pushed from start to target . . . . .	25
3.1	Schematic of Tele-micromanipulation system . . . . .	31
3.2	Tele-Micromanipulation Setup . . . . .	32
3.3	Custom built parts in the slave mechanism . . . . .	32
4.1	Electromechanical model of a PZT actuator . . . . .	35
4.2	Hysteresis multibranch nonlinearity . . . . .	39
4.3	z-x curves of several combination $\alpha$ , $\beta$ , $\gamma$ . (a) $\alpha = 1.0$ , $\beta = 0.5$ , and $\gamma = 0.5$ ; (b) $\alpha = 1.0$ , $\beta = 0.1$ , and $\gamma = 0.9$ ; (c) $\alpha = 1.0$ , $\beta = 0.5$ , and $\gamma = -0.5$ ; (d) $\alpha = 1.0$ , $\beta = 0.25$ , and $\gamma = -0.5$ ; adapted from [6] . . . . .	40
4.4	Schematic of the experimental setup . . . . .	41
4.5	Structure of the experimental setup . . . . .	42
4.6	Hysteresis Loop for Sinusoidal input with 1 Hz and varying Amplitude . . . . .	43

4.7	Sinusoidal Input with varying frequencies of 0.5 Hz, 1 Hz and 2 Hz with constant Amplitude . . . . .	44
4.8	Sinusoidal Input of 1 Hz frequency and 20 V amplitude . . . . .	45
4.9	Sinusoidal Input of 1 Hz frequency and 60 V amplitude . . . . .	46
4.10	Controller and disturbance observer for position control of the PZT actuator, adapted from [7] . . . . .	52
4.11	Position response for a reference of 100nm [8] . . . . .	55
4.12	Position response for a reference of 50nm [8] . . . . .	56
4.13	Position response for a reference of 5nm [8] . . . . .	57
4.14	Position response for a trapezoidal reference for 0.5 $\mu$ . . . . .	58
4.15	Position response for a sinusoidal reference for 1 $\mu$ m amplitude . . . . .	59
4.16	Position response for a sinusoidal reference for 10 $\mu$ m amplitude . . . . .	60
4.17	Block diagram of the closed loop system with friction observer . . . . .	61
4.18	X-Y stages of linear drive . . . . .	62
4.19	Block diagram of the system with two linear axes driven by dSpace1103 . . . . .	63
4.20	Response of two consecutive smooth step of less than 1 $\mu$ m for a single axis . . . . .	63
4.21	Experimental results for circular motion of two axes of radius 1 $\mu$ m . . . . .	64
5.1	Piezoresistive AFM Cantilever with inbuilt Wheatstone bridge . . . . .	66
5.2	Force measurement setup . . . . .	67
5.3	Force for smooth step position reference. . . . .	69
5.4	Pulling in-out for smooth step position references . . . . .	70
5.5	Force curve for interaction between a silicon tip and a glass surface . . . . .	71
5.6	Scaled bilateral teleoperation control structure . . . . .	71
5.7	Position Tracking of the Bilateral Controller for zig-zag motion with amplitude 20nm . . . . .	73
5.8	Position Tracking of the Bilateral Controller for random motion with amplitude 0.6 $\mu$ m . . . . .	74
5.9	Position Tracking of the Bilateral Controller for sinusoidal reference with amplitude 5 $\mu$ m . . . . .	75

---

5.10	Position Tracking of the Bilateral Controller for step motion with amplitude $0.5 \mu m$ . . . . .	75
5.11	Force tracking of the bilateral controller and tracking error . . . . .	76
5.12	Force tracking of the bilateral controller and tracking error . . . . .	76
5.13	Force tracking of the bilateral controller and tracking error . . . . .	77
6.1	Semi-automated pushing scheme . . . . .	79
6.2	Hybrid control structure for semi-automated pushing . . . . .	80
6.3	Sliding of micro-object [9] . . . . .	83
6.4	Calculation of friction cone . . . . .	85
6.5	Calculation of velocity vector for known center of friction . . . . .	86
6.6	Reference frame and object frame . . . . .	88
6.7	Instantaneous center of rotation . . . . .	89
6.8	Image Processing Procedures . . . . .	94
6.9	Snapshot of tracking polygonal micro-object . . . . .	95
6.10	Snapshot of pushing rectangular object at the mid-point of the rectangle and line of action passes through center of mass of the object. . . . .	97
6.11	Snapshot of pushing rectangular object by changing the contact point depending upon the orientation angle . . . . .	98
6.12	Snapshot of pushing rectangular object such that the line of action passes through the center of friction . . . . .	99
6.13	Snapshot of pushing rectangular object such that the line of action passes through the center of friction . . . . .	100

# List of Tables

2.1	The features of meso-, micro- and nanoscale assembly systems [10] . . .	8
2.2	Force Ranges . . . . .	16
4.1	Properties Of Piezo-Stage . . . . .	54
4.2	Parameters of The Linear Drive . . . . .	61
4.3	Parameters of the frictional observer . . . . .	61
A.1	PI P-854 PiezoMike: Piezoelectric Micrometer Drive Technical Data .	111
A.2	PI P-611 3-S NanoCube XYZ Piezo Nanopositioning System Techni- cal Data . . . . .	112
A.3	PI E664 NanoCube Piezo Controller Technical Data . . . . .	113
A.4	Maxon RE 40 DC Motor Data . . . . .	114
A.5	Maxon 4-Q-DC Servoamplifier Data . . . . .	114



# Chapter 1

## Introduction

### 1.1 Overview

As the nature has provided us with things in a dimension ranging down till micro/nanometers likewise humans also were able to fabricate components in the same scales as shown in Figure 1.1, but the prominent challenge lies in the fact to assemble incompatible components in a single and functionalized product or micro/nano systems. In this thesis, the focuss is on the products whose dimensions are in the range of micrometers, thus referring only to microsystems. Microsystems that are optimized as an entire device offer considerable advantage over conventional systems, as for example high functionality and compact density, very good performance, high reliability, low weight, and low consumption of material and energy. Moreover, their small size allows placing sophisticated functionality where it was never possible before. Hence, in many applications micro/nano systems will prove more accurate, faster, gentler and less expensive than present day used macrosystems. It will be, therefore, not incorrect to say that microsystems are finding applications in all parts of the daily lives including instrumentation and process control, automotive engineering, aeromechanics, telecommunication, medicines, microbiology, environment technologies and consumer electronics.

Complex microsystems contain, in general, much distinct functionality in single products. Thereby it is often about application-specific products which are required in many different variants, and thus barring few exceptions- in only small and

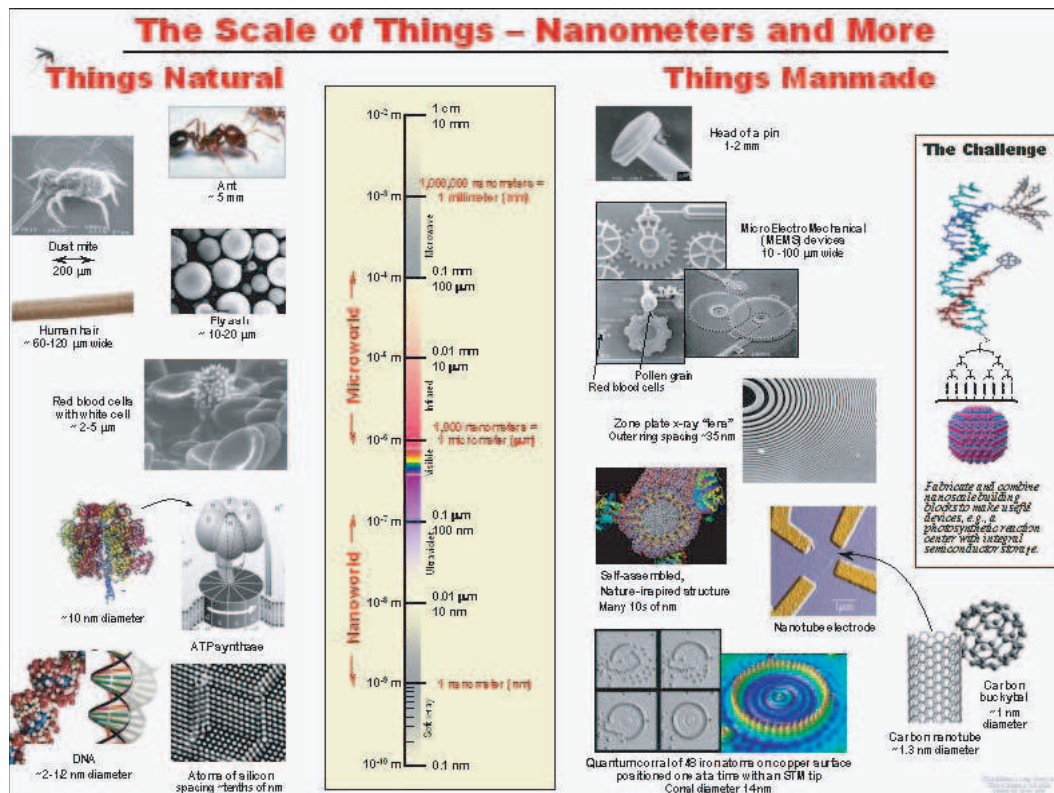


Figure 1.1: The Scale of Things

medium piece numbers. Even though a monolithic ways of integrating would be more desirable, when building entire micro/nano systems but unfortunately in general its not feasible. The small sizes of components, and in particular also incompatibilities among the variety of materials and different processing of the technologies of the individual components, as well as the need for interfacing the microsystems to the macro-world makes microassembly indispensable. Hence, in the manufacturing of hybrid microsystems, precise manipulation of individual micro component is a very important and unavoidable phase.

Precise manipulation can be defined as positioning, assembling, cutting, pushing, pulling, indenting, scratching, twisting, grabbing, releasing, injecting, or any type of interaction which would change the relative position and relation of entities through direct or indirect human operator control. Among the various forms of manipulation process, my research is mostly directed towards pushing of an object in order to make it to reach its destination position and orientation. Pushing is a useful technique for manipulating delicate, small, or slippery parts, parts with uncertain location, or

parts that are otherwise difficult to grasp and carry. The process of manipulation by pushing of micro objects poses many challenges for present researcher due to the requirement of sub-nanometer precision motion, robust teleoperation controller for human intervention and compensating the frictional forces existing between the object and substrate to achieve smooth movement of the objects. Thus, pushing using only visual feedback is not sufficient but it is also indispensable to sense and control the interaction forces involved in the manipulation process with nano-newton resolution, in other words to adopt vision/force hybrid scheme for force controlled pushing. Pushing in micro-scale with force control is an emerging area that appears certain to eventually become an important component in microsystem technologies.

## 1.2 Problem Definition and Approach

The problem dealt within this work concerns utilizing semi-autonomous manipulation scheme for pushing of polygonal micro-object, by point contact to achieve pure translational motion with the aid of a human operator employing scaled bilateral teleoperation with force-feedback and visual display. In order to achieve pure translation motion, the proper line of action of the pushing force needs to always pass through the varying center of friction of the polygonal micro-objects. Thus, while the pushing operation is in progress, it is inevitable to online estimate the center of friction and align the probe such that line of action passes through the center of friction of the micro-object.

The above mentioned problem is coped with by utilizing a proposed method for pushing polygonal micro objects using semi-autonomous scheme with human assistance. The whole process of pushing a micro-object is divided into two concurrent process: in one process pushing is performed by the human operator which acts as an impedance controller to switch between force-position control and alters the velocity of the pusher while in contact with the micro-object. In the second part, the desired line of pushing for the micro-object is determined continuously so that it always passes through the varying center of friction. Visual feedback procedures are adopted to align the resultant velocity vector at the contact point to pass

through the center of friction in order to achieve pure translational motion of the micro-object. In this thesis, a semi-autonomous scheme is adopted for pushing of micro-objects. Experimental results are demonstrated to prove the effectiveness of the proposed method.

## 1.3 Contribution

*In this thesis, a semi-autonomous manipulation scheme is proposed to push micro-objects with human assistance using a custom built tele-micromanipulation setup to achieve pure translational motion.* The pushing operation is administered by the human operator through a scaled bilateral control architecture. Visual feedback is also provided for the operator to monitor the motion of the object. As assistance, visual servoing procedures aligns the micro-cantilever such that the line of pushing always passes through the estimated center of friction of the micro-object to attain pure translational motion. The center of friction is estimated online using recursive least squares method.

Several intermediate steps are performed to achieve the above can be listed as follows:

- A custom and open architecture **tele-micromanipulation setup** is constructed for pushing of the micro-objects.
- Implementation of discrete time sliding mode controller along with the disturbance observer is utilized to achieve **nanometer scale motion using piezoelectric actuators**.
- **Force sensing with nano-newton ( $nN$ )** resolution is demonstrated using a commercial available piezoresistive microcantilever.
- **Scaled bilateral teleoperation** controller is developed and force/position tracking between the master and the slave is demonstrated.
- **Image processing procedures** are developed to track polygonal micro-object to estimate the positions/velocities of feature points along with the orientation angle.

- **Semi-autonomous pushing scheme** is proposed and implemented in which visual feedback procedure assists human operator during pushing of the micro-object to achieve pure translational motion.

## 1.4 Outline of the Thesis

The organization of this thesis is divided into several chapters as follows:

- **Chapter 2:** The present state of the art in microassembly is presented along with several approaches in micromanipulation process. Several issues related with dominant surface force in the micro world is discussed and finally literature survey on mechanism of pushing is illustrated.
- **Chapter 3:** This chapter explains the custom built tele-micromanipulation setup along with the utilized modules for the overall operation.
- **Chapter 4:** This chapter focus on the several methodologies adopted to achieve high precision motion using open-loop, closed loop piezoelectric actuators and linear drives. Implementation of discrete time sliding mode controller and disturbance observer is demonstrated to achieve nanometer resolution motion using closed loop piezo actuators.
- **Chapter 5:** In this chapter implementation of scaled bilateral control is demonstrated. Force sensing with  $nN$  resolution using piezoresistive AFM micro-cantilever is demonstrated. Force/position tracking and transparency between the master and the slave is presented.
- **Chapter 6:** This chapter presents a method for pushing polygonal micro objects using hybrid force-position controller to achieve pure translational motion with the aid of human operator.
- **Chapter 7:** The conclusion of the thesis is presented along with the future works.

# Chapter 2

## State of the Art

In this chapter, the present state of the art in microassembly is presented along with several approaches in micromanipulation process. Several issues related with dominant surface force in the micro world is discussed along with the bilateral control for human intervention. Finally literature survey on mechanism of pushing is illustrated.

### 2.1 What is a Microsystem?

#### 2.1.1 Introduction

The term “microsystem” is composed from the word “micro”, an English prefix of Greek origin which refers to an object as being smaller than an object or scale of focus, in contrast with macro. The first representation that crosses the mind when talking about ‘micro’ is that it surely must be ‘small’. The prefix ‘micro’ is technically standardized as defining the size of a component ( $10^{-6}m$ ). The terms “microsystem” and “microsystem technology” (MST) have widely been used in Europe to describe the same technology which goes under the name MEMS (Microelectromechanical Systems) in the USA and “micromachines” in Japan. The use of different terminology does not only indicate geographical source but also reflect a different conceptual approach. The background of MEMS lays in the solid-state silicon IC technology. After the integrated circuits, the next steps towards MEMS

were the maturity of microfabricated silicon sensors, then the innovation of movable micromechanical parts and finally the concept of microsystems came ahead. MEMS have eventually been intended to be mass-produced with a low unit cost and this term mainly refers to bulk-produced silicon microsensors or microactuators. The concept of micromachine has, in turn, precision and mechanical engineering background and the idea behind it has been the development of real miniaturized three dimensional machines. Micromachines are not necessarily to be manufactured in large quantities and their unit price may be high. In this thesis, we will refer to the term microsystem to cover both extremes and everything in between: from silicon microsensors and actuators to polymer and glass chips, active materials and hybrid microsystems and machines.

### 2.1.2 Several issues for “Micro” World

We will focus on microproducts or microsystems, made up of microparts or microcomponents. Generally speaking, we will consider that microsystems have sizes ranging from a few  $cm^3$  to a few  $dm^3$ .

These microsystems are made up of several microparts or microcomponents that have a size ranging from  $10\ \mu m$  to  $10\ mm$ , but they can have some features with a size reaching  $1\ \mu m$ . For example, the pumping mechanism of a micropump can be smaller than a cube with  $10\ mm$  edge, having at least one dimension smaller than  $100\ \mu m$ . [11] generally refers to  $1\ \mu m$  to  $100\ \mu m$  as ‘microscale’ and  $100\ \mu m$  to  $1\ mm$  as ‘mesoscale’. As far as assembly equipment is concerned, most microfactories are desktop factories, having external dimensions of  $1\ m^2 \times 40\ cm$  height. [12] locates the field of microassembly between conventional assembly, dealing with part dimensions higher than  $1\ mm$  and what they call as ‘the emerging field of nanoassembly’ (with part dimensions  $< 1\ \mu m$ ).

## 2.2 Trend from Macro to Microassembly

One of the features of microsystem technology, concerning the size of constituent part and the overall system are very unique but it also includes even more attractive

features. The three primary unique features (the three “M’s”) define microsystems technology as miniaturization, multiplicity, and microelectronics. Miniaturization is clearly indispensable. A small manipulator has the capability to handle microobjects much more gently and dexterously than its macro counterparts. With micro-machines, precise positioning in shorter response times is achievable in comparison with macroscopic machines. Micromachines have the luxury to travel freely into narrow spaces such as blood vessels. Connectors and harnesses hindering the further miniaturization of electronic equipment will be miniaturized by microsystems technologies. However, it should be also noted that mere miniaturization of macroscopic machines is not the best way to realize microsystem because of scaling effects.

Some features of the mesoscale, microscale and nanoscale assembly are depicted in Table 2.1.

Table 2.1: The features of meso-, micro- and nanoscale assembly systems [10]

Assembly Attribute	Mesoscale	Microscale	Nanoscale
Positioning	Easy	Difficult	Very difficult
Velocity	$cm/s$ or $m/s$ are not usual	Slow ( $\mu m/s$ ) or ( $mm/s$ ), vibration suppression	Very Slow $Nm/s$ or $\mu m/s$
Force Sensing and Control	Easy, necessary to avoid part damage and improve manipulability	Difficult, The range of forces could be as low as $\mu N$	Difficult, AFM used to measure forces
Dominant Forces	Gravity, Friction	Surface forces (stiction, friction, electrostatic, Van der Waals)	Molecular/Atomic Forces
Throughput	Serial assembly provides adequate throughput	Serial assembly is usually not sufficient. Parallel manipulation methods are preferred	Parallel manipulation methods, or self-assembly are necessary
Gripper	Mechanical, many examples, RCC, Utah/MIT hand etc.	Micromechanical, gripper-free manipulation preferred	Other, optical, proximity force etc.
Fixturing	Mechanical	Micromechanical fixturing must be used	Chemical
Compliance	Gripper compliance is not necessary if force is measured	Gripper compliance is usually necessary	Mechanical compliance does not apply
Vision	Easy	Difficult (expensive optics)	Impossible in visible wavelength, SEM, TEM are used

The table shows a straight comparison between assembly characteristics at three different scales: meso, micro, and nano. A major difference between assembly in micro and macro domains is the mechanics of object interactions. In the macroworld, the mechanics of manipulation are predictable, e.g. when a gripper opens, gravity



causes the part to drop. In the microworld, things are highly unpredictable as forces other than gravity dominate due to scaling effects and the parts may not drop due to surface forces. Surface-related forces, such as electrostatic, Van der Waals and surface tension forces become dominant over gravitational forces. These attractive forces depend on environmental conditions, such as humidity, temperature, surface condition, material, etc. For the manipulation of the microobjects, the physics in the micro world should be carefully considered. Thermal, optical, electrical, and magnetic effects will change or become dominant when the objects are miniaturized. Micro parts stick to the manipulator surface as a result of these attractive forces and the manipulation becomes a very challenging task. Due to this unevenly scaling behavior, manipulation in the microworld is completely different from manipulation in the macroworld. Manipulation in this ‘strange’ world, therefore, requires special techniques and methodologies.

### 2.2.1 Microassembly Systems

Even today, micro-system technology dominates the technology market of the 21st century. The dramatic development of the manufacturing procedure from micro-electronics technology has made feasible to combine electronics, optical, and mechanical function to complex, miniaturized systems, so-called microsystems. Due to the increasing use of these microsystems in medical devices, such as in endoscopes for minimally invasive surgery or in sensors - just to mention acceleration sensors for air bag systems - the requirements on the relative manufacturing procedures are getting higher and higher. An exceptional feature of microsystems technology can be seen in the fact that by integrating most different functionalities it deals with highly application-specific and thus highly variant products. The production can be confined to a small to medium number of parts [13]. In order to keep the manufacturing cost as low as possible guaranteeing the products marketability, it is reasonable to manufacture standard elements in large numbers and to assemble them into individual single products.

### 2.2.2 Serial and Parallel Microassembly

Till now the conventional approach in microworld has been serial process which means the micro-parts are put together one-by-one according to traditional pick-and-place paradigm. It involves a sequential process, in which assembly tasks are performed one after another. To complete assembly, a series of sub task are required to be accomplished prior. Typical examples for serial micro-assembly techniques includes manual operation with microscope and optical tweezers, visually based and teleoperated microassembly, [14]high precision macroscopic robot with sub- $\mu m$  motion resolution [15], and micro-grippers. All the mentioned techniques requires considerable amount of time before completing the assembly process for the final products as its sequential process. Thus there is a need to make the process in parallel giving rise to parallel assembly techniques the time needed for assembling process is decreased, high package density and consistency, decrease in the cost can be achieved in comparison with serial assembling process.

### 2.2.3 Existing Microassembly Systems - Microfactory

In today's literature many examples of microassembly systems exist but very few of them are fully operational, in a sense suffers from few drawbacks which are indeed as obligatory requirements. Microassembly systems or microfactory involves several modules that are presented in Figure 2.1. In most of the cases the presented systems are part of the research setups for providing facilities for research in the manipulation of microparts.

The microfactories developed by several research institutes illustrate several complementary approaches: miniaturization of conventional production equipment (MEL), vision oriented station (OLYMPUS), modular designed microfactory (AMMS project), factory integrating new plug-and-produce equipment (LAB), microfactory in mastered environment (EPFL), case study for the understanding and the exploitation of the forces in the microworld (TU Delft). Additional examples illustrate realizations achieved in Europe (IPT), Japan (MITI) and USA (MSL).

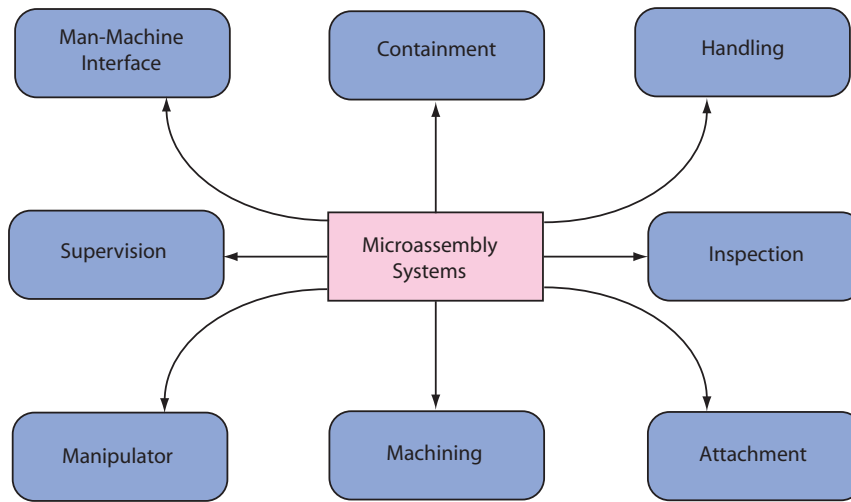


Figure 2.1: Microassembly Functions according to, adapted from [1]

## 2.3 Manipulation of Micro Object and Approaches

One of the most desirable tasks to achieve microassembly is to be able to precisely manipulate micro-scale components. Precise manipulation can be defined as positioning, assembling, cutting, pushing, pulling, indenting, scratching, twisting, grabbing, releasing, injecting, or any type of interaction which would change the relative position and relation of entities through direct or indirect human operator control. Micro/Nano manipulation approaches can be classified depending upon starting point, process, interaction and operation as depicted in Figure 2.2.

This section discusses the various approaches available in the literature for micro/nano object manipulation along with comparison of various standard tools utilized by several researchers in the past.

### 2.3.1 Starting Point Based

With respect to starting point for manipulation, manipulation system can be classified as bottom-up and top-down approaches. In bottom-up approach small objects are integrated to form a final product. Such kind of micro/nano technologies is the ultimate goal towards the miniaturization process. On the other hand, top-down approach, starts from macroscopic world and move towards smaller object requiring more precision of handling.

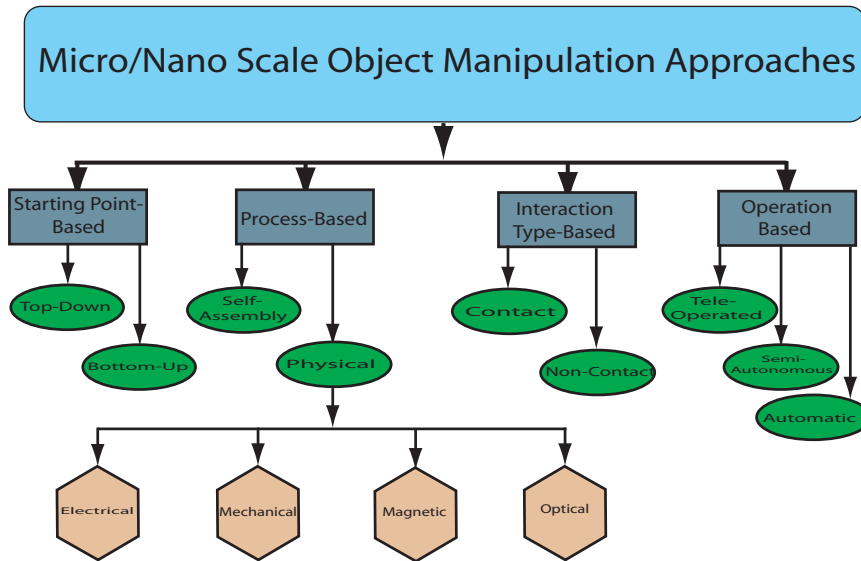


Figure 2.2: Micro/nano scale manipulation approaches, adapted from [2]

### 2.3.2 Process Based

With regards to process based manipulation approach, biochemical process such as self-assembly can be utilized for constructing micro/nano devices or materials. The second approach which can be called as physical manipulation is aimed in manipulating selected particular micro/nano objects in high precision using physical forces, i.e. forces such as electrical, mechanical, magnetic and optical forces. By physical manipulation, an external force required for positioning or assembling objects in 2D or 3D, cutting, drilling, twisting, bending, pick-and-place, push and pull kind of tasks are meant. Our Focus lies on utilizing physical manipulation based on mechanical procedures.

### 2.3.3 Interaction Type Based

Depending on the interaction type, non-contact and contact manipulation systems exist. In the former, laser trapping (optical tweezers) or electrostatic or magnetic field forces are utilized. In case of contact manipulation, AFM probe tip is utilized for pushing particles on substrate by contact pushing or pulling operations. In our case, we are interested in contact mode manipulation scheme.

### 2.3.4 Operation Based

The operation based approach can be divided into manual, teleoperated and automatic approaches and subsequently the automated process can be subdivided into semi-automated and fully automated microassembly processes as depicted in Figure 2.3. Since the micro/nano physical and chemical phenomena are not yet clearly understood, thus automation of the manipulation process is still a challenging task but teleoperation technology is at a premature stage and is considered to understand the uncertainties and improve towards an automatic manipulation process using human intelligence.

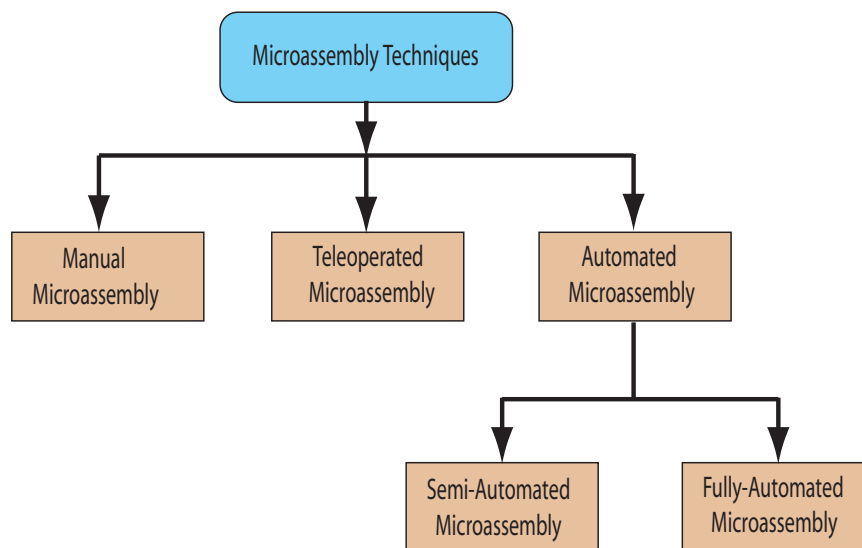


Figure 2.3: Classification of microassembly operation-based techniques

#### Manual Microassembly

Manual microassembly is one of the processes for the realization of assembly tasks by the involvement of trained professionals where high-precision hand motion is performed by the aid of human eye as feedback.

#### Teleoperated Microassembly

In teleoperated microassembly, motions of the human operator are transferred into the actuators by means of a MMI (Man-Machine Interface). MMI having more

number of degrees of freedom enables the control of the motion with the same number of DOF (Degrees of Freedom) in the microworld workspace.

### **Automatic Microassembly**

One of the major requirements of microassembly process is the capability to handle microcomponents with high precision to deliver a final product with high quality. The handling of micro-component requires submicron precision for the high quality of the final product and the limit of human capabilities makes indispensable to utilize the process of automated microassembly operation.

Automatic microassembly can be divided into two categories:

- Semi-automated Microassembly
- Fully-automated Microassembly

In semi-automatic microassembly, operator intervention is allowed but to some level. The operator can define some parameters for the operation such as pushing the micro-object and operation for finding the line of pushing is executed automatically. In fully-automated microassembly, all the tasks and the parameters are predefined. With the aid of sensory feedbacks such as visual feedback, force sensors, etc. the assembly task is realized automatically.

## **2.4 Forces in the Manipulation Process**

Due to the scaling effect, volumic forces (e.g. the gravity) tend to decrease faster than other kind of forces such as van der waals, electrostatic and the capillary forces as depicted in Figure 2.4. Although they still exist on the macroscopic scale, these forces are often negligible (and neglected) in macroscopic assembly. A micro-component is consequently brought in contact with the relative increase of this so-called surface force. According to the literature on microassembly, these surface forces mainly consist of the electrostatic forces, the van der waals forces, the liquid bridge (also called capillary or surface tension) forces and the forces due to the

mechanical clamping. These surface forces creates a lot of hindrance in the manipulation process as it's difficult to speculate the quantitative values of the forces as it's depends upon several parameters such as material, environment and geometries. There are several ways to tackle this problem: these forces can be reduced by controlling the environment etc, it can be overcome if the correct quantitative estimation of the forces can be made. This section presents a first general classification of the forces according to their range and introduces the most often cited forces in microassembly literature.

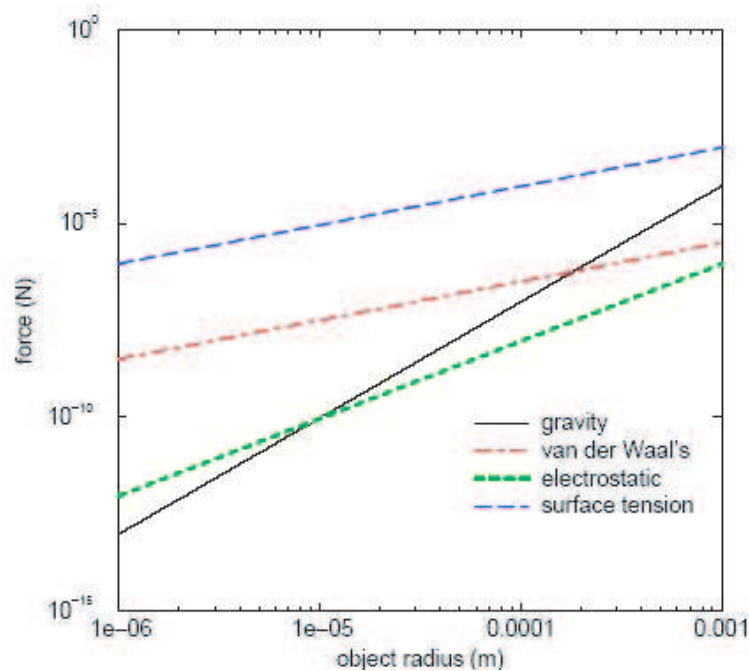


Figure 2.4: Comparison of surfaces forces effect, adapted from [3]

### 2.4.1 Classification Scheme of the Forces

In general, the forces can be broadly classified into four main categories as follows:

- *Gravity*, with an infinite range.
- *Electromagnetic Force*, with an infinite range.
- *Weak Nuclear Force*, with a range smaller than  $10^{-18} m$ .

- *Strong Nuclear Force*, with a range smaller than  $10^{-15} m$ .

These last two forces are outside the scope of this thesis due to their very short range (inside the nucleus). Electromagnetic forces represent the source of all intermolecular interactions and their influence can be combined to that of gravity in some phenomena such as the rise of a liquid in small capillaries. Intermolecular interaction due is the dominant force in the micro world which falls in the region of our interest.

### 2.4.2 Surface Forces Acting in the Micro World

As mentioned in the previous section, the intermolecular interaction between atoms, molecules and solids gives rise to dominant interaction between micro bodies with different ranges as defined by Table 2.2 and characterized by several forces.

Table 2.2: Force Ranges

Interaction distance	Predominant force
Up to infinite range	Gravity
From a few $nm$ up to $1 mm$	Capillary forces
$> 0.3 nm$	Coulomb (electrostatic) forces
$0.3 nm < \text{separation distance} < 100 nm$	Lifshitz - Van Der Waals
$< 0.3 nm$	Molecular interactions
From $0.1 nm$ to $0.2 nm$	Chemical interactions

### 2.4.3 Force Sensing in the Micro World

Manipulating an object, in broad aspect can be defined as the ability to observe, position, and physically transform (with force) the object. When manipulating microobjects, especially delicate parts or biological materials that are usually fragile, pure position control is usually not enough in ensuring successful operation and avoiding damage to the object. Force control is often needed to augment the operation with the position information in order to achieve better manipulation results.



To achieve the task, force sensing and control in microscale is one of the mandatory requirements. Micromanipulation with force control is a promising area that appears certainly to eventually become an important component in microsystems technology.

Force sensor is used to measure the interaction forces between the manipulator and its environment. Depending upon the external force applied to the force sensor, its sensing unit will deform in proportion to the external forces. The deformation is either detected by measuring the changes in certain properties of the sensing element (e.g. change in resistance or capacitance), or directly measured by optical devices (e.g. atomic force microscope). In micromanipulation application, the magnitude of the force varies from  $1mN$  down to  $1\mu N$ . The design and construction of sensors may face many challenges due to the requirement of high resolution and high accuracy. To meet these requirements, semiconductor and microfabrication techniques have been applied to build sensitive and stable sensing elements. Currently, the types of widely used microforce sensors are as follows:

- Strain Gauge;
- Piezoelectric Force Sensor;
- Capacitive Force Sensor;
- Optical Sensor;
- Piezoresistive Sensors;

In our case, Piezoresistive AFM (Atomic Force Microscope) cantilever [16] is utilized to sense the force in  $nN$  range and capable capable of measuring forces down to about  $100 pN$ . Since in our application, it is tedious to employ optical detection scheme due to the complexity to integrate with the system thus piezoresistive sensor provides the best alternatives. The sensed forced are utilized for human intervention in the bilateral control framework.

## 2.5 Bilateral Control

A compact definition of the word bilateral can be defined as having two sides [17]. In robotics systems, the term bilateral control is used to define two systems actively interacting with each other by means of position and/or force information. Generally bilateral systems aims to provide a “feeling” or the force sensation of the remote environment to the human operator for delicate teleoperation. Typically, it is used for teleoperation, in which one system is called the “master” side and the other is called the “slave” side of bilateral action. Slave subsystem is tracking the positions of the master subsystem and master side provides the forces encountered by the slave side to the operator and hence, teleoperation is achieved [18]. A simple bilateral systems is represented in Figure 2.5 consisting of a human operator, a bilateral system and an environment. While the human operator controls the master device, the communication channel controls the transfer of force and position/velocity information and the slave device manipulates the environment.

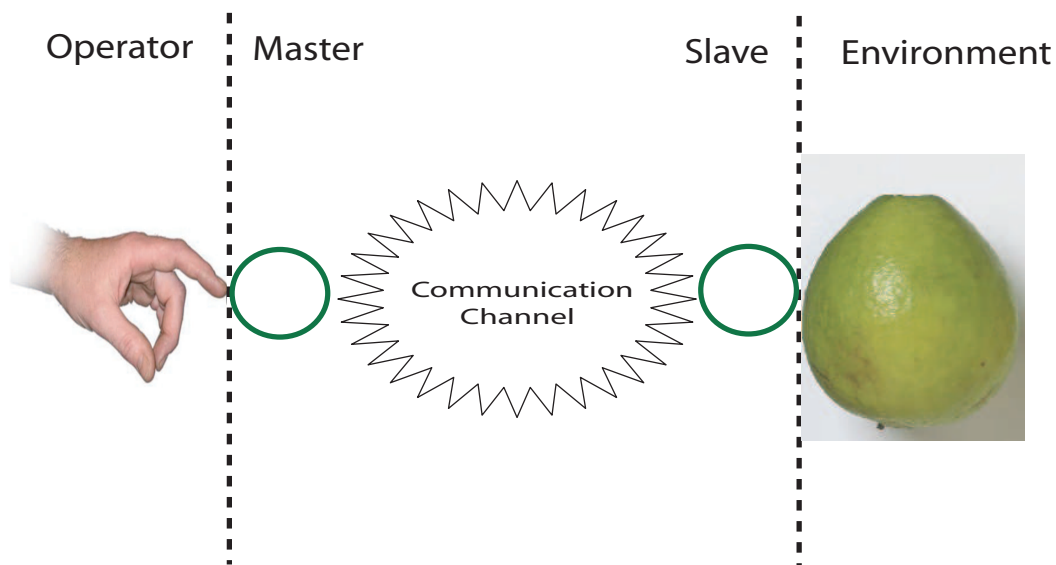


Figure 2.5: General force reflecting teleoperation systems/bilateral systems, adapted from [4]

In order to perform tele-micromanipulation it is indispensable to achieve robust and transparent bilateral controllers for human intervention so that high fidelity position/force interaction between the operator and the remote micro/nano environ-

ment can be achieved. As bilateral control enables skilled teleoperation on several tasks, it offers better safety, lower cost and high accuracy, if carefully designed

### 2.5.1 Teleoperation vs Bilateral Control

Many researcher have proposed several ways of defining or explaining terms bilateral control and teleoperation which ar defined as follows:

- *Teleoperation* is operation of system from remote location, such as controlling an irrigation valve or controlling the Mars observer robots movements from a ground station.
- *Bilateral Control* is control of a system mechanically coupled with environment (slave) by using another mechanically coupled system with human operator (master). Master side has the control over slave side with a force sensation from slave environment. These two sides don't have to be distant from each other so bilateral control can be without teleoperation like in robotic minimal invasive surgery.

### 2.5.2 Ideal Characteristics of Bilateral Control

The definition of ideal characteristics of bilateral control is defined by Yokokohji [19] as mandatory requirement of following three points:

1. Having the same position response at the master and the slave sides apart from of the object dynamics;
2. Having the same force response at the master and the slave sides;
3. Having the same force-position response at the master and the slave sides;

The third definition provided by Yokokohji indicates that the operator is working with the real objects and is defined this as the ideal kinesthetic coupling. A mechanical analogy of an ideal bilateral teleoperation system for 1 DOF connecting the operating and the environment with a infinitely stiff, zero mass rod can be represented as shown in Figure 2.6. Some of the necessary requirements that needs to be

considered for ideal bilateral teleoperation will be discussed in detail in the following sub-sections.



Figure 2.6: Rigid coupled ideal bilateral teleoperation system, adapted from [5]

### Transparency

In a general way, transparency, as the name implies, is defined as the ability of the bilateral controller to be invisible to the human operator. An ideal bilateral teleoperation is called perfectly transparent when the human operator feels the same forces and velocities as the master device as if the operator was directly manipulating the environment.

Katsura [20] and Onal [18] showed that ideal transparency of a bilateral system is not achievable even without the absence time delay. Transparency, used as the evaluation index for bilateral controller indicates the extent of invisibility of the master-slave transmission line to the human operator. Even though transparency is the evaluation index for ideality of the bilateral system, there is no standardized agreed numerical representation for transparency.

### Stability

Lawrence [5] proposed that transparency and stability of the system are two conflicting design goals in bilateral teleoperation systems. Thus, more inclination to achieve transparency while designing a bilateral system may delimit the overall stability of the system and vice-versa. Thus a trade-off exist between transparency and

stability of the bilateral systems and the designer needs to decide keeping in mind desired goals.

### **Scaling**

Generally, bilateral control is used for teleoperation on micro-environments not reachable by human beings like as in our micromanipulation applications. Therefore, a general bilateral controller should be able to scale the motions and forces between the two sides for extensive applicability.

### **Time Delay**

Since bilateral teleoperation system posses a communication link between the two sides as shown in Figure 2.5, it inherently has an unavoidable time-delay. Since it is physically impossible to eliminate time delays in a network structure bilateral teleoperation with time delays resulting in degradation of transparency, thus the time delay problem has received much attention from researchers [21].

In this thesis since the master and the slave are connected to single computer so the time delay problem is not considered to a matter of concern.

### **Impedance Shaping**

Since the ideal realization of the transparent bilateral system is not possible, another bilateral teleoperation design philosophy is discussed by several researchers [22]. Instead of designing fully transparent bilateral systems, the focus is concentrated on impedance shaping, in other words the impedance perceived by the human operator is shaped in order to create a feeling of virtual tool in the operators hand. By implementing this method, a human operator can execute a task smoothly for a specific application.

### **Human Operator Modeling**

Its quite necessary to have an understanding of the various ranges of the frequencies of the force that creates a range of impact on human operator. This information will provide a mean to design the master side much effectively to be felt by the human

operator. Study of human operator should be done in two parts, human motion control and the human force perception. If the environment is assumed as passive, then all the motion originates from human operator.

### 2.5.3 Two Channel Bilateral Control Architecture

There are many bilateral channel proposed such as:

- Position-Force Scheme (Direct force feedback).
- Position-Position scheme.
- Position Error Based Position Force Architecture
- Force-Force Architecture.
- Force-Position Architecture.

In this thesis, position-force scheme is implemented due to the fact that, robust position controller is already implemented as discussed in chapter 4 to track the commanded master position and information of the slave force is available from the force sensor as discussed in Section 5.1. The control architecture of Position-Force, Direct Force Feedback is represented in Figure 2.7. The commanded position from the master robot is tracked by the slave robot and the interaction forces between the slave robot and environment is sent to the master robot.

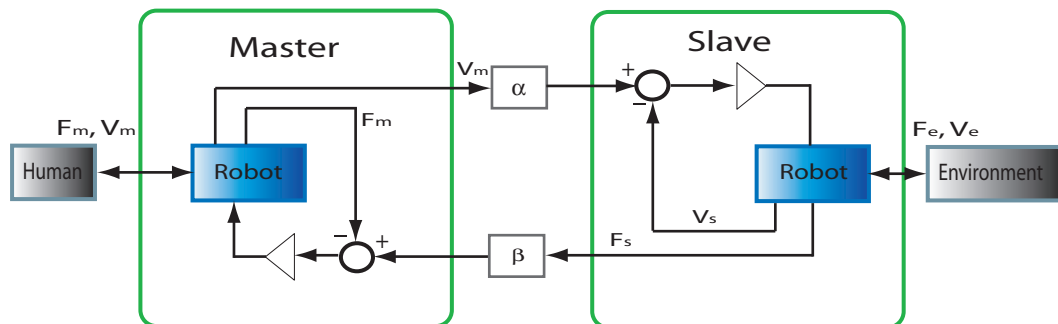


Figure 2.7: Position-Force Direct Force Feedback scheme

## 2.6 Manipulation by Pushing

Positioning of workpieces and/or aligning them with other objects are the basic requirement of tele/semi/fully-automated assembly process. Often, it is sufficient to perform this task on a horizontal plane, i.e. with only three kinematics degrees of freedom (DOF). More or less accurate positioning can be the goal itself, or serves as a pre-requisite for the next process, e.g. a 3D assembly operation performed by a robot. As Mason and Lynch [23], [24] showed, moving objects by actively pushing them with a manipulator is flexible, also mechanically less complex than pick-and-place, for planar positioning due to following reasons:

- To pick up objects that are too small or too numerous to grasp easily, rather you can scoop off the edge of a table into your hand;
- To move objects that are too bulky to grasp, as when rearranging the furniture you can push them;
- Manufacturing automation systems make frequent use of pushing. Often a conveyer belt, in conjunction with guides, is used to move objects through such a system.

Thus we can clearly state that pushing can be a good way to reduce or eliminate uncertainty in the state of the task as it does not require a special grasping tool, nor the manipulator needs to lift and support the workpieces. This hypothesis is also vital for micromanipulation, the problems of precisely releasing the object is circumvented. Pick-and-place manipulation, i.e. grasping, transporting and depositing the object with a manipulator arm equipped with a microgripper [25], allows programmable execution of the positioning task and is well suited for environments clogged with obstacles but on the other hand suffers from above mentioned drawbacks. However, pushing introduces certain restrictions. The moving object is subject to (dry) friction at the contact with the substrate. Previous work has lead to a good understanding of pushing with robots, including stability [23]. In general, these strategies work well for macroscopic parts since the forces involved, such as friction, are well known or can be tightly bounded. Also, the typical accuracy in the millimeter range

is relatively easy to achieve. This is not the case in the microscopic domain, i.e., for part dimensions below 1 *mm*, where adhesion and other surface effects become significant. Thus it's necessary to look into the various models which describe the adhesion behavior between the micro-part and substrate.

### 2.6.1 Models of Contact Mechanics

The sliding friction between micro objects and substrate depends upon the 'real' contact area which is caused by normal adhesion force between the surfaces [26], [27]. In contrast with macro-scale friction, micro-scale friction is dominated by adhesion force at low loads, objects are almost wearless [28] and friction becomes an intrinsic property of the particular interface.

In the literature, several models based on continuum mechanics exists such as Hertz, Johnson-Kendall-Roberts (JKR), Derjaguin-Muller-Toporov (DMT), Maugis-Dugdale (MD), which have been used by several researcher to estimate the real contact area. The Hertz model is rational when the external loads are much larger than the adhesion forces. However, load amounts may have comparable magnitudes to adhesion forces during micromanipulation tasks, thus this model should not be exploited in the case of small loads. The DMT model includes the effect of adhesion to the Hertz model, and it can be used in the case of rigid systems, low adhesion, and small radii of curvature. But it may underestimate the true contact area, and the hysteresis between loading and unloading cannot be modeled with this model. On the other hand, the JKR model includes the effect of adhesion forces and hysteresis behavior where it is realistic for small loads. But, it assumes that short-ranged surface forces act only inside the contact area, and this may underestimate loading due to the surface forces. Finally, the MD model is currently the best model since it can be used for any case and does not underestimate surface forces and contact area.



### 2.6.2 Mechanism of Pushing

In this section of discussion regarding the mechanism of pushing, we will restrict ourselves for stable pushing in which the object is effectively attached to the pusher. A pushing path is formed by stringing together stable pushes, as depicted in Figure 2.8.

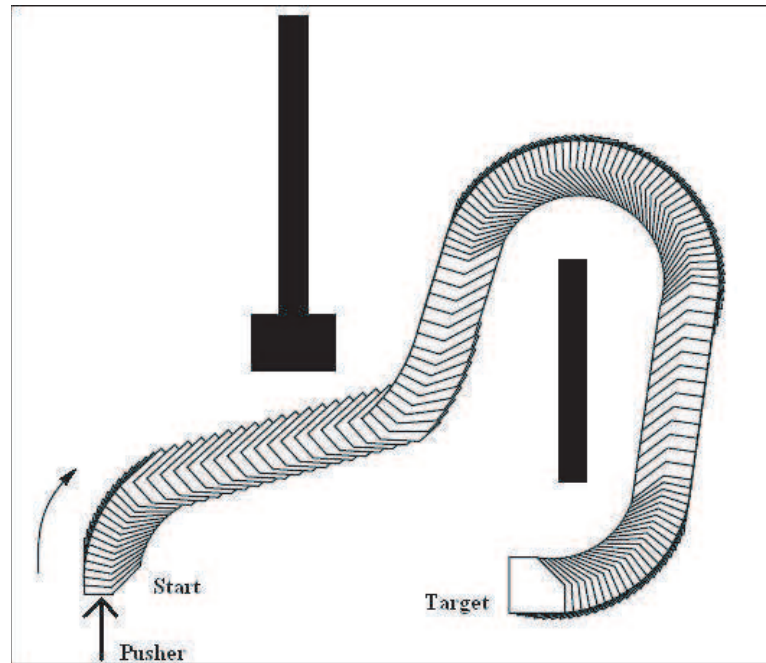


Figure 2.8: The object is stable pushed from start to target

The aim of the task is to develop algorithm to automatically find pushing plans to position and orient parts in the plane in order to follow a desired trajectory starting from the initial location to final destination. As per [24], the final goal is to develop algorithms to automatically find pushing plans to position and orient parts in the plane. There are three main issues which need to be dealt with in pushing operation as follows:

- *Mechanics.* How does an object move when it is pushed? Some standard procedure is required that identifies a set of stable pushing directions when the pusher attains line contact with the object.
- *Controllability.* The directions an object can move during pushing are limited due to the limited set of forces that can be applied by the pusher. Given these

limitations, the study of controllability is motivated by questions of whether or not it is possible to push the object to the goal configuration, with and without obstacles. It's necessary to examine the local and global controllability of objects pushed with either point contact or stable line contact.

- *Planning.* Pushing paths consist of sequences of stable pushes, and the space of stable pushing directions imposes nonholonomic constraints on the motion of the object. It's required to work on path planning for nonholonomic to construct a planner to find stable pushing paths among obstacles.

With regard to above mentioned issues, many researchers have proposed several theories for stable pushing operation. Mason [23] identified pushing as an important manipulation process for manipulating several objects at once, for reducing uncertainty in part orientation, and as a precursor to grasping. Building on early work by Prescott [29] and MacMillan [30], Mason implemented a numerical routine to find the motion of an object with a known support distribution being pushed at a single point of contact. Recognizing that the support distribution is usually unknown, Mason derived a simple rule for determining the rotation sense of the pushed object that depends only on the center of mass of the object. Mason and Brost [31] and Peshkin and Sanderson [32] followed this work by finding bounds on the rotation rate of the pushed object. Goyal, Ruina, and Papadopoulos [33] studied the relationship between the motion of the sliding object and the associated support friction when the support distribution is completely specified. Alexander and Maddocks [34] considered the other extreme, when only the geometric extent of the support area is known, and described techniques to bound the possible motions of the pushed object. These results have been used to plan manipulator pushing and grasping operations. Mason [23] used pushing and grasping to reduce uncertainty. Wilson [35] built a system for orienting a part in an initially unknown orientation by executing a series of linear pushes with a fence. Brost [31] has also shown how to find the linear pushing motions resulting in a desired pusher/object equilibrium configuration. This is like "catching" the object by pushing it. Balorda [36] has investigated catching by pushing with two points of contact. Mason [37] has shown

how to synthesize robot pushing motions to slide a block along a wall, a problem later studied by Wakatsuki [38], who considered pushing forces out of the plane. Feedback control of the motion of an object pushed with a single point of contact has been studied by many researchers. Using only single point of contact for pushing objects removes the complications of controlling several pushers and it's an effective solution for translating object from one location to other. The prominent challenge lies in finding the desired line of pushing which varies with respect to time while pushing a micro-object.

### 2.6.3 Requirements for Reliable Pushing

In order to achieve stable pushing operation for micromanipulation application to attain desired translational and rotational motion of micro objects, it's indispensable to fulfill some of the requirements are as follows:

- *High Precision Motion:* Actuators needs to be driven with very high resolution (in nanometer range), high bandwidth (up to several kilo hertz), and relatively large travel range (up to a few millimeters) . Moreover, a robust controller needs to be designed and utilized for high precision motion with no overshoot because even a very low overshoot can damage either the micro object or the manipulator.
- *Visual Feedback:* Vision based algorithms is needed to estimate location of objects being manipulated along with visual feedback procedures to position manipulators so that these objects can be pushed along a desired trajectory [39].
- *Force Sensing:* Since manipulating an object requires not only the ability to observe and position, but also to physically interact with the object. Thus, micromanipulators solely based on visual feedback and position control are not effective for dexterous micromanipulation. Force control is often needed to augment the operation in order to achieve better manipulation results. Thus it's inevitable to sense the force with nano-newton resolution and with milli-newton range.

- *Scaled Bilateral Teleoperation:* Robust and transparent bilateral controllers is necessary for human intervention so that high fidelity position/force interaction between the operator and the remote micro/nano environment can be achieved.
- *Force Controller for Pushing:* Force controller is required to generate the desired pushing forces for compensating the surface forces arising between the object and the environment. This condition is needed to achieve automatic pushing of the object.

All of the above mentioned points need to be fulfilled for reliable pushing of micro object lying on a homogenous substrate.

## 2.7 Conclusion

This chapter starts the discussion with several issues related to the microsystems and how the micro world differs from the macro world. The aim is directed to the future developments concerning miniaturization of the products which will be composed of incompatible hybrid micro objects which cannot be produced using traditional monolithic process. Microassembly is proposed to be as one of the most effective solution to integrate the micro parts one by one. Some of the recent techniques concerning microassembly are presented along with the trend from serial assembly to parallel assembly approach for mass production. As an initial step several approaches dealing with manipulation of micro objects are presented which is indeed a mandatory requirement for microassembly. Due to scaling effect, the task micro-manipulation of objects become difficult as the surface forces becomes much more dominant than the inertial forces. Several discussion related with forces in the micro world are presented and how to sense the forces which are in milli/nano-newton range. Forces acting in the micro-world are transferred to human operator with the framework of scaled bilateral control is presented. Finally, manipulation by pushing is focused more due to the fact that it has more flexibility with respect to manipulation by pick-and-place operation. Pushing is more affected by the friction between

the micro object and substrate caused by adhesion forces. Several models which predict the real contact area between the micro object and substrate in presence of adhesion forces are presented. Several mechanism implemented by some researcher for pushing operation is presented and finally all the requirements needed for the reliable pushing are enlisted.

# Chapter 3

## Tele-Micromanipulation Setup

This chapter briefly describes the experimental setup of custom built tele-micromanipulation setup along with the working procedures. The setup is comprised of motion control, force sensing, visual feedback and Human-Machine Interface Modules.

### 3.1 Description of the Setup

A custom and open structure tele-micromanipulation setup is developed with human-computer interface containing the master and the slave mechanism as demonstrated in schematic Figure 3.1 and the experimental setup in Figure 3.2. The setup is broadly classified into three categories comprising master side, slave side and human-computer interface. Master mechanism is realized using DC servo with a rigid rod connected to the shaft of the motor to enable the human operator to rotate and transfer the commanded position to the slave mechanism. The slave mechanism employs closed loop piezoelectric actuator to attain motion with nanometer resolution directed from the master side as shown in zoomed Figure 3.3 and the control structure to attain nanometer resolution motion discussed in Chapter 4. Moreover, the substrate is supported by open-loop piezoelectric actuator to bring the micro-object lying on the substrate to the desired location and the control structure for hysteresis elimination is discussed in Chapter 4. Force sensing piezoresistive probes is utilized to sense the interaction forces in  $nN$  range while the probe is contact with the micro-object and the procedures for force sensing part is discusses in Sec-

tion 5.1. Human operator sends the commanded reference position after scaling to the slave side through the master device so the micro-cantilever can manipulate the micro-object and feels the interaction force after necessary scaling of the forces from the slave side. The bilateral control procedures is demonstrated in Section 5.2. Human-computer interface between the master and slave side is realized with a computer attached with dSpace1103 which assist human being as a visual display during the manipulation process. The visual feedback from the camera mounted on top of the microscope is utilized for proper aligning the micro-cantilever and the methodologies is discussed in Chapter 6.

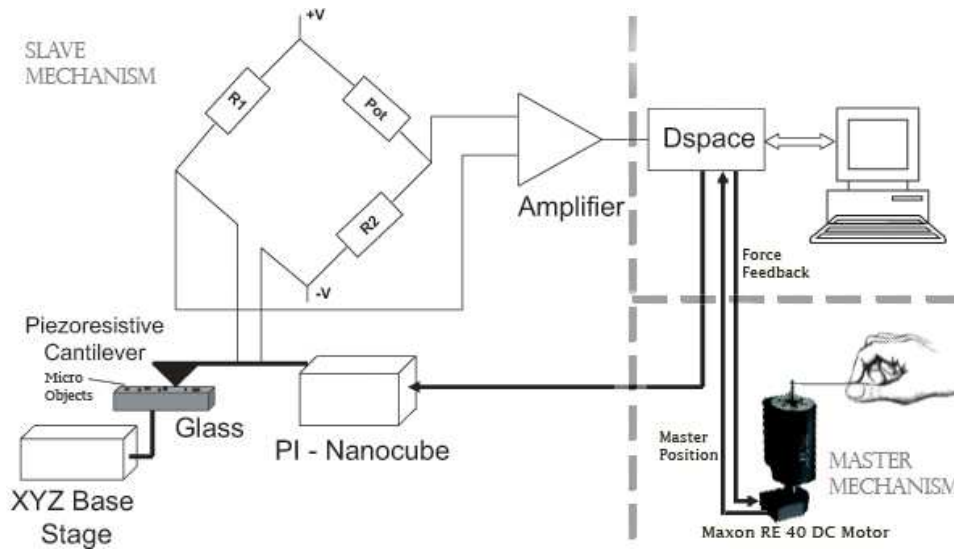


Figure 3.1: Schematic of Tele-micromanipulation system

## 3.2 Conclusion

In this chapter, description of the experimental setup along with the working procedure for manipulation of the micro-objects is explained. The detail working for each component of the experimental setup is discussed in the respective chapters.

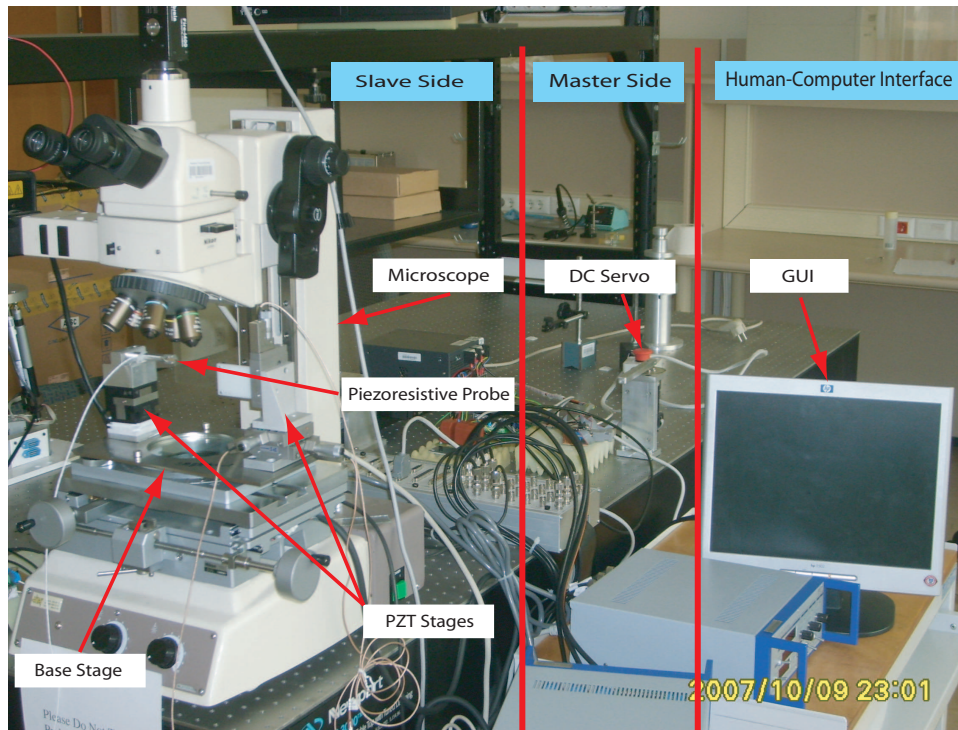


Figure 3.2: Tele-Micromanipulation Setup

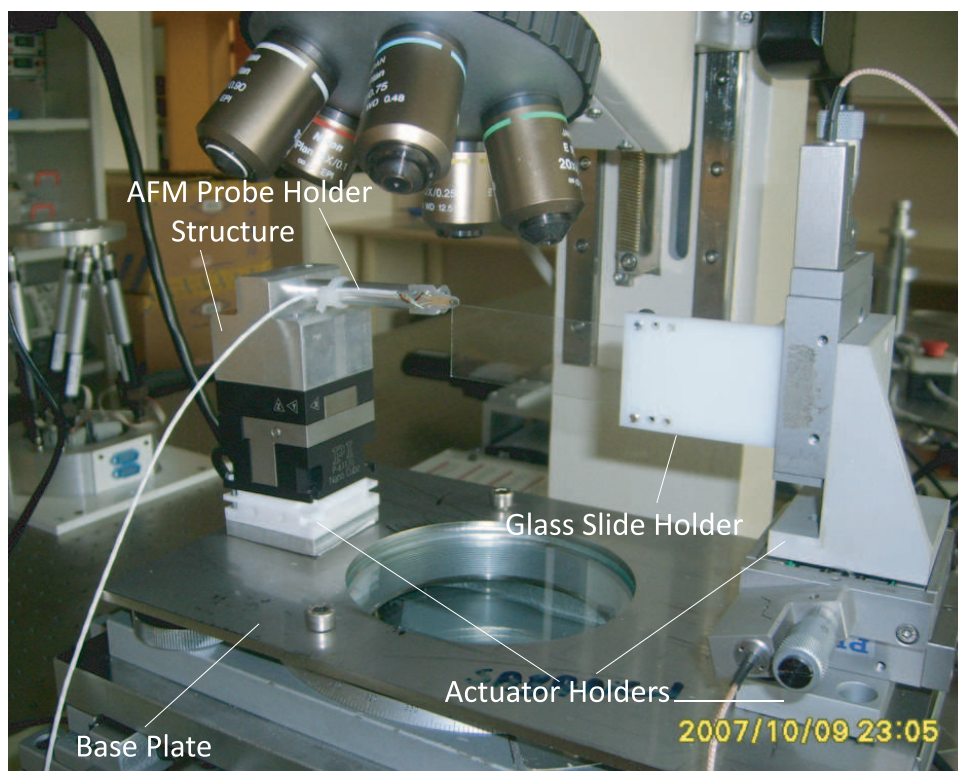


Figure 3.3: Custom built parts in the slave mechanism



# Chapter 4

## High Precision Motion Control

High precision motion control has become an essential requirement in today's advanced manufacturing systems such as machine tools, micro-manipulators, surface mounting robots, etc. In our micromanipulation application, there are strict requirements of the motion to be in range of nanometers, without any overshoot as it may cause damage to the micro-object and/or the micro-manipulator. Moreover, the low-amplitude position tracking is also necessary for trajectory tracking with varying loads. As performance requirements become more stringent, classical controllers such as the PID controller, which has been the most preferred controller and widely used in industry for generations, can no longer provide acceptable results. Although several approaches to the design of better controllers have been proposed in the literature, control problems associated with system uncertainties, presence of high-order dynamics and system inherent nonlinearities remain big challenges for control engineers.

High precision motion control is first challenged by the presence of several uncertainties present in the real-world systems. These nonlinearities limit the high precision positioning/tracking of the actuator which simply cannot be eliminated by introducing an integral action in the controller. The uncertainties which may also be regarded as parasitic effects are often present in real-world systems such as:

- Parametric uncertainty, such as parameter changes due to different operating conditions and load changes.

- Actuator/sensor nonlinearities, such as hysteresis, dead-zone, saturation, input-output slope changes in operating ranges as well as the nonlinearity of quantization when using AD converters for digital-computer control.
- Backlash and compliance in gear-trains.
- Time delay.

The goal of this chapter is to develop a simplified control methodology for implementation into real systems that are required to have very high-precision motion. The main efforts are concentrated on handling internal nonlinear disturbances and friction of mechanical systems using discrete sliding mode controller along with disturbance observer. The chapter focuses more on actual implementation of control methodologies in open-loop PZT, closed-loop PZT and linear drive rather than rigorous theoretical analysis.

## 4.1 Modeling and Control of Open Loop PZT Actuator

Piezoelectricity is a fundamental process in electromechanical energy conversion. It relates electric polarization to mechanical stress/strain in piezoelectric materials. Under the direct effect, an electric charge can be observed when the materials are deformed. The converse or the reciprocal effect is when the application of electric field can cause mechanical stress/strain in the Piezo materials. The former effect is known as the piezoelectric effect and was discovered in 1880 by the Curies. The latter effect is the inverse piezoelectric effect. The word “Piezo” is derived from the Greek word “piezen”, which means “to push”. The effect was discovered when a pushing force or, in other words pressure, was applied to the material. In the beginning, both pressure electricity and piezoelectricity was used to describe the same phenomenon.

### 4.1.1 Modeling of PZT Actuator

Since piezoceramics are dielectrics, one could expect a PZT stack actuator to exhibit capacitive behavior along with rate-independent hysteresis exhibited which affects the net electrical charge delivered to the actuator. Additionally, dynamic observation indicates that endpoint displacement as a function of electrical charge is well approximated by second-order linear dynamics.

By keeping the above factors in mind, a fairly accurate model was chosen [40] for the Piezo-stage due to its easiness for implementation and accuracy for estimating the actual behavior of these actuators. The Piezo-stage consists of a Piezo-drive with a flexure guided structure which is designed to possess zero stiction and friction. Moreover the flexure stages exhibit high stiffness, high load capacity and insensitive to shock and vibration. Figure 4.1 describes the overall electromechanical model [40] of a PZT actuator.

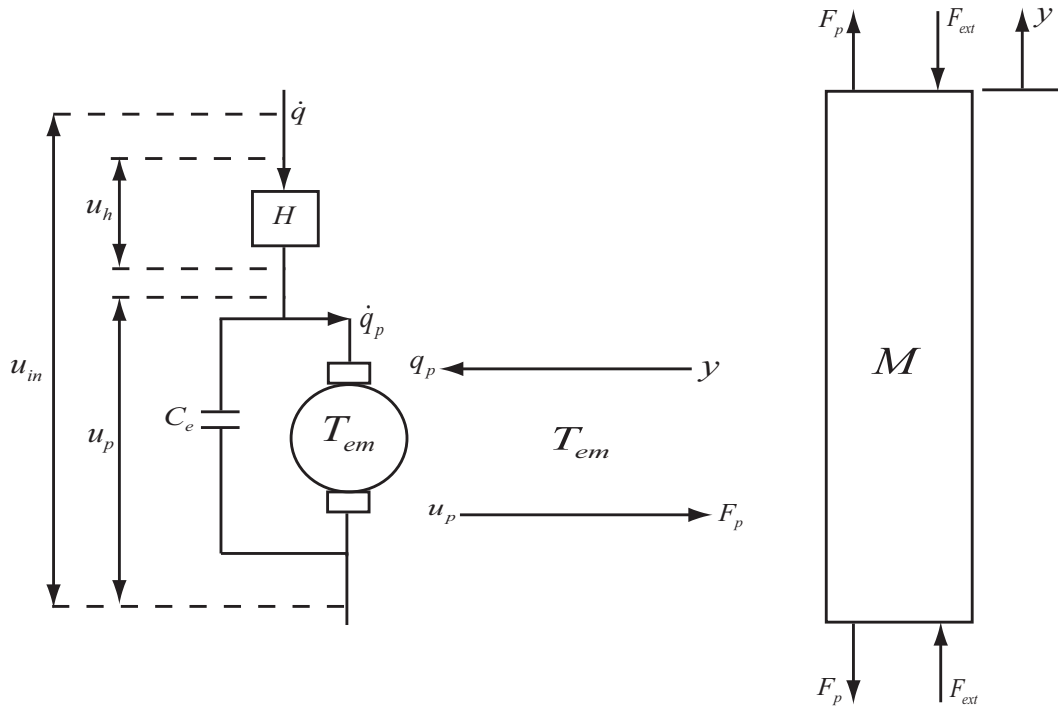


Figure 4.1: Electromechanical model of a PZT actuator

The hysteresis and piezoelectric effects are separated.  $H$  Represents the hysteresis effect and  $u_h$  is the voltage due to this effect. The piezoelectric effect is represented by  $T_{em}$  which is an electromechanical transducer with transformer ra-

tio. The capacitance  $C_e$  represents the sum of the capacitances of the individual PZT wafers, which are connected in parallel. The total current flowing through the circuit is  $\dot{q}$ . Furthermore,  $q$  may be seen as the total charge in the PZT actuator. The charge  $q_p$  is the transducer charge from the mechanical side. The voltage  $u_p$  is due to the Piezo effect. The total voltage over the PZT actuator is  $u_{in}$ ,  $F_p$  is the transducer force from the electrical side,  $F_{ext}$  is the external applied force, and the resulting elongation of the PZT actuator is denoted by  $x$ . The mechanical relation between  $F_p$  and  $x$  is denoted by  $M$ . Note that one have equal electrical and mechanical energy at the ports of interaction i.e.  $u_p q_p = F_p x$ .

The piezoelectric ceramic has elasticity modulus  $E$ , viscosity  $\eta$ , and mass density  $\rho$ . Furthermore, the geometric properties of the PZT actuator are length  $L$  and cross-sectional area  $A_p$ . Effective Mass  $m_p$ , Effective stiffness  $k_p$  and damping co-efficient  $c_p$  can be calculated as follows:

$$\begin{aligned} m_p &= \rho A_p L \\ k_p &= \frac{\rho A_p}{L} \\ c_p &= \frac{\eta A_p}{L} \end{aligned} \tag{4.1.1}$$

The complete electromechanical equations can be written as:

$$m_p \ddot{y} + c_p \dot{y} + k_p y = T_{em}(u_{in}(t) - H(y, u_{in})) - F_{ext} \tag{4.1.2}$$

Here  $y$  represents the displacement of the Piezo stage and  $H(y, u_{in})$  denotes the non-linear hysteresis which is a function of  $y$  and  $u_{in}$ .

### 4.1.2 Introduction to Hysteresis in PZT

An inherent non-linearity in piezoelectric actuator is hysteresis, which is a rate-independent nonlinearity i.e. the output displacement depends on the present input voltage as well as on how the inputs were applied previously, but not the input voltage in the past. The hysteresis behavior, if not considered carefully in the control system design, may cause limit cycles or even instability [41]. This hysteresis non-linearity is usually 15 – 20 percent of the output thereby greatly reducing the performance by the actuator. One effective way to cancel hysteresis is to construct

a model which can describe its behavior and then reshape the input voltage based on the inverse behavior of the model. Similar to the inverse dynamics control in the literature, the effectiveness relies on the accuracy of system model.

Motivated by canceling hysteresis using model inverse, extensive research has been devoted for developing hysteresis models. For instance one can use a nonlinear differential equation, or so-called Duhem-Madelung's model, to describe hysteresis [42]. Hysteresis models formed by a weighted superposition of many/infinite elementary hysteresis operator has also been reported. Depending on the hysteresis operator chosen, the model can be Preisach type [43], and [44]. These hysteresis models are mathematically combined with the piezoelectric actuator linear dynamics to form the overall system model. Such models do not emphasize the physical aspect of the system's characteristics. In comparison, PEA model proposed by Goldfarb and Celanovic [40] is completely based on physical principles. Their model consists of an electric and a mechanical domain, as well as the energy transfer between the two domains. Hysteresis therein is modeled via Generalized Maxwell Slip [45] as a nonlinear resistive-capacitive element in the electrical domain. The complete parameterizations is obtained by fitting the model behavior with the initial ascending part of the experimental curve.

The modeling and identification approaches in all above approaches suffers from three basic limitations. First of all, these approaches either ignore the impact of piezoelectric actuators initial charges/strain or assumed it to be in relaxed state before the voltage is applied [40]. Secondly, hysteresis loops produced by the models are restricted in the sense they are mainly anti-symmetric, does not match the experimental behavior of piezoelectric actuators. Though, it requires much more complicated and repeated experimental procedure. Thirdly, there is no guarantee that the resultant model behavior can accurately reproduce the whole major hysteresis loops as well as other minor loops.

In this paper, a well established model from Bouch-Wen [46] has been utilized in a directed effort to drastically reduce the hysteresis behavior. Since our major application is focused on micromanipulation application which indeed requires a relatively slow and constant velocity, thus the operating frequency has been fixed.

Moreover, an experimental challenge has been overtaken by using a laser interferometer to achieve the displacement feedback from open-loop piezoelectric actuator.

### 4.1.3 Model for Hysteresis

The phenomenon of hysteresis is encountered in many areas of science. But the very interpretation of hysteresis varies from one area to another and from one context to another context. As a result, rigorous mathematical definitions of hysteresis are needed in order to avoid confusion and ambiguity. Such definitions serve a twofold purpose: they are substitute's far vague notions, and they create machinery for elegant proofs.

A transducer can be characterized by an input  $u(t)$  and an output  $f(t)$ . This transducer is called a hysteresis transducer (HT) if its input-output relationship is a multibranch nonlinearity for which a branch-to-branch transition occurs after each input extremes as shown in Figure 4.3. Only the case of static hysteresis nonlinearity will be further discussed. The term "static" means that branches of hysteresis nonlinearities are determined by the past extremes values of input, while the speed of input variation between extremes points has no influence on branching. But in our case due to slow motion requirement, the problem can be neglected. According to the given definition, branching constitutes the essence of hysteresis, while looping is a consequence of branching.

Consequently, control input is not known beforehand but it is determined by the interaction of the transducer with the rest of the system. For this reason, a mathematical model is needed which itself (due to its structure) will detect and accumulate input extremes and will choose the appropriate branch of the hysteresis nonlinearity with respect to the accumulated history. By using such models [44] one can attempt mathematical descriptions of systems with hysteresis. These models are of particular interest because they have been used successfully in general control design algorithms for broad classes of hysteretic systems. For the purpose of characterizing the dynamics of mechanical structures, the Bouch-Wen [46] nonlinear hysteresis model appears to be a good choice because of its form (mass-spring-viscous damper equivalent differential equation of motion) and its versatility. Hence, this model has

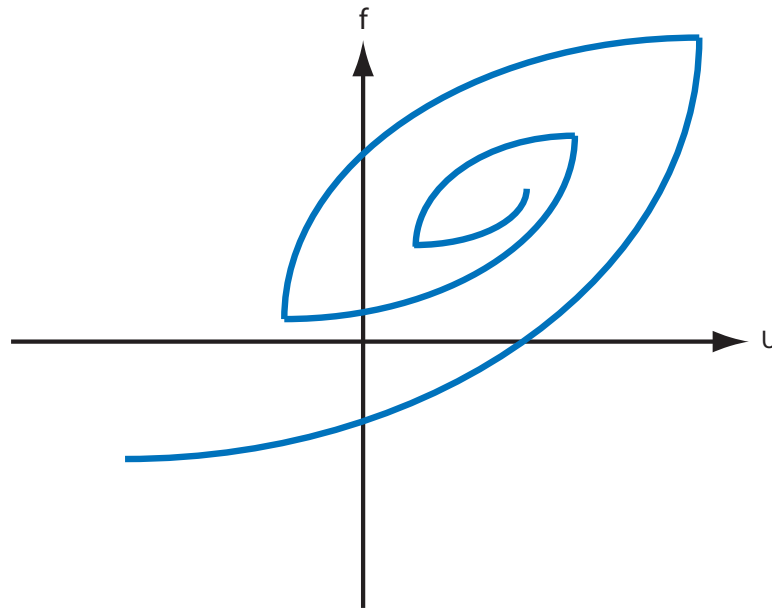


Figure 4.2: Hysteresis multibranch nonlinearity

been selected in the current work to compensate for the hysteresis loop arising in open-loop Piezo actuator. Numerous researchers have successfully used this model. For example Constantinou [47] used it for the study of nonlinear hysteretic isolators; Smyth [48] for adaptive application and Heine [49] for an optimization approach for degrading hysteretic joints with slack behavior.

The Bouch-Wen hysteresis model is a system of nonlinear differential equations defined by Eqn.(4.1.3).

$$\dot{z} = \alpha\dot{x} - \beta|\dot{x}|z|\dot{z}|^{n-1} - \gamma\dot{x}|z|^n \quad (4.1.3)$$

Where parameter  $\alpha$  controls the restoring force amplitude,  $\beta$  and  $\gamma$  controls the shape of the hysteresis loop, and control the smoothness of the transition from elastic to plastic response. Because of the assumption for the elastic structure and materials, then letting  $n = 1$ , Eqn.(4.1.3) can be rewritten as Eqn.(4.1.4)

$$\dot{z} = \alpha\dot{x} - \beta|\dot{x}|z - \gamma\dot{x}|z| \quad (4.1.4)$$

which represents the hysteretic relationship between the state variable  $z$  or voltage and excitation  $x$  or displacement. The hysteretic variable  $z$  is a "fictitious" displacement related to actual displacement,  $x$ . Different combinations of the parameters

yield also different shapes for the hysteresis loops. To illustrate this let  $n = 1$  and vary only the parameters  $\beta$  and  $\gamma$ . Different possible stable hysteresis curves [50] are shown in Figure and the versatility of the system response of differential equations can be observed as described in Eqn.(4.1.4). By appropriate selection of the values of parameters,  $\alpha$ ,  $\beta$  and  $\gamma$  this model can describe the behavior of piezoelectric actuator very well.

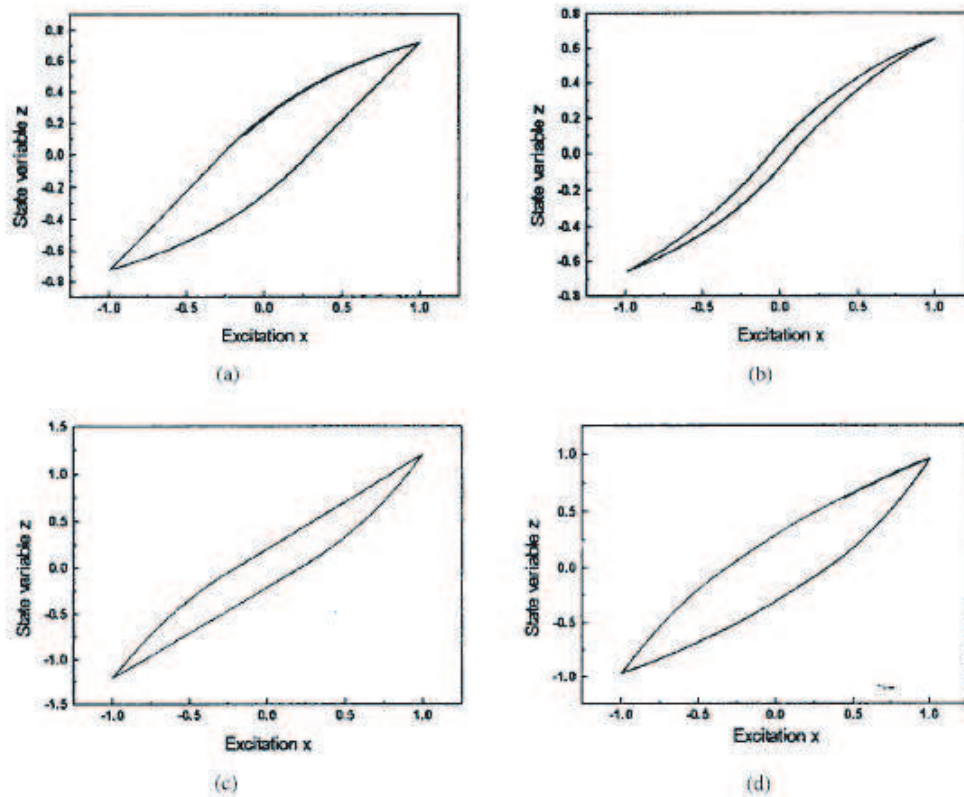


Figure 4.3:  $z$ - $x$  curves of several combination  $\alpha$ ,  $\beta$ ,  $\gamma$ . (a)  $\alpha = 1.0$ ,  $\beta = 0.5$ , and  $\gamma = 0.5$ ; (b)  $\alpha = 1.0$ ,  $\beta = 0.1$ , and  $\gamma = 0.9$ ; (c)  $\alpha = 1.0$ ,  $\beta = 0.5$ , and  $\gamma = -0.5$ ; (d)  $\alpha = 1.0$ ,  $\beta = 0.25$ , and  $\gamma = -0.5$ ; adapted from [6]

#### 4.1.4 Description of Experimental Setup

To verify the established model, an open loop piezoelectric micrometer drive PiezoMike PI-854 from *Physik Instrumente<sup>TM</sup>* has been utilized. It's equipped with integrated high-resolution Piezo linear drives. They can be operated manually with a resolution of  $1 \mu m$ . By controlling the Piezo voltage, the micrometer tip is automatically



moved in and out up to  $25\ \mu\text{m}$  with respect to the manually set position. Resolution of Piezoelectric motion is in the sub-nanometer range. The piezoelectric actuators are being driven by E-663 low voltage Piezo driver from PI in external control mode. In external control mode, the input voltage is provided from DAC module of *dSpace*<sup>TM</sup> 1103 in the range from -2 volts to 2 volts which is amplified by 10 times and feed to Piezo actuators. In order to achieve the displacement of piezoactuator, a laser interferometer LK-2001 from *Keyence*<sup>TM</sup> has been utilized. It is equipped with CCD as a light-receiving element, which enables high accurate displacement measurement, regardless of the light quantity distribution of the beam spot. It has resolution of  $1\ \mu\text{m}$  with a travel range of  $18\ \text{mm}$ . The technical specification of the drive is provided in Appendix A.1. The overall schematics is shown in Figure 4.4, with a corresponding experimental setup demonstrated in Figure 4.5.

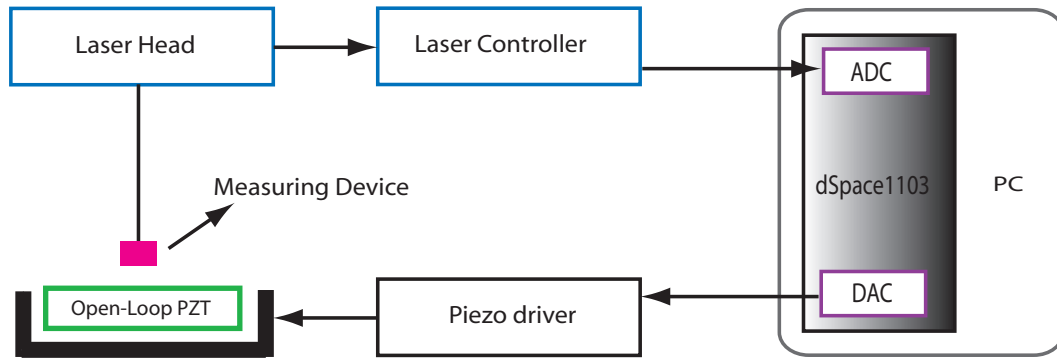


Figure 4.4: Schematic of the experimental setup

The PZT actuator is driven by Piezo driver to which input voltage is provided by DAC module of *dSpace* 1103 and the displacement of the open-loop piezo are sensed by laser head and corresponding analog voltage is generated by the laser module controller. The resulting voltage in terms of displacement is read by ADC module. The incorporated Bouch-Wen model generates the necessary voltage along with the reference signal in order to eliminate the hysteresis behavior.

#### 4.1.5 Experimental Validation

In order to validate the Bouch-Wen model, the parameters values were tuned as  $\alpha = 0.1049$ ,  $\beta = 1.1115$  and  $\gamma = -1.0387$  to eliminate or reduce the hysteresis

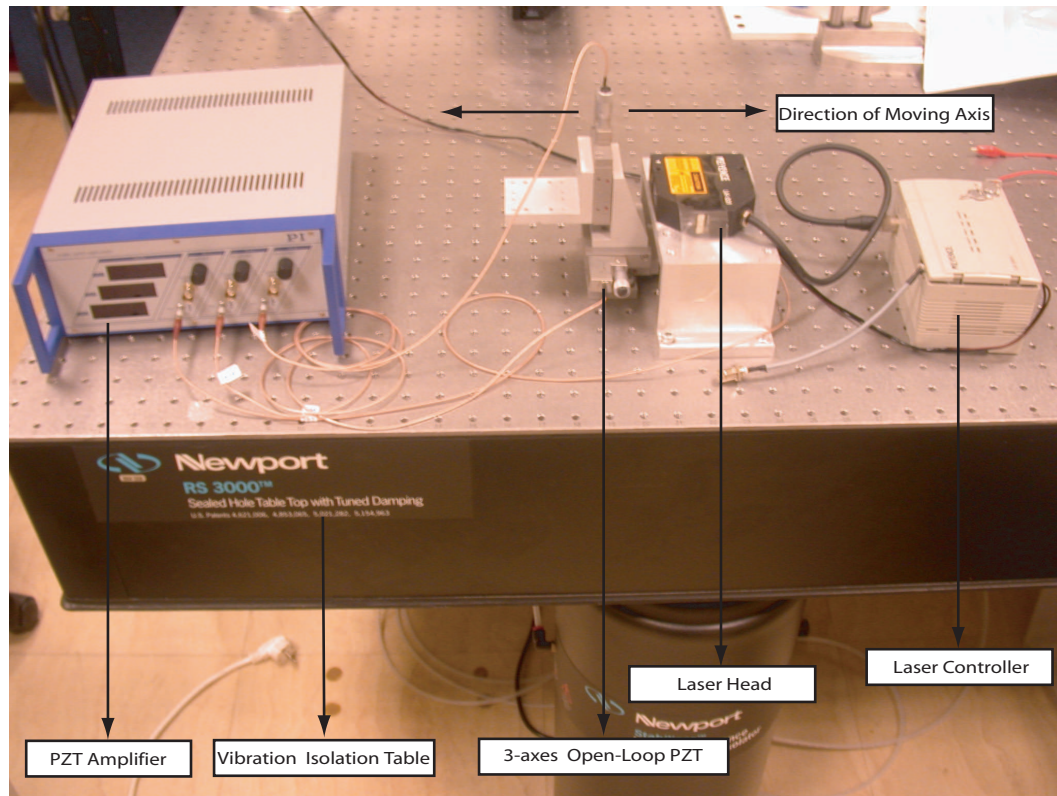


Figure 4.5: Structure of the experimental setup

behavior present in open-loop PZT.

It is a well established fact that hysteretic behavior increases with respect to travel range; this is illustrated in Figure 4.6 where the sinusoidal input frequency is fixed at 1 Hz and with varying amplitude. The hysteretic behavior increases with increasing frequencies which is clearly illustrated in Figure 4.7 where sinusoidal input frequencies of 0.5 Hz, 1 Hz and 2 Hz and constant amplitude are applied to the piezoelectric drives.

Sinusoidal input with constant frequencies of 1 Hz is applied with varying amplitudes and its hysteresis behavior is compensated. Since in our micromanipulation applications all the motion needs to be very slow, as a results driving frequency is set constant to 1 Hz. Figure 4.8 and 4.9 shows the hysteresis compensation for input Voltage of 20 V and 80 V respectively. Figures 4.8 and 4.9 clearly shows that there is an immense reduction of the hysteretic behavior and the dynamics of the PZT actuator is enhanced and linearized after applying the model. Thus the reference can be generated with respect to modified dynamics of PZT actuator.

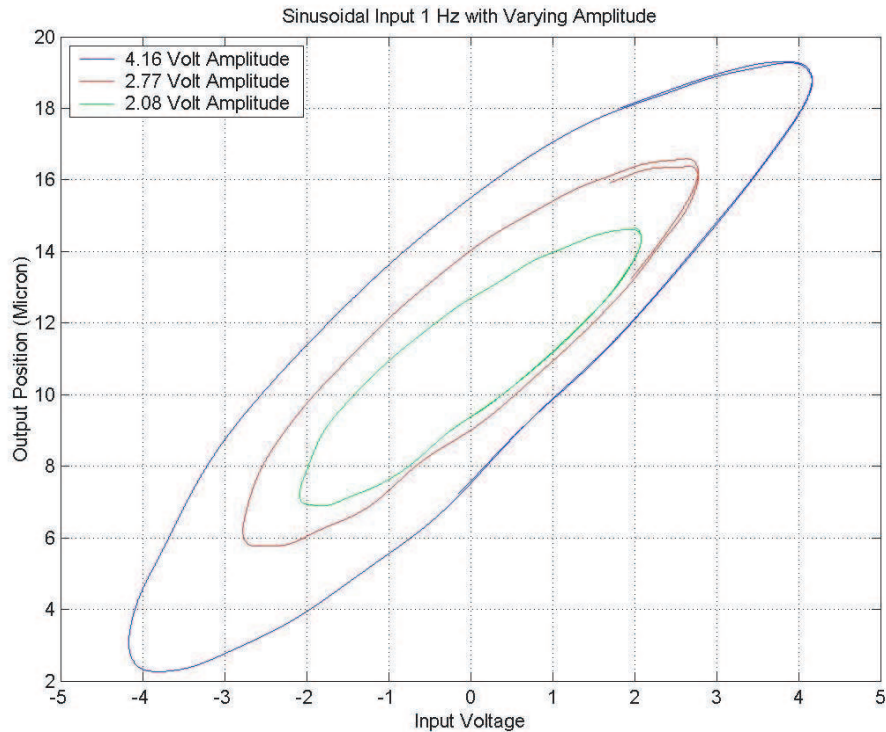


Figure 4.6: Hysteresis Loop for Sinusoidal input with 1 Hz and varying Amplitude

## 4.2 Closed Loop Control of PZT Actuator

As discussed above piezoelectric actuator has been demonstrated with immense potentialities in application with required accuracy within the range from sub micrometer to nanometer motion. The main advantage to use piezoelectric as an actuator is due to the fact that it does not possess any frictional or static characteristics which generally exist in other forms of actuators. The main characteristics of piezoelectric actuator are: high resolution in nanometer range, high bandwidth up to several kilohertz range, a large force up to few tons and short travel range along with millimeter range [51]. Some of the major areas where piezoelectric actuator can be used is in micromanipulation, force feedback as in AFM, micro-assembly and in dual stage hard disk drives. In all of these applications it is highly desired to have accurate positioning which can only be achieved using closed-loop control. Though some attempts have been made in the past [40], [52] to control piezoelectric actuator in open loop system with fine compensation for hysteresis non-linearity in the system.

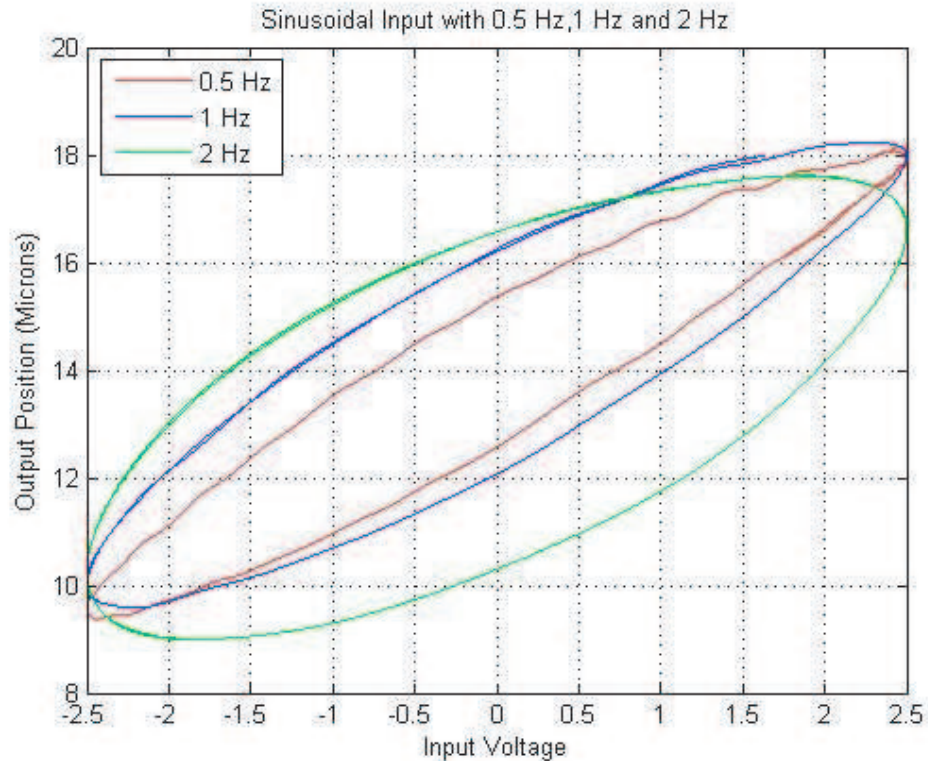


Figure 4.7: Sinusoidal Input with varying frequencies of 0.5 Hz, 1 Hz and 2 Hz with constant Amplitude

Due to the development of accurate positioning sensors it has become possible to use robust feedback based nonlinear control methods in order to eliminate the hysteresis effect.

Many researcher has applied several control methodologies for feedback control to achieve high-precision motion without any overshoot and to eliminate non-linearities present in the system. In [53],  $H_\infty$  based closed-loop is proposed with model based hysteresis compensation. The model described is too complex in spite of good outcome but could be replaced by a simpler model. In [54], a neural-network based feed-forward assisted proportional integral derivative (PID) controller was proposed. In [55] variable structure control (VSC) for accurate positioning control in sub-micron ranges is demonstrated.

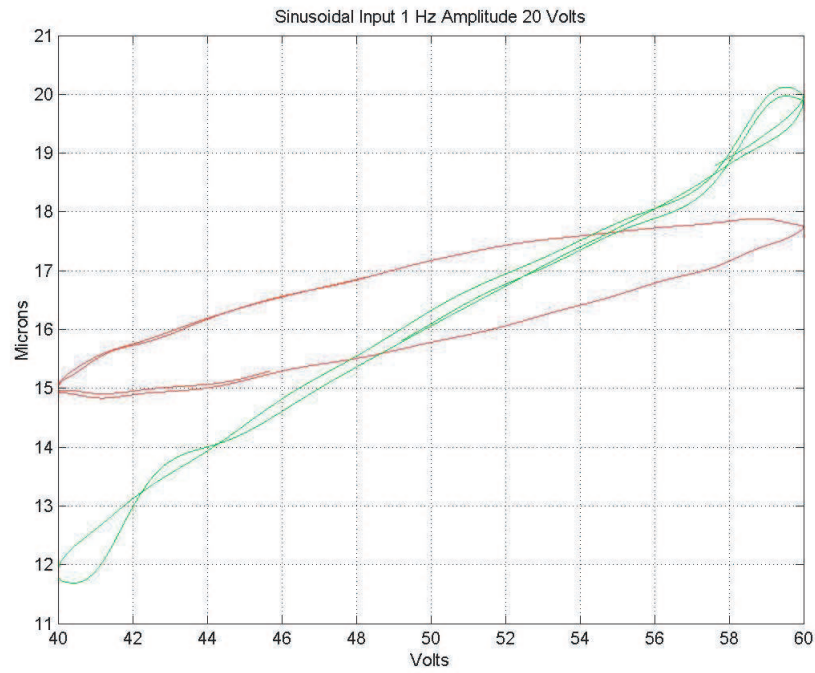


Figure 4.8: Sinusoidal Input of 1 Hz frequency and 20 V amplitude

### 4.2.1 Sliding Mode in Variable Structure System

Sliding mode control (SMC), which is sometimes known as variable structure control (VSC), is characterized by a discontinuous control action which changes structure upon reaching a set of predetermined switching surfaces. This kind of control may result in a very robust system and thus provides a possibility for achieving the goals of high-precision motion with a very fast response. Some promising features of SMC are listed below:

- The order of the motion can be reduced.
- The motion equation of the sliding mode can be designed linear and homogeneous, despite the original system may be governed by non-linear equations.
- The sliding mode does not depend on the system dynamics, but is determined by parameters selected by the user.
- Once the sliding motion occurs, the system develops invariant properties which make the motion independent of certain system parameter variations and dis-



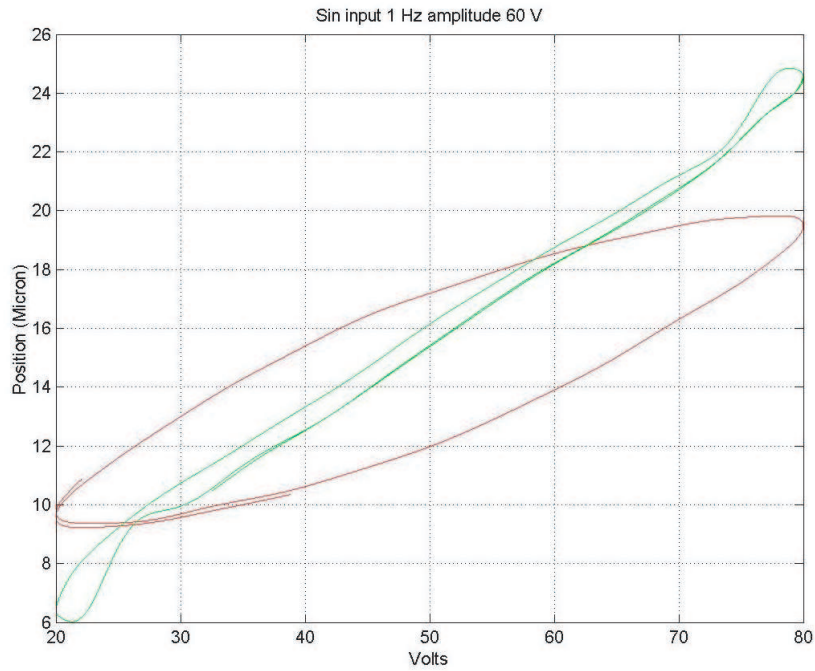


Figure 4.9: Sinusoidal Input of 1 Hz frequency and 60 V amplitude

turbances. Thus the system performance can be completely established by the dynamics of the sliding manifold.

Consider the system as below,

$$\dot{x} = f(x, t) + B(x, t)u(x, t), \quad x \in R^n, u \in R^m \quad (4.2.1)$$

where all the elements of vector  $f(x, t)$  and matrix  $B(x, t)$  are continuous and bounded along with their first order time derivatives;  $rank(B(x, t)) = m, \forall x, t > 0$

The discontinuous control is given by,

$$u = \begin{cases} u^+(x, t), \sigma(x) > 0 \\ u^-(x, t), \sigma(x) < 0 \end{cases} \quad (4.2.2)$$

$$\sigma(x)^T = \{\sigma_1(x), \sigma_2(x), \dots, \sigma_m(x)\}, \sigma(x) = G(x^r - x) \quad (4.2.3)$$

here  $u^+(x, t)$ ,  $u^-(x, t)$  and  $\sigma(x)$  are continuous functions. Since  $u(x, t)$  undergoes discontinuity on the surfaces, it is called the *switching surface* or the *switching hyperplane*.

Let  $S = X|_{\sigma(x)=0}$  be a switching surface that includes the origin  $x = 0$ . If, for any  $x_0$  in  $S$ ,  $x(t)$  is in  $S$  for all  $t > t_0$ , then  $x(t)$  is a sliding mode of the system and the switching surface  $S$  is called a sliding surface or sliding manifold. A sliding mode exists, if in the vicinity of the switching surface  $S$ , the tangent or the velocity vectors of the state trajectory always point towards the switching surface. Existence of a sliding mode requires stability of the state trajectory towards sliding surface  $S = X|_{\sigma(x)=0}$  at least in the neighborhood of  $S$ , i.e., the representative point must approach the sliding surface at least asymptotically. This sufficiency for sliding mode is called reaching condition, and state trajectory under the condition is called the reaching mode or reaching phase. The largest neighborhood for which the reaching condition is satisfied is called the region of attraction.

In order to guarantee desired behavior of the closed-loop system, the sliding mode controller requires infinitely fast switching mechanism. However, due to physical limitations in real-world systems, direct application of the above control will always lead to some oscillations in some vicinity of the sliding surface, i.e. the so called chattering problem. The main restrictions come from the implementation of controllers in digital computers which work on discrete-time principles and cannot permit infinitely fast switching. Since modern controllers are most likely implemented in digital computers, it is inevitable to approach a practical SMC design in discrete-time.

### 4.2.2 Design of Sliding Mode Controller and Realization in Discrete Form

SMC theory was initially developed from a continuous time perspective. It has been realized that directly applying the continuous-time SMC algorithms to discrete time systems will lead to some indomitable problems, such as the limited sampling frequency, sample/hold effects and discretization errors. Since the switching frequency in sampled-data systems cannot exceed the sampling frequency, a discontinuous con-

control does will not enable generation of motion in a random manifold in discrete-time systems. This leads to chattering at the sampling frequency along the designed sliding surface, or even instability in case of a too large switching gain.

The discontinuous sliding-mode controller involves a continuous plant model with a discontinuous right-hand-side due to the switching control function as mentioned above. Drakunov and Utkin [56] introduced a continuous approach to SMC for an arbitrary finite dimensional discrete-time system. This approach implies that for a sampled-data controller, as the system becomes discrete, the controller should be continuous to overcome the sampling frequency limitations of the discontinuous approach. For such continuous implementation of SMC, plant motion is proven to reach the sliding manifold of predefined state trajectory in finite time.

The derivation of the controller structure starts with the proper selection of the Lyapunov function  $V(\sigma)$ , and an appropriate form of the derivatives of the Lyapunov function,  $\dot{V}(\sigma)$ .

Natural selection of the Lyapunov function candidate seems in the form

$$V(\sigma) = \frac{\sigma^2}{2} \quad (4.2.4)$$

$$\dot{V}(\sigma) = \sigma \dot{\sigma} \quad (4.2.5)$$

In order to guarantee the asymptotic stability of the solution  $\sigma(x, x^r) = 0$ , the derivatives of the Lyapunov function may be selected to be

$$\dot{V}(\sigma) = -D\sigma^2 - \mu \frac{\sigma^2}{|\sigma|} \quad (4.2.6)$$

Here  $D$  and  $\mu$  is a positive constant. Hence, if the control can be determined from Eqn.(4.2.5) and Eqn.(4.2.6), the asymptotic stability will be guaranteed since  $V(\sigma) > 0$ ,  $V(0) = 0$  and  $\dot{V}(\sigma) < 0$ . By combining Eqn.(4.2.5) and Eqn.(4.2.6) the following Equation can be deduced,

$$\sigma(\dot{\sigma} + D\sigma + \mu \frac{\sigma}{|\sigma|}) = 0 \quad (4.2.7)$$



which means,

$$\dot{\sigma} + D\sigma + \mu \frac{\sigma}{|\sigma|} = 0 \quad (4.2.8)$$

The derivation of the sliding function can be written as

$$\dot{\sigma} = G(\dot{x}^r - \dot{x}) = G\dot{x}^r - G\dot{x} \quad (4.2.9)$$

after some simplification, we can get

$$\dot{\sigma} = G\dot{x}^r - Gf - GBu(t) = GB(u_{eq} - u(t)) \quad (4.2.10)$$

solving the above equation, we get

$$u(t) = u_{eq} + (GB)^{-1}(D\sigma + \mu \frac{\sigma}{|\sigma|}) \quad (4.2.11)$$

It can be seen from above equation that  $u_{eq}$  are difficult to calculate. Using the fact that  $u_{eq}$  is a continuous function, it can be rewritten in discrete form using Euler's approximation as,

$$\frac{\sigma((k+1)T_s) - \sigma(kT_s)}{T_s} = GB(u_{eq}(kT_s) - u(kT_s)) \quad (4.2.12)$$

Here  $T_s$  is the sampling time and  $k = Z^+$ . It is also necessary to write  $u(t)$  in the discrete form which results in,

$$u(kT_s) = u_{eq}(kT_s) + (GB)^{-1}(D\sigma(kT_s) + \mu \frac{\sigma(kT_s)}{|\sigma(kT_s)|}) \quad (4.2.13)$$

The value of  $u_{eq}(kT_s)$  can be written as,

$$u_{eq}(kT_s) = u(kT_s) + (GB)^{-1}(\frac{\sigma((k+1)T_s) - \sigma(kT_s)}{T_s}) \quad (4.2.14)$$

Since the system is casual, and it is required to avoid the calculation of the predicted value for  $\sigma$ , as control cannot be dependent on future value of  $\sigma$ . Since the equivalent control is a continuous function, the current value of the equivalent control can be approximated with the single-step backward value calculated for  $u_{eq}(kT_s)$  as,

$$u_{eq_{k-1}} = u_{k-1} + (GB)^{-1} \left( \frac{\sigma_k - \sigma_{k-1}}{T_s} \right) \quad (4.2.15)$$

here  $\hat{u}_{eq_k}$  (or  $\hat{u}_{eq}(kT_s)$ ) is the estimate of the current value of the equivalent control. After some simplification the resulting control structure as be written as,

$$u_k = u_{k-1} + (GBT_s)^{-1} \left( (DT_s + 1)\sigma_k - \sigma_{k-1} + \mu \frac{\sigma(k)}{|\sigma(k)|} \right) \quad (4.2.16)$$

The control structure Eqn.(4.2.16) is suitable for implementation, since it requires measurement of the sliding mode function and the value of the control applied in the preceding step. For a discrete-time system, the discrete sliding mode can be interpreted as that the states are only required to be kept on the sliding surface at each sampling instant. Between the samples, the states are allowed to diverge from the surface within a boundary layer. Note that the control defined by Eqn.(4.2.16) is continuous unlike the case for continuous time. Estimation of boundary layer is explained in next section.

### 4.2.3 Estimation of Boundary layer in Discrete Sliding-Mode Control

During the course of designing the controller, it is crucial to analyze the robustness of the controller or, in other words, whether it satisfy the condition defined by Eqn.(4.2.8). Moreover the estimation of boundary layer of the sliding manifold is significant in relation with the robustness of the controller. The analysis that will be shown are concerned with a general system affine with control such as Eqn.(4.2.1). Consider the system defined in Eqn.(4.2.1), where  $f(x, t)$  and  $B(x, t)$  are assumed to be continuous and bounded. The derivative of the sliding surface is given by,

$$\frac{d\sigma(t)}{dt} = G(\dot{x}^r - \dot{x}) + \frac{\delta\sigma(t)}{\delta t} = G\dot{x}^r(t) - Gf(t) + \frac{\delta\sigma(t)}{\delta t} \quad (4.2.17)$$

Instead of  $O(T_s)$  the control defined by Eqn.(4.2.16) assuming  $\sigma = 0$  is used and following result is obtained

$$\begin{aligned} \frac{d\sigma(t)}{dt} = G\dot{x}^r(t) - Gf(t) - GB\{u(t^-) + \\ (GB)^{-1}(D\sigma + \dot{\sigma})|_t^- + \frac{\delta\sigma(t)}{\delta t} \end{aligned} \quad (4.2.18)$$

here  $t^- = t - T_s$  for discrete time applications with  $T_s$  is the sampling time. Further simplification of Eqn.(4.2.18) leads to,

$$\frac{d\sigma(t)}{dt} = G\dot{x}^r(t) - Gf(t) - GBu(t^-) + \frac{\delta\sigma(t)}{\delta t} - (D\sigma + \frac{d\sigma}{dt})|_{t^-} \quad (4.2.19)$$

Finally Eqn.(4.2.19) can be written as

$$\begin{aligned} \frac{d\sigma(t)}{dt} = \frac{d\sigma(t^-)}{dt} - \frac{d\sigma(t^-)}{dt} - D\sigma(t) + \\ \underbrace{G\Delta\dot{x}^r - G\Delta f + \Delta\left(\frac{\delta\sigma}{\delta t}\right) - D\Delta\sigma}_{\zeta(T_s)} \end{aligned} \quad (4.2.20)$$

Here,

$$\begin{aligned} \Delta\dot{x}^r &= \dot{x}^t - \dot{x}^r(t^-), \\ \Delta f &= f(t) - f(t^-), \\ \Delta\sigma &= \sigma(t) - \sigma(t^-), \\ \Delta\left(\frac{\delta\sigma}{\delta t}\right) &= \frac{\delta\sigma(t)}{\delta t} - \frac{\delta\sigma(t^-)}{\delta t}, \end{aligned} \quad (4.2.21)$$

Hence,

$$\frac{d\sigma(t)}{dt} + D\sigma(t) = \zeta(T_s) \quad (4.2.22)$$

Since  $f(t)$ ,  $x^r(t)$  and  $\sigma(t)$  are smooth functions,  $\zeta(T_s)$  has order  $O(T_s)$ . Hence, the states will remain within an  $O(T_s^2)$  boundary layer of the sliding surface.

#### 4.2.4 Design of Disturbance Observer based on Sliding-Mode Control

There are several hindrances for high precision motion which are highly nonlinear in nature and arises from several factors such as hysteresis, dead zone, saturation, backlash etc of the actuators and/or sensing devices, high parameter variations and time delay.

It might be possible to combine all the effects of these different kind of disturbances on the plant response (i.e. observe their position) and provide a compensation for them as an addition to the controller output and use this sum as the plant input. This kind of compensation is called “disturbance compensation” and the observer used is called “disturbance observer”.

The observer structure is deduced based on Eqn.(4.1.2) under the assumption that all the plant parameters uncertainties, nonlinearities and external disturbances can be represented as a lumped disturbance. It is assumed that  $y$  is the displacement and measurable and similarly  $u_t$  is the input and also a measurable quantity.

$$m_p \ddot{y} + c_p \dot{y} + k_p y = T_p u(t) - F_{dis} \quad (4.2.23)$$

$$F_{dis} = T_p H + \Delta T (v_{in} + v_h) + \Delta m \ddot{y} + \Delta k y$$

Here  $m_p$ ,  $c_p$ ,  $k_p$  and  $T_p$  are the nominal plant parameters while  $\Delta m$ ,  $\Delta c$ ,  $\Delta k$  and  $\Delta T$  are the uncertainties associated with the plant parameters. Since  $y$  and  $u(t)$  are measurable quantity, observer structure can be written in following form,

$$m_p \ddot{\hat{y}} + c_p \dot{\hat{y}} + k_p \hat{y} = T_p u - T_p u_c \quad (4.2.24)$$

Here  $\hat{y}$ ,  $\dot{\hat{y}}$  and  $\ddot{\hat{y}}$  are position, velocity and acceleration respectively.  $u$  is the plant control input and  $u_c$  is the observer control input as shown in Figure 4.10.

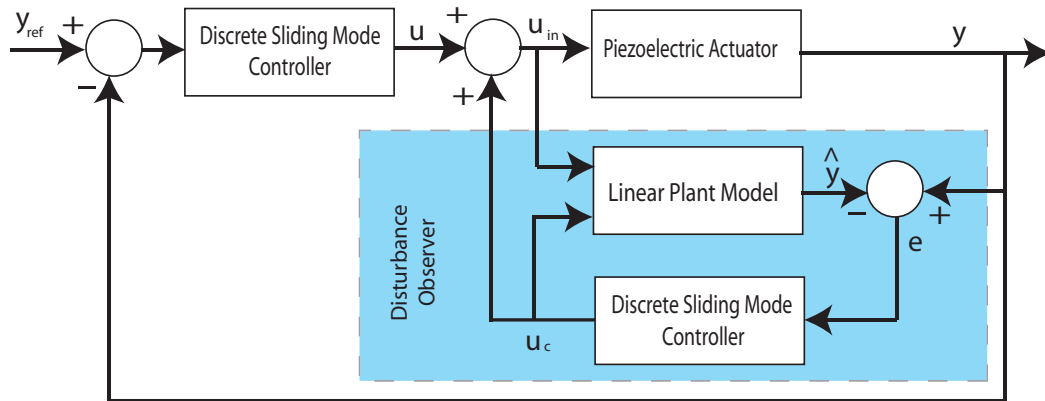


Figure 4.10: Controller and disturbance observer for position control of the PZT actuator, adapted from [7]

The estimated position  $\hat{y}$  should be forced to track  $y$ . The SMC structure is used for deriving the observer controller whose sliding manifold is defined as,

$$\sigma_{obs} = \lambda_{obs}(y - \hat{y}) + (\dot{y} - \dot{\hat{y}}) \quad (4.2.25)$$

Here  $\lambda_{obs}$  is a positive constant. If  $\sigma_{obs}$  is forced to become zero then  $\hat{y}$  should be forced to  $y$ . As described in the previous section, with the same analogy it can be written as,

$$\dot{\sigma}_{obs} + D_{obs}\sigma_{obs} = 0 \quad (4.2.26)$$

which guarantees  $\sigma_{obs} \rightarrow 0$ . After some modification the resulting equation can be written as,

$$(\ddot{y} - \ddot{\hat{y}}) + (\lambda_{obs} + D_{obs})(\dot{y} - \dot{\hat{y}}) + \lambda_{obs}D_{obs}(y - \hat{y}) = 0 \quad (4.2.27)$$

It can be seen that the transient of the closed-loop system are defined by the roots  $-\lambda_{obs}$  and  $-D_{obs}$ . The same structure of the controller will be used in the observer as described in Eqn.(4.2.16). From structure Eqn.(4.2.24) it can be seen that the input matrix is given by,

$$B_{obs} = \begin{bmatrix} 0 & -\frac{T_p}{m_p} \end{bmatrix}^T \quad (4.2.28)$$

The matrix  $G$  for this case is defined as,

$$G = [\lambda_{obs} \quad 1] \quad (4.2.29)$$

Thus, after some simplification the controller structure can be written as,

$$u_{ck} = u_{ck-1} - \frac{m_p}{T_p} \left( D_{obs}\lambda_{obsk} + \frac{\sigma_{obsk} - \sigma_{obsk-1}}{T_s} \right) \quad (4.2.30)$$

Here  $u_c$  is the compensated control input to the system. The positive feedback by input  $u_c$  forces the system to behave closely towards the ideal system having the nominal parameters. But in reality there is also some amount of difference between the real disturbance and estimated disturbances.

### 4.2.5 Experimental Validation of Position Control

In order to illustrate the effectiveness of the proposed controller with the disturbance observer, experiments were carried out on a single axis of a 3-axis Piezo-stage. The Piezo stage is manufactured by *Physik Instrumente<sup>PI</sup>* and driven by E-664 power amplifier. The technical specification of the piezo stages and the driver is provided in Appendix A.2 and A.3 respectively. Table 4.1 shows the parameters of the Piezo-stage. As hardware to drive the Piezo-stage *dSpace<sup>TM</sup> 1103* is used and coded in the C language using the libraries provided by the software. The closed loop performance of the Piezo stage was investigated while using the overall structure as shown in Figure 4.10 by applying several input references.

Table 4.1: Properties Of Piezo-Stage

Symbol	Quantity	Value in SI
$m_p$	Nominal Mass	$1.5 \times 10^{-3} Kg$
$c_p$	Nominal Damping	$220 \frac{Ns}{m}$
$k_p$	Nominal Stiffness	$300000 \frac{N}{m}$
$f_r$	Resonant Frequency	$350 Hz$
$T_{em}$	Transformation Ratio	$0.3 \frac{N}{V}$

In order to verify the performance of discrete time sliding mode controller along with the disturbance observer, smooth step inputs are given to one of the piezo stages and responses were drawn in Figure 4.11, 4.12 and 4.13 which represents the smooth step response for position reference of  $100nm$ ,  $50nm$  and  $5nm$  respectively. The rise times and steady state errors are  $30 ms$ ,  $23 ms$ , and  $22.5 ms$ ; and 1%, 2%, and 8%, for 100, 50 and 5 nanometer step inputs, respectively. An overshoot behavior is not observed in any of these tested cases. Operation with no overshoot is the foremost requirement for micromanipulation applications since overshoot may result damage to the probe or micro-object. However, the system suffers from noise coming from the measurement devices, which shows up in the steady state plots.

Figure 4.14 represents the response for trapezoidal input with a height of  $0.5 \mu m$ . The result shows that it precisely follows the reference and tracking error are found to be less than  $\pm 10 nm$ . Figure 4.15 and Figure 4.16 demonstrates the position

response for sinusoidal input with an amplitude of  $1\mu m$  and  $10\mu m$  respectively with a frequency  $1Hz$ . It can be clearly observed that the actual position tracks the reference with high accuracy and the tracking error is found to be within  $\pm 20 nm$  and  $\pm 0.4\mu m$ . These experimental results suggests that the proposed controller along with the disturbance observer produces acceptable results for positioning with very high-precision.

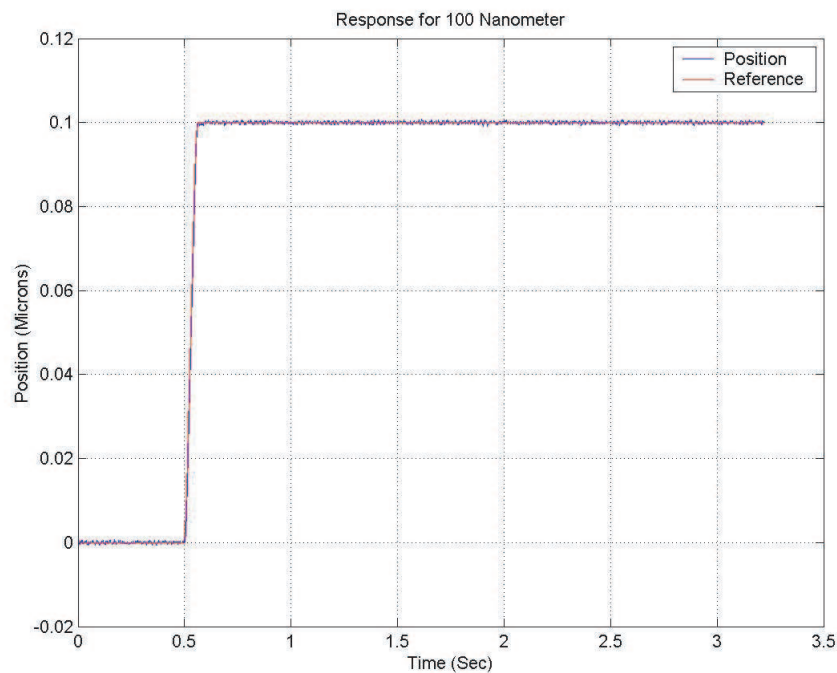


Figure 4.11: Position response for a reference of  $100nm$  [8]

### 4.3 Motion Control of Linear drives

In many micromanipulation applications, it is desirable for the actuators to possess a long travel range as well as high accuracy of the motion, and linear drives provide the best option to fulfill the goal. For high precision control it becomes mandatory to control the shaft of the linear drive to a varying reference angle with high accuracy in spite of the high disturbance present in the system mostly dominated by the highly disturbance component. In case of the multidimensional motion of a linear drive it becomes inevitable to compensate the effect of friction in order to accurately place

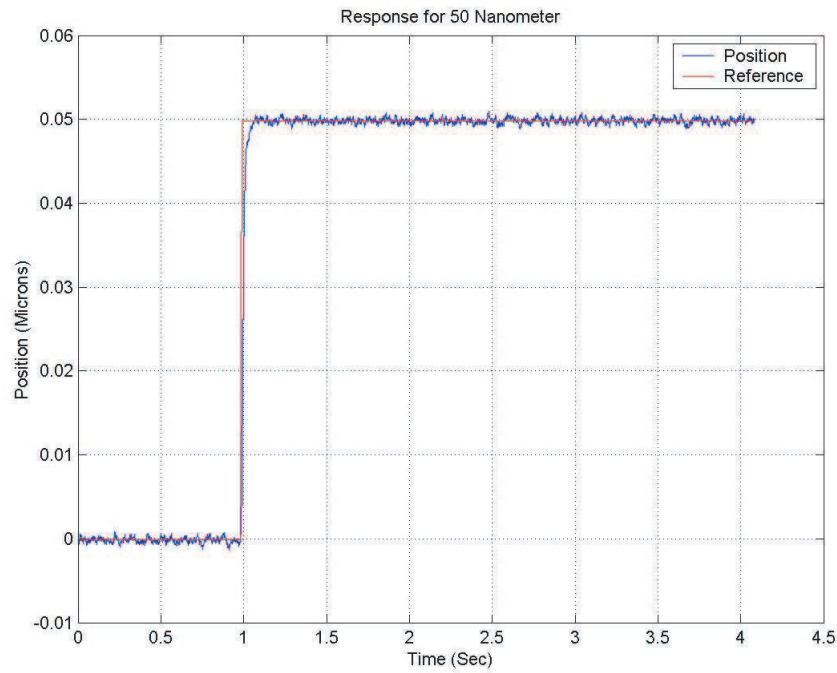


Figure 4.12: Position response for a reference of  $50nm$  [8]

the end effectors of the system in the desired location as well as desired dynamics.

The most dominant disturbance which hinders the precise positioning and the dynamics is due to frictional part which is highly non-linear in nature. Thus there is immense need to remove the frictional part present in the system and to come out with a robust controller in order to achieve a high accuracy and desired dynamics. In the literature many methods are proposed in order to compensate for the disturbance, Yang and Tomizuka [57] compensated the friction component by adaptively changing the frequency of the control input, Tung et al. [58] compensated the friction with a repetitive control scheme. Rao et al [59] have proposed a friction observer and disturbance observer. Pan [60] used a PID controller using a defined model [61] for angular positioning. Apart from these, many recent approaches fuzzy control [62] and learning control [63] can be found on the literature. In all the approaches the frictional model imposes destabilizing effects in the low velocities. The above approaches did not take the hysteretic behavior when studying friction for non stationary velocities nor variation in the break-away force with the experimental conditions nor small displacement that occur at the contact interface during



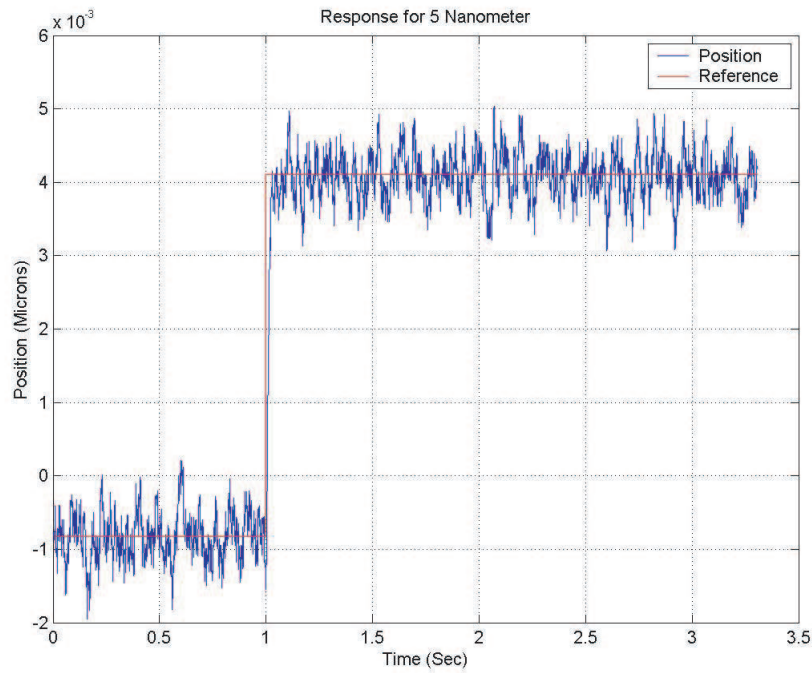


Figure 4.13: Position response for a reference of  $5nm$  [8]

stiction.

In this section a dynamic friction model [64] is implemented which describes the stiction behavior along with coulombs friction, viscous friction, and stribek effect. This section also describes the implementation of variable structure control for continuous system with discrete-time implementation of the control algorithm by maintaining sliding mode as discussed in previous section. A considerable amount of work has been done for analyzing discrete-time sliding modes [65]. Most of the proposed control strategies uses, in one or another way, the calculation or estimation of the discrete-time equivalent control explicitly, which requires the transformation of the plant model into a discrete-time form.

### 4.3.1 Canudas Frictional Model

In most of the cases disturbance acting on the plant is considered as smooth disturbance but for friction the smoothness of the disturbance  $d_k$  is lost in the vicinity of zero velocity hence the tracking error may be large due to  $|d_k - d_{k-1}|$ , may be large in this region e.g. zero-velocity crossing,  $d_k$  and  $d_{k-1}$  have opposite signs.

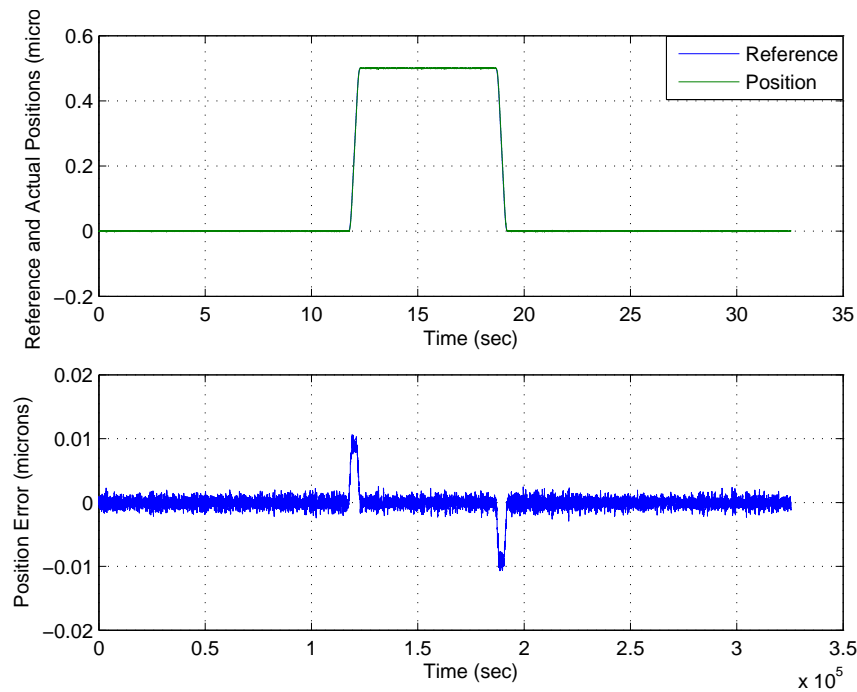


Figure 4.14: Position response for a trapezoidal reference for  $0.5 \mu$

Clearly, the amplitude of the tracking error depends on the difference in friction amplitude between two sampling values. It is a well established fact that friction cannot be described by a pure discontinuity at zero velocity, instead friction is a continuous function of time with complicated and fast dynamics around the zero velocity. Therefore the difference in friction values between two successive sampling instances is made smaller by selecting a smaller time period, which reduces the friction estimated error and the following tracking error during zero-velocity crossing is also reduced. The obvious solution is to decrease the sampling period as the friction becomes more “discontinuous”. However, as sampling time  $T \rightarrow 0$ , the control signal saturates  $\pm u_{sat}$  and due to the saturation the  $u_k$  will actually chatter with amplitude of  $u_{min} \leq sat(\cdot) \leq u_{max}$ , which is unacceptable as it may excite the high frequency modes in the system.

In order to cope up with the above written problem, the dynamic friction model proposed by Canudas de Wit [64] is used as a friction acting on the system. The advantage for selecting this model is because it inherits most of the frictional phenomena that gives rise to control problem such as stick-slip behavior as explained above. The observer for the frictional model is expressed as,

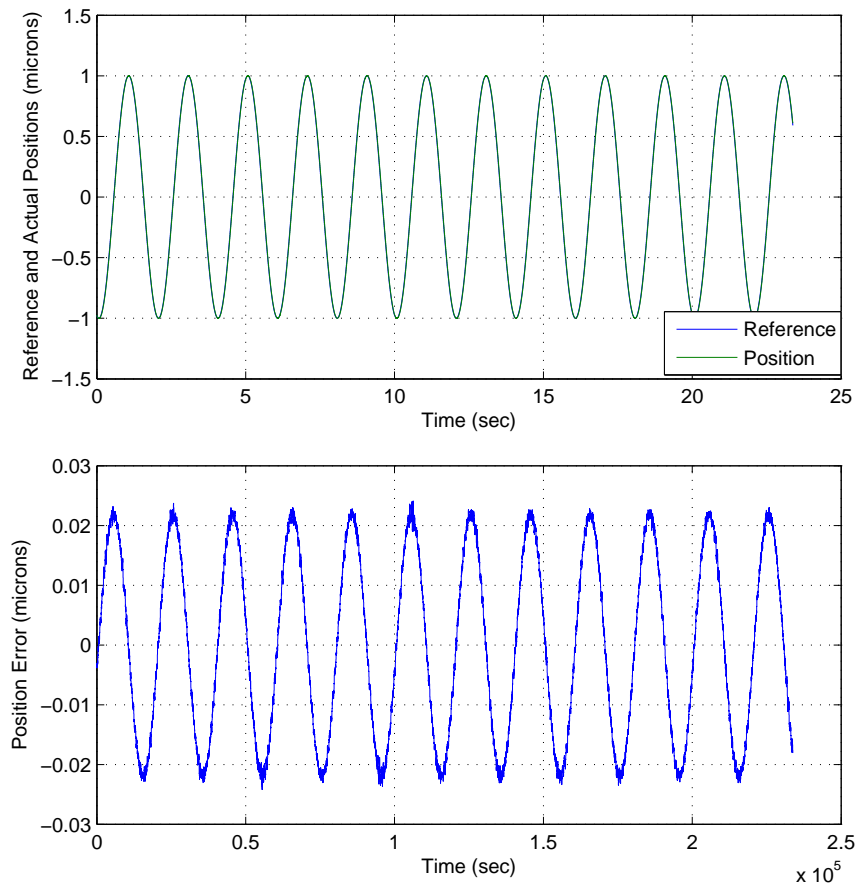


Figure 4.15: Position response for a sinusoidal reference for  $1\mu m$  amplitude

$$\hat{F} = \sigma_0 \hat{z} + \sigma_1 \frac{d\hat{z}}{dt} + \sigma_2 v$$

Where  $\frac{dz}{dt}$  and  $\sigma_0 g(v)$  is represented as,

$$\begin{aligned} \frac{d\hat{z}}{dt} &= v - |v| \frac{\hat{z}}{g(v)} - ke \\ \sigma_0 g(v) &= F_c + (F_s - F_c) e^{-\left(\frac{v}{v_s}\right)^2} \end{aligned} \quad (4.3.1)$$

Where  $F_s$  denotes the static friction level,  $F_c$  is the level of Coulomb force and  $v_s$  is the stribek velocity.  $\sigma_0$ ,  $\sigma_1$  and  $\sigma_2$  represents stiffness, damping co-efficient and viscous friction co-efficient respectively.  $e$  denotes the position error and the term  $k$  is a correction term for the position error. The closed loop system block diagram is shown in Figure 4.17.

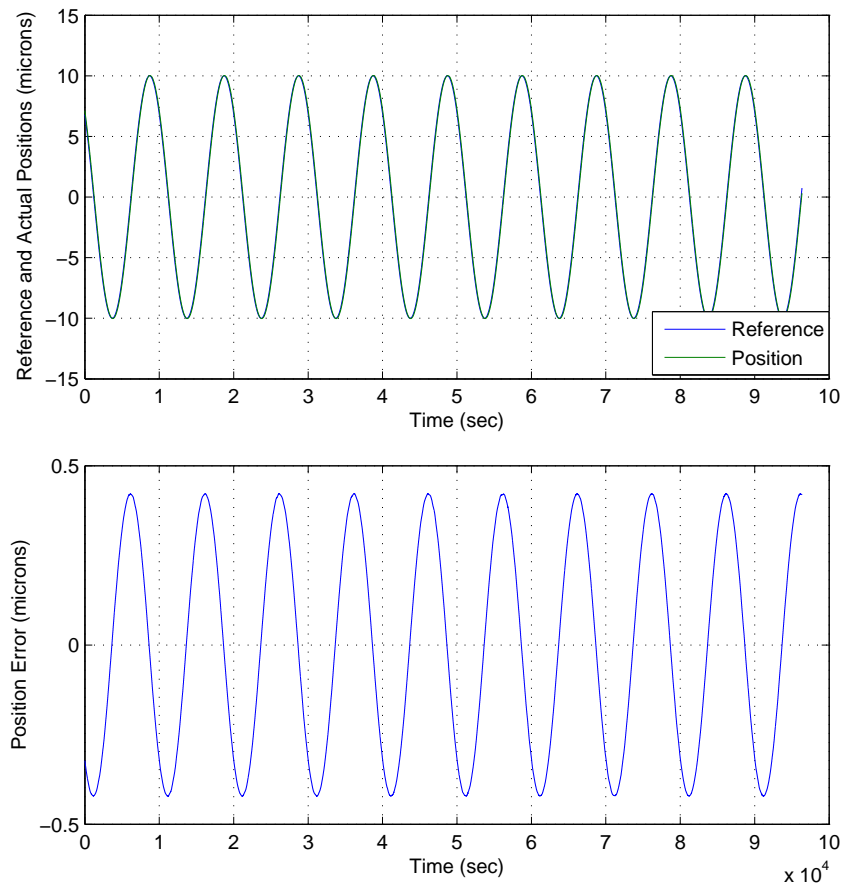


Figure 4.16: Position response for a sinusoidal reference for  $10\mu m$  amplitude

### 4.3.2 Experimental Description

In order to validate the frictional model, a linear drive system equipped with DC servo from PI *Physik Instrumente*<sup>TM</sup> model M-415.DG has been utilized, which uses closed loop DC motor with shaft mounted position encoders and backlash-free gear heads. Two such linear drive systems were used for the x-y stage motion as shown in the Figure 4.18 and Table 4.2 describes the parameters of the linear drives. The block diagram of the experimental setup is represented in Figure 4.19. According to the motor specification the design resolution of the linear drive is  $0.0085\mu m$ , which means theoretical minimum movement that can be achieved based on the selection of the mechanical drive components (drive screw, gear ratio, angular motor position etc). Design resolution is much higher than the practical position resolution or minimum incremental motion. Thus using a robust discrete time SMC controller as discussed in previous section and frictional compensation a high accurate system

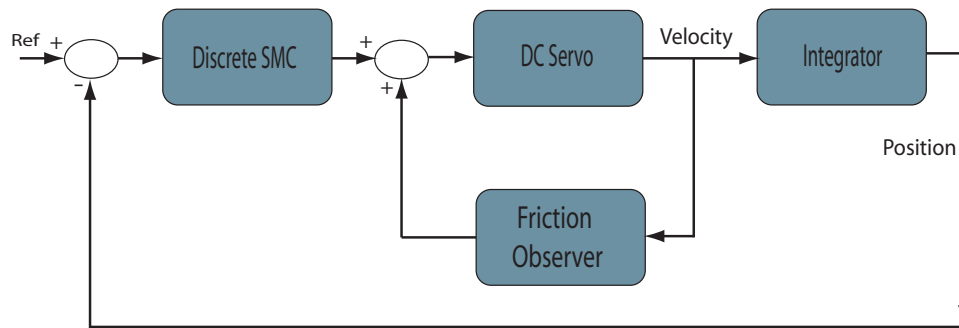


Figure 4.17: Block diagram of the closed loop system with friction observer

Table 4.2: Parameters of The Linear Drive

<b>Motor Voltage</b>	12 V	<b><math>J</math> (Moment of Inertia)</b>	$2.1992e^{-7} Nm/A$
<b>Motor Power</b>	3 W	<b><math>K_t</math> (Torque constant)</b>	$0.0133908 Nm/A$
<b>Encoder Resolution</b>	2000 counts/rev	<b><math>B</math> (Friction constant)</b>	$0.00012002 Nm$
<b>Gear Head Ratio</b>	29.641975309 : 1	<b>Travel Range</b>	150 mm
<b>Lead-Screw Pitch</b>	0.5 mm/r	<b>Design Resolution</b>	$0.0085 \mu m$

along with the desired dynamics is achieved in the vicinity of the design resolution without any stick slip motion which arises from the disturbance due to friction.

The parameters for the Canudas friction model is tuned as shown in Table 4.3 to achieve high-precision motion without any stick-slip motion due to frictional component.

Table 4.3: Parameters of the frictional observer

$\sigma_0$	100000 N/m	$v_s$	0.001 m/s
$\sigma_1$	316.2277 Ns/m	$T(\text{SampleTime})$	0.0001 s
$\sigma_2$	0.4 Ns/m	$k$	0.0001
$F_c$	1 N	$F_s$	1.5 N

Figure 4.20 represents the experimental results for two consecutive smooth response of less than  $1 \mu m$  with the implementation of the frictional observer and it is seen that it tracks the reference position and the dynamics very accurately. Figure 4.21 represents the experimental result of circular path of radius of  $1 \mu m$  followed by the X and Y axis of the linear drive and the result indicates that it follows the

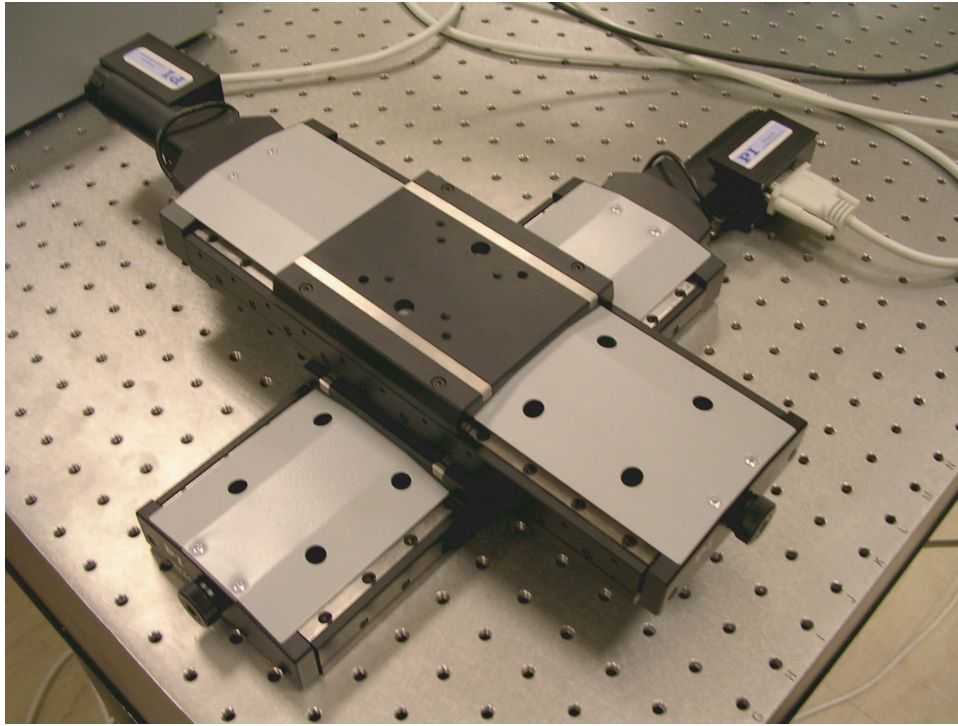


Figure 4.18: X-Y stages of linear drive

trajectory very accurately but suffers from vibration at some point.

## 4.4 Conclusion

In this chapter, high precision motion control for micromanipulation application using open-loop piezoelectric actuator, closed-loop piezoelectric actuator and linear drives is demonstrated. Open-loop piezoelectric actuator are utilized to achieve high precision motion by canceling the hysteresis effect using a well established model in feed-forward fashion. Experimental results are shown to prove the minimization of hysteresis effect. Discrete-time sliding mode controller along with the disturbance observer is utilized for closed-loop piezoelectric actuator in order to achieve closed loop motion with nanometers accuracy. Finally, linear drive mechanism is driven by sliding mode controller along with the friction observer to minimize the effect of friction around the vicinity of zero-velocity. Experimental results are demonstrated with micrometer resolution motion for the X-Y axes linear drives.

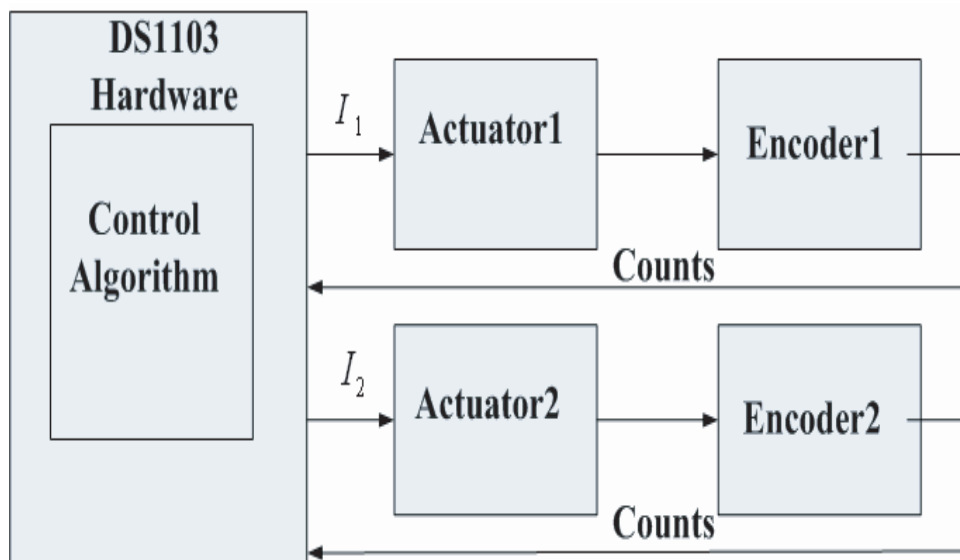


Figure 4.19: Block diagram of the system with two linear axes driven by dSpace1103

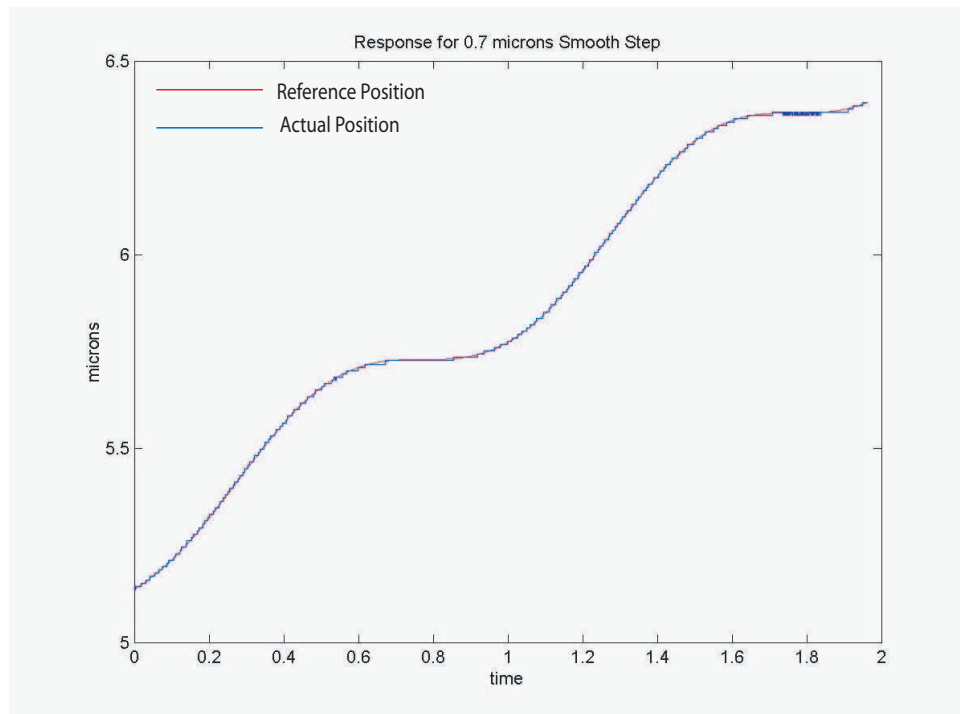


Figure 4.20: Response of two consecutive smooth steps of less than  $1 \mu\text{m}$  for a single axis

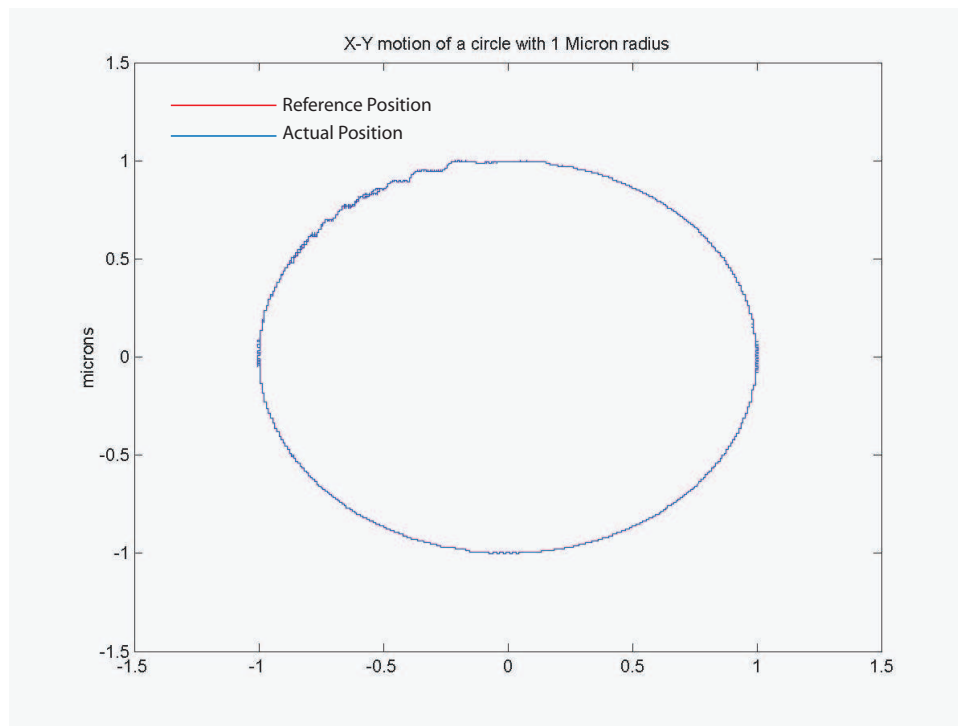


Figure 4.21: Experimental results for circular motion of two axes of radius  $1 \mu m$



# Chapter 5

## Bilateral Control in Micromanipulation

In this chapter implementation of scaled bilateral control in a custom built tele-micromanipulation setup is presented. Force sensing with  $nN$  resolution using piezoresistive AFM (Atomic Force Microscope) micro-cantilever is demonstrated and validated with the theoretical estimates. Force/position tracking and transparency between the master and the slave is presented with varying references after necessary scaling.

### 5.1 Force Sensing Using Piezoresistive AFM Cantilever

In order to achieve force transparency between master and slave, it's necessary to sense the force in nano-newton range with high accuracy. Many researchers have used different ways for sensing or estimating force using PZT actuator [7], Capacitive sensors, optical deflection as in AFM scheme, tunneling as in STM etc. In complex micro-manipulation applications, it may be necessary to utilize more than one manipulator thus using optical detection mechanism as like AFM may become very cumbersome process and complicate to integrate in the system. Thus there is a need to utilize inbuilt force sensors integrated in the probe or the manipulator.

Piezoresistive AFM cantilever with inbuilt Wheatstone bridge from *Applied Nanostructures* is utilized as a force sensor as well as probe for pushing operation as shown in Figure 5.1. Piezoresistive sensors have been used for many other MEMS applications, including accelerometers, gyroscopes and AFM cantilevers. The primary advantage of this approach is that the sensor impedance is relatively low (a few  $K\Omega$ ), and it is possible to extract small signals without interference from noise with off-chip integrated circuits.

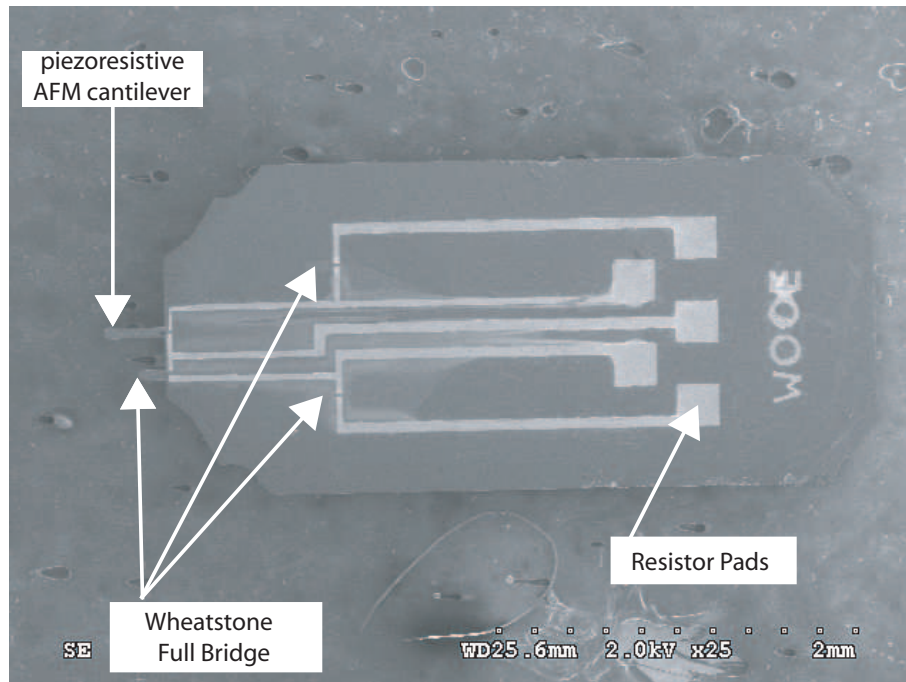


Figure 5.1: Piezoresistive AFM Cantilever with inbuilt Wheatstone bridge

The working principle of force sensing is demonstrated in Figure 5.2. As the force is applied at the free end of the cantilever using the PZT actuator with the glass slide, the change of resistance takes place depending on deflection of the cantilever. The amount of deflection is measured by the inbuilt Wheatstone bridge providing a voltage output, which is amplified by the custom built amplifier. To match with the initial cantilever resistance value, one of the active resistors in the full bridge is replaced by a potentiometer. The amplified voltage is sent to the data acquisition *dSpace1103* card for further processing.

The force is calculated using Hooke's law as Eqn.5.1.1.

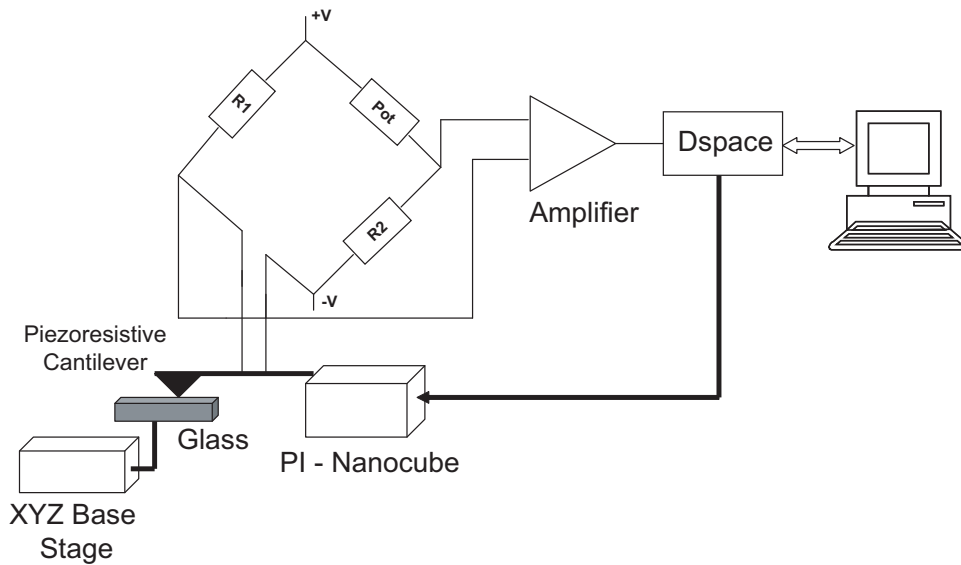


Figure 5.2: Force measurement setup

$$F = K_c z \quad (5.1.1)$$

where  $K_c$  is the known spring constant of  $0.3603 \text{ N/m}$  and  $z$  is the amount of cantilever deflection. The spring constant is calculated by considering a linear beam equation and verified via a natural frequency test using an AFM [66].

### 5.1.1 Modeling of the AFM Cantilever

The piezoresistive AFM cantilever is modeled as linear beam equation as represented in Eqn.(5.1.2).

$$K = \frac{3EI}{L^3} \quad (5.1.2)$$

where  $E$  represents the modulus of elasticity ( $190 \text{ GPa}$  for silicon),  $L$  represents the length of the cantilever ( $300 \mu\text{m}$ ) and  $I$  represent the moment of inertia calculated as Eqn.(5.1.3).

$$I = \frac{bh^3}{12} \quad (5.1.3)$$

where  $b$  and  $h$  represents the width and height of the microcantilever which is  $50 \mu\text{m}$  and  $1.6 \mu\text{m}$  respectively and the calculated value of inertia is  $17.067 \times 10^{-24} \text{ m}^4$ .

### 5.1.2 Experimental Validation of Force Sensing

The cantilever is mounted on the three axes closed loop stage and the interaction (contact and non-contact) forces between the tip and glass slide are measured. The position of the cantilever is selected to be perpendicular to the plane of the optical axis in order to achieve better visibility of the distance between the cantilever and the glass slide. Since the displacement range of the x-axis of the closed loop stage is  $100\ \mu m$ , the glass slide is brought within the range using open-loop manual PZT axes. Finally, the change of the resistance is converted to change in voltage (millivolt range) using the inbuilt full bridge along with offset potentiometer, which in turn is converted to  $\pm 10V$  ranges using the amplifier.

Figure 5.3 and Figure 5.4 [67], [68] represents the attractive forces for pulling in and in-out phase respectively between the tip and glass slide. The decreasing distance between the tip and glass slides is represented by the increase in the position of PZT axis. As the distance between the tip and glass slide decreases the attractive forces increases and vice-versa. Electrostatic force is inversely proportional with the square of the separation distance but Van der Waals depends with sixth root. Thus it can be clearly stated that during initial phase of pulling in/out electrostatic force will be dominant and has lower slope as compared to Van der Waals. This can be clearly seen as change in slope of the force measurement plot corresponding to these two regions can be observed from Figure 5.3 and Figure 5.4.

In order to verify force measurement, theoretical values of pull-off force (breaking load during the withdrawal of tip) between the silicon tip and the glass surface is compared with the experimental results. In case of the interaction between a spherical tip and a flat surface, the interaction force can be approximated by Dugdale model [69] as Eqn.(5.1.4)

$$F_{pull-off} = \left( \frac{7}{4} - \frac{1}{4} \frac{4.04\lambda^{\frac{1}{4}} - 1}{4.04\lambda^{\frac{1}{4}} + 1} \right) \pi W R \quad (5.1.4)$$

where  $W$  is the work of adhesion between the two mediums,  $R$  is the radius of the sphere and  $\lambda$  is a coefficient, which can be used to choose the most appropriate contact model for a given case [70]. Using the interfacial energy the pull-off force

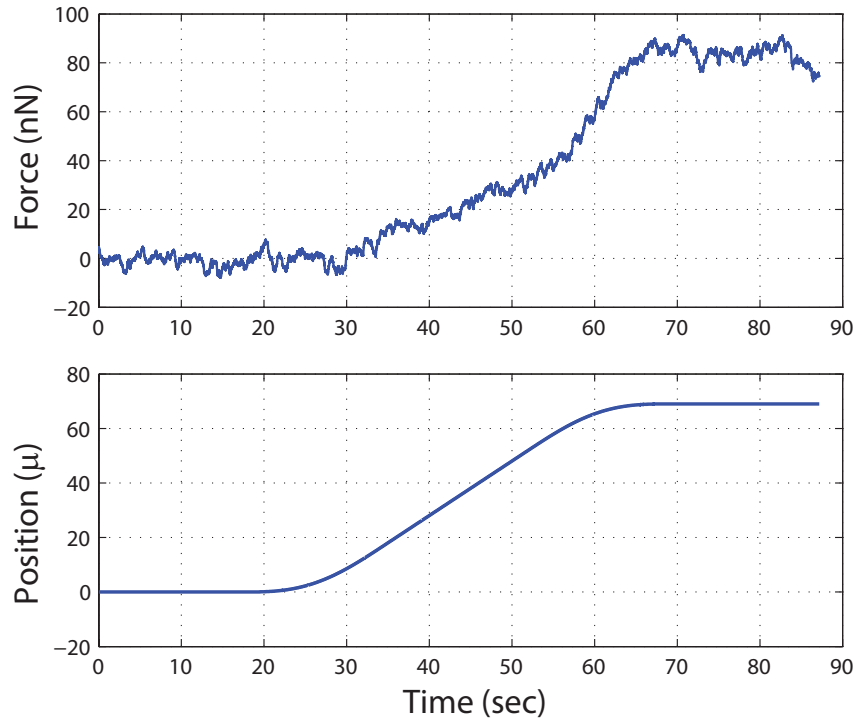


Figure 5.3: Force for smooth step position reference.

can be calculated for  $\lambda = 0.54$  according to the Dugdale model as  $39.43 \text{ nN}$  [71, 72]. Figure 5.5 demonstrates that experimentally determined pull-off force is close to  $40 \text{ nN}$ , indicating a close match between the theoretically and experimentally determined values.

## 5.2 Implementation of Scaled Bilateral Teleoperation

In the micromanipulation applications, scaled bilateral control is used for teleoperation where master/human is not able to access the micro environment on the slave side. Since the master and slave are working on macro and micro scales respectively, thus its indispensable to use general bilateral controller to scale the position and forces between two sides for extensive capability. In other words, position information from the master is scaled down to slave and force information from the slave side is scaled up to master.

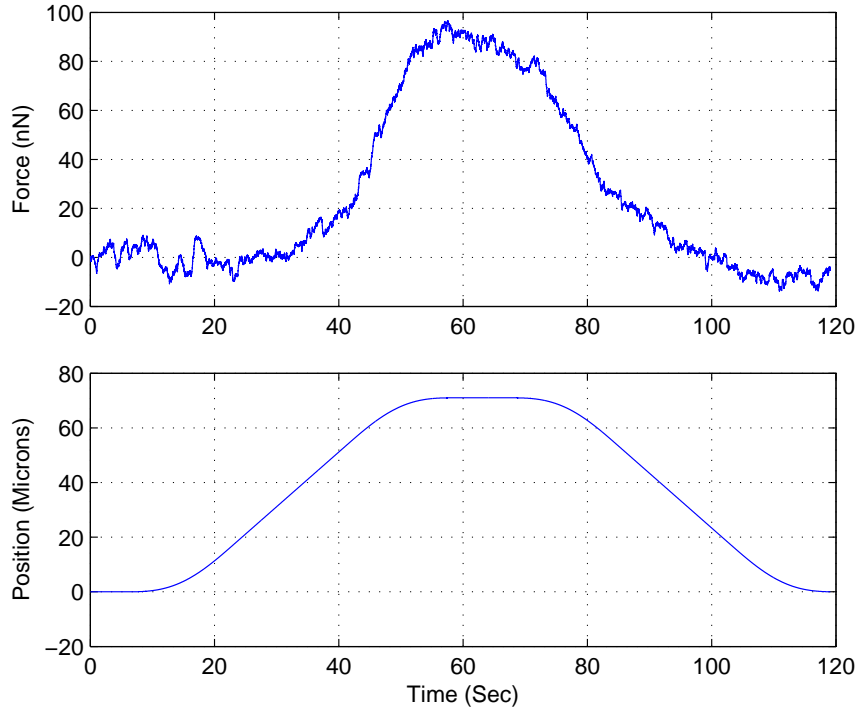


Figure 5.4: Pulling in-out for smooth step position references

### 5.2.1 Schematic of Bilateral Control Structure

The scaled bilateral control structure is shown in Figure 5.6 comprising of master and slave side. Piezo-stage on the slave side is required to track master's position as dictated by operator using discrete sliding mode controller structure as discussed in Chapter 4. The  $1D$  force of interaction with environment, generated by piezoresistive cantilever, on the slave side is transferred to the master as a force opposing its motion, therefore causing a “feeling” of the environment by the operator. The conformity of this feeling with the real forces is called the “transparency”. Transparency is crucial for micro/nanomanipulation application for stability of the overall system. Furthermore, for micro system applications, position and forces should be scaled in order to adjust to operator requirements. Position of the master manipulator, scaled by a factor  $\alpha$ , is used as a position reference for the slave manipulator, while the calculated force due to contact with environment, scaled by a factor  $\beta$ , is fed-back to the operator through the master manipulator. As a master device Maxon DC servo is utilized along with the driver and the technical specification is mentioned in Appendix A.4 and A.5 respectively.

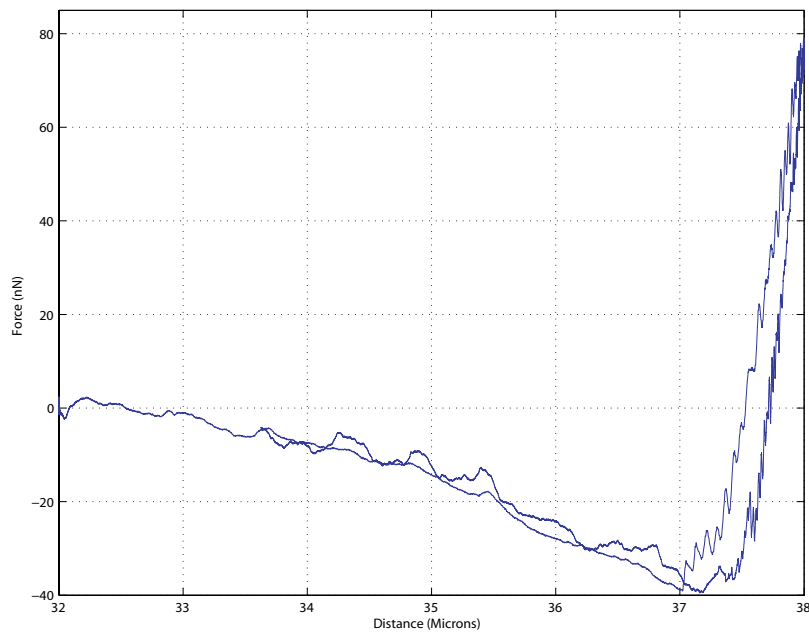


Figure 5.5: Force curve for interaction between a silicon tip and a glass surface

In order to eliminate oscillations both on master side because of oscillatory human hand and on the slave side due to piezoresistive cantilever dynamics, position of master manipulator and force of slave manipulator are filtered by low pass filters before scaling.

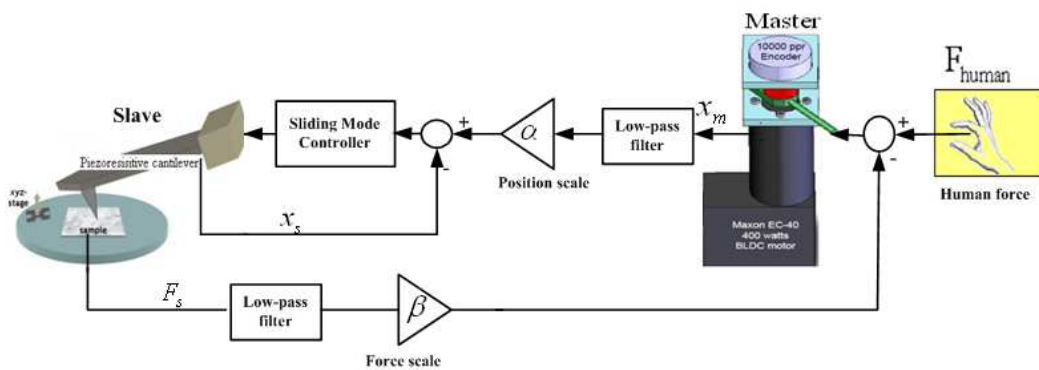


Figure 5.6: Scaled bilateral teleoperation control structure

### 5.2.2 Scaling of the Position and Force Information

Since the master and slave side resides on macro and micro scales respectively, thus its very vital to appropriately choose the scaling factor in order to attain the optimum performance. In the ideal condition, the steady state condition of the bilateral controller should be Eqn.(5.2.1).

$$\begin{aligned}x_s &= \alpha x_m \\ F_m &= \beta F_s\end{aligned}\tag{5.2.1}$$

Where  $\alpha$  and  $\beta$  represents the position and force scaling respectively.  $x_m, x_s$  denotes the master and slave position respectively and  $F_m, F_s$  denotes the master and slave force respectively. To be able to meaningfully interact with the micro environment, positions and forces are scaled to match the operator requirements.

In the first and second experiments, scaling factors of  $\alpha = 0.027 \frac{\mu m}{deg}$  and  $\beta = 0.00366 \frac{N}{nN}$  are used, that is an angular displacement of  $1deg$  on the master side corresponds to a linear displacement of  $1\mu m$  on the slave side and a force of  $0.00366nN$  on the slave side corresponds to a force of  $1N$  on the master side. The objective of these experiments is to provide very fine motion on the slave side for a relatively larger displacement on the master side, hence  $\alpha$  is selected according to this objective. Then the corresponding forces/torques for each amount of displacement were compared for the selection of  $\beta$ , keeping in mind that the DC motor on the master side has low torques.

### 5.2.3 Experimental Validation of Position Tracking

In order to validate the position tracking between the master and slave, the commanded position from the master is transferred after necessary scaling to be tracked by the slave side. Figure 5.7, 5.8, 5.9, 5.10 illustrates the experimental results for position tracking along with the tracking error of the bilateral controller. It can be clearly seen that under different references, the slave tracks the master position with high accuracy. This position tracking performance is acceptable for precisely positioning the micro cantilever.



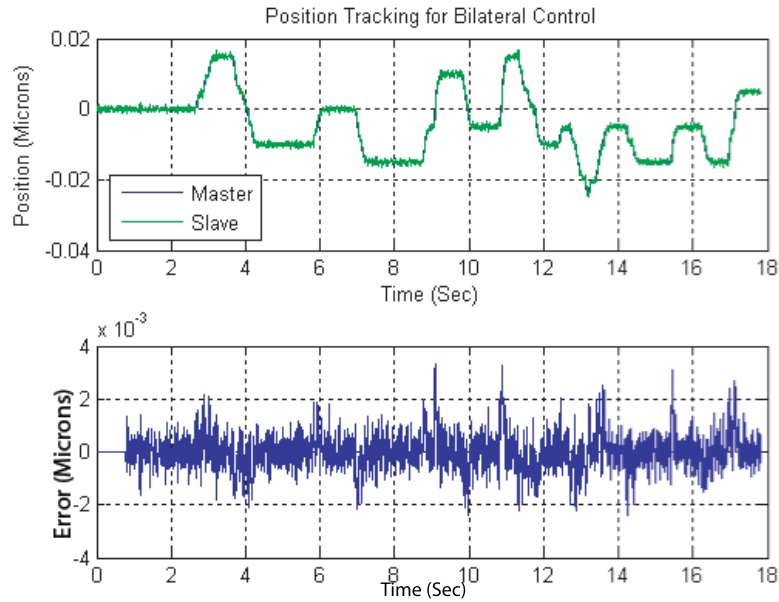


Figure 5.7: Position Tracking of the Bilateral Controller for zig-zag motion with amplitude  $20nm$

#### 5.2.4 Experimental Validation of Force Tracking

In order to validate the force tracking, the slave forces encountered from the environment is being transferred to the master side after necessary scaling. Figure 5.11, 5.12, 5.13 demonstrates the force tracking between the master and slave along with the tracking error. It can be clearly observed from the three figures that the master tracks the slave force precisely and tracking error is found to be within  $\pm 20nN$ .

### 5.3 Conclusion

In this Chapter, Piezoresistive cantilever is utilized along with a full bridge in order to achieve the nano-Newton level interaction forces between piezoresistive probe tip and a glass surface. Experimental results are compared to the theoretical estimates of the change in attractive forces as a function of decreasing distance and of the pull off force between a silicon tip and a glass surface, respectively. Good agreement among the experimental data and the theoretical estimates has been demonstrated.

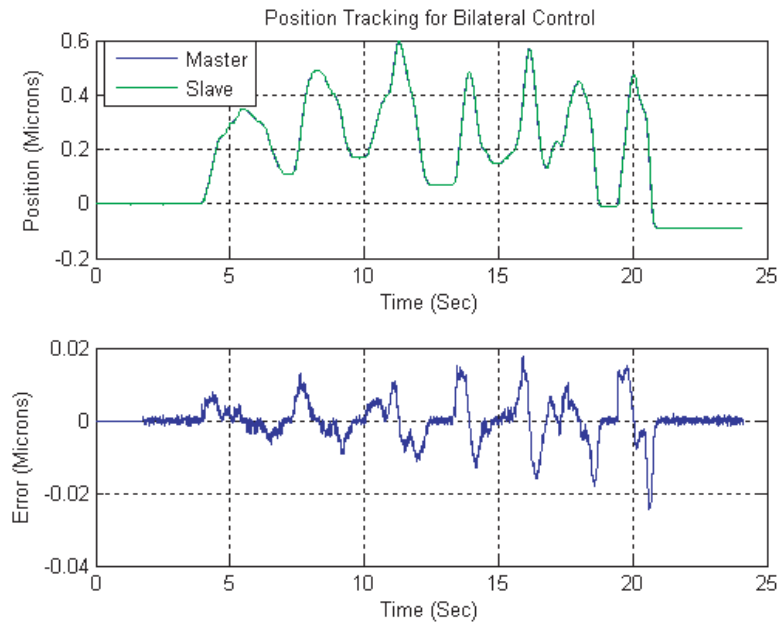


Figure 5.8: Position Tracking of the Bilateral Controller for random motion with amplitude  $0.6 \mu m$

Force/Position tracking between master and slave has been clearly demonstrated after necessary scaling. It is clearly demonstrated that the slave position tracks the master position with high precision using discrete time sliding mode controller as discussed in chapter 4 structure along with disturbance observer yield, which is necessary for micromanipulation applications. The master feels the interaction forces between the slave and environment in one dimension. Force tracking also confirms the transparency between the master and slave which is an essential requirement to conduct the task effectively.

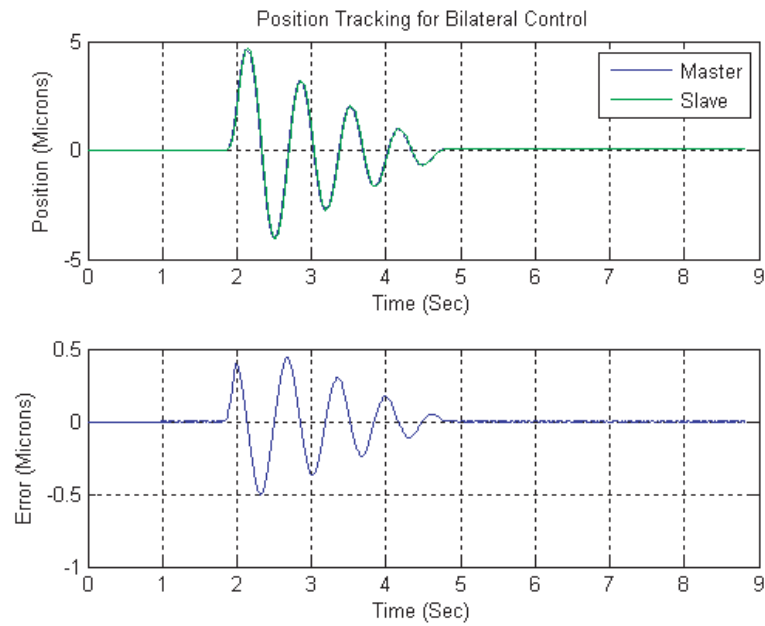


Figure 5.9: Position Tracking of the Bilateral Controller for sinusoidal reference with amplitude  $5 \mu m$

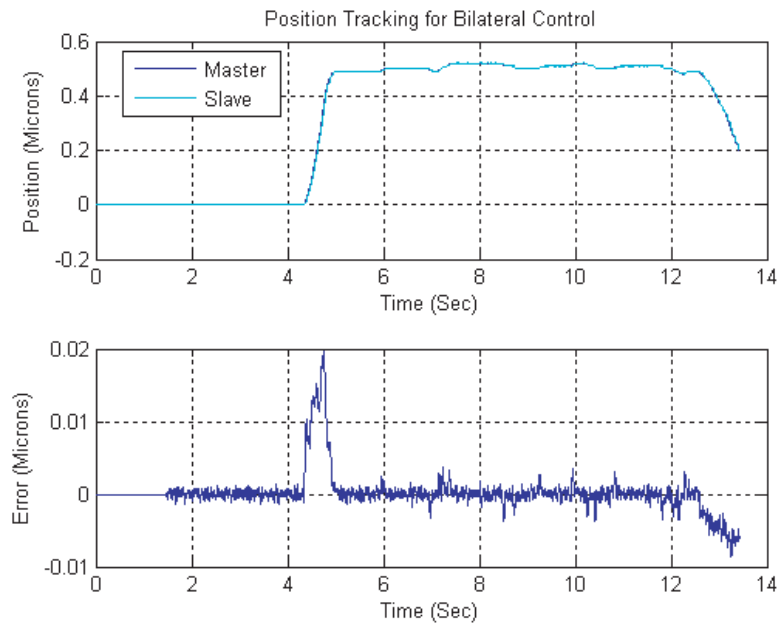


Figure 5.10: Position Tracking of the Bilateral Controller for step motion with amplitude  $0.5 \mu m$

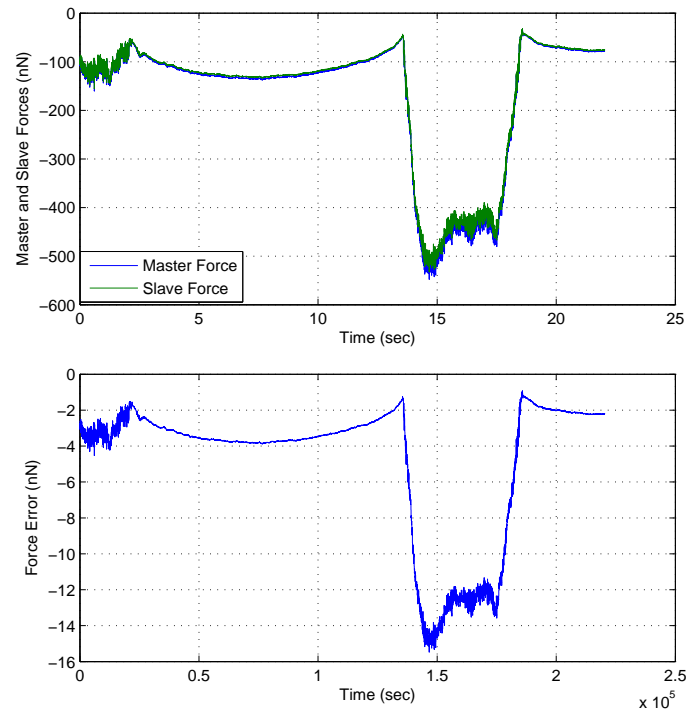


Figure 5.11: Force tracking of the bilateral controller and tracking error

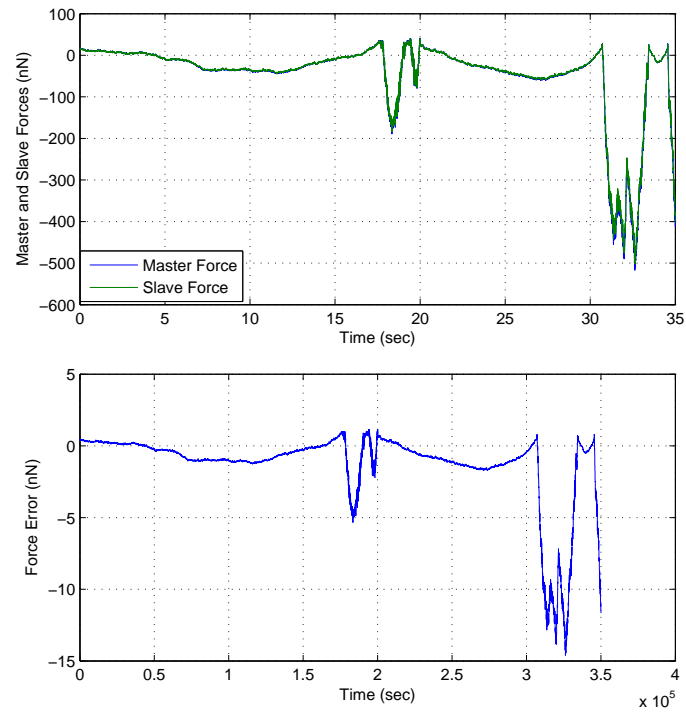


Figure 5.12: Force tracking of the bilateral controller and tracking error

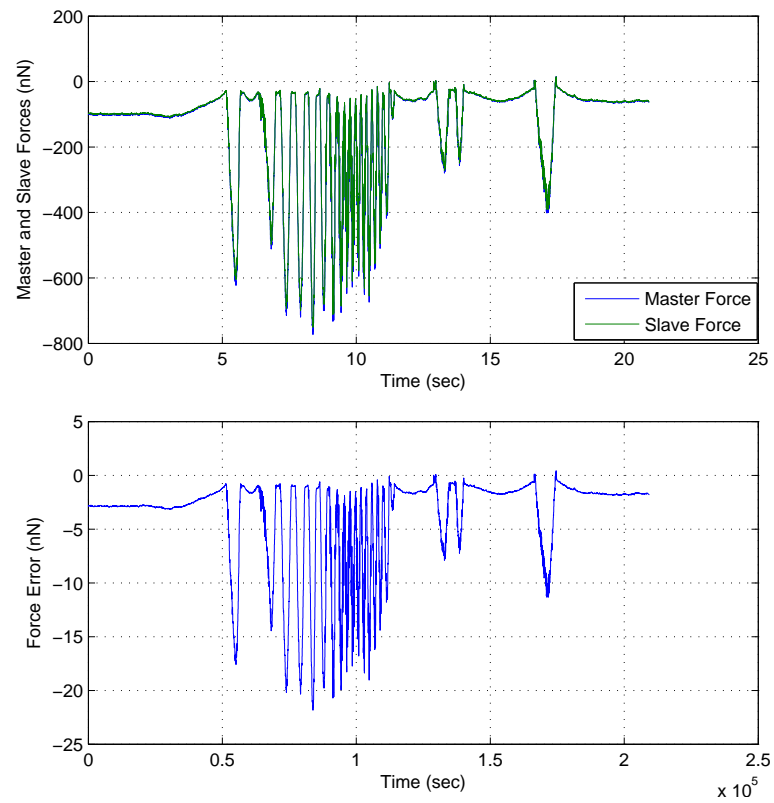


Figure 5.13: Force tracking of the bilateral controller and tracking error

# Chapter 6

## Semi-Automated Pushing of Micro Object

In this chapter, a method for pushing polygonal micro objects using hybrid force-position controller is proposed. The pushing task is accomplished through semi-autonomous fashion. In the semi-autonomous process, velocity controlled pushing with force feedback is realized along x-axis by the human operator with the aid of visual display and velocity control along y-axis is undertaken automatically using visual feedback. Visual feedback control is utilized to track the micro object and generate the necessary velocity so that the resultant velocity vector passes through the center of friction of the micro-object to achieve pure translation motion. Since the location of the center of friction in the micro-world is subjected to unpredictable changes with respect to time, thus an procedure is demonstrated for online estimation for the location of center of friction.

### 6.0.1 Introduction

It is a well established fact that human operators are much more adaptable to force changes and can react much effectively under unexpected situations as compared with other robotic manipulators. In other words, human operator can perform force control and motion operation much more skillfully, thus human intervention can be employed in pushing of the micro-object. The whole process of pushing of

micro-object can be divided into two concurrent process: in one process pushing is performed by human operator which acts as a impedance controller and alters the velocity of the pusher while in contact with the micro-object. In another process, the desired line of pushing for the micro-object is achieved through visual feedback procedures in one dimension to attain the desired trajectory for the motion of the micro-object. In this thesis, a hybrid force/position control structure is adopted for semi-automated pushing of micro-objects.

## 6.0.2 Problem Definition

The scheme [73] of semi-automated pushing of micro-objects is illustrated in Figure 6.1. A hybrid force-position controller is proposed in which the proper velocity direction of the micro cantilever is performed through visual feedback procedures to achieve pure translational motion of the micro-object while pushing is administered by a human operator with the aid of visual display.

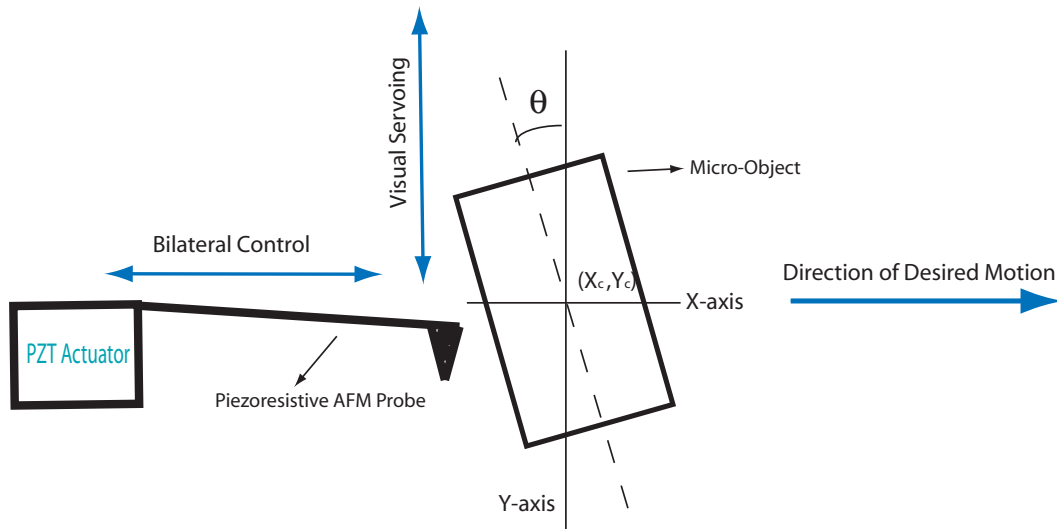


Figure 6.1: Semi-automated pushing scheme

Figure 6.1 presents an illustration of the pushing problem where  $\theta$  represents angle between the Y-axis and the image axes, and  $X_c$  and  $Y_c$  denotes center of the rectangular object. To achieve pure translation along the X-axis, that is to keep the angle  $\theta$  close to zero, the velocity of micro cantilever needs to be automatically adjusted to pass through center of friction while human operator pushes the object through

scaled bilateral teleoperation as demonstrated in Chapter 5.

The velocity control of the micro cantilever is critical during planar pushing to ensure that the object tracks the desired straight line trajectory with desired zero-angle orientation. In order to achieve pure translation motion, the proper line of action of the pushing force needs to be determined with the help of feedback gathered through image processing techniques and force feedback from the piezoresistive force sensor. Once the position and orientation of the micro-object is determined along with the sensed force, proper vector of the micro cantilever and its components along the Y-axis can to be calculated to compensate for the orientation error of the object.

### 6.0.3 Proposed Approach - Hybrid Force-Position Control

The overall mechanism for hybrid force-position control structure for semi-automated pushing of micro-objects is depicted in Figure 6.2.

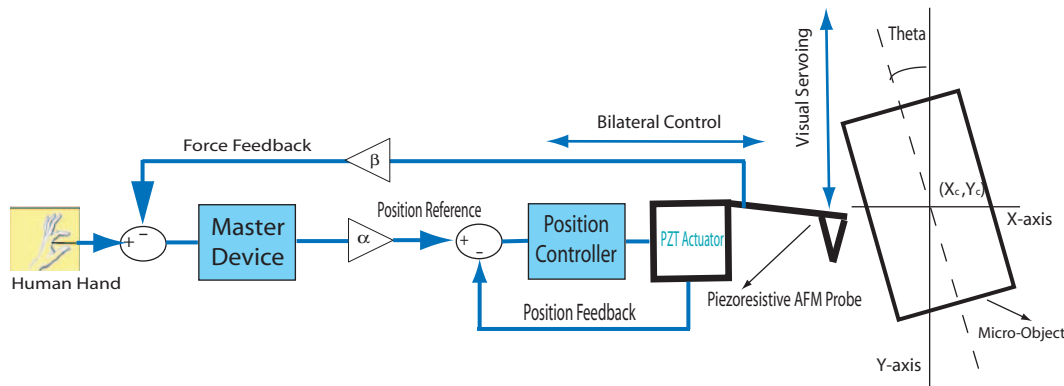


Figure 6.2: Hybrid control structure for semi-automated pushing

Human operator utilizes the scaled bilateral control structure as demonstrated in Chapter 5 to generate the desired position which is scaled with a factor  $\alpha$  before feeding to the position controller. The position controller uses the feedback from PZT actuator to compensate the position error to achieve the desired position of the piezoresistive micro-cantilever. As the micro-cantilever comes in contact with the micro-object the interaction resultant forces are felt by the human operator through the force fed from the piezoresistive micro-cantilever after scaling by a factor of  $\beta$ . Depending upon the situation human operator which acts an impedance controller



can adjust the impedance (effective muscle stiffness) to change from position control to force control to push that micro-object along X-axes with the commanded position/force. Moreover, the operator has the access to the visual information for monitoring the pushing process. Visual feedback procedures is performed automatically to estimate the correct line of pushing to achieve pure translational motion. Visual processing algorithms are employed to detect position and orientation of the micro-object for the estimation of the location of the center of friction. Finally, the velocity of the piezoresistive cantilever is varied at the contact point using visual feedback process to ensure that resultant line of pushing passes through the center of friction to achieve pure translation motion along the X-axes.

#### 6.0.4 Pushing Mechanism

Precise positioning of micro-objects lying on a substrate using a point contact pushing to track a desired trajectory poses lot of challenges. The pusher or probe needs to controlled in such a way to reorient and transport the microobject to its final location using a stable pushing<sup>1</sup> operation. Using only a point contact with a limited number of freedom the task of pushing on a horizontal plane can be realized. In the micro-world, the inertial effect can be neglected with compared to the frictional forces existing between the micro-object and substrate. Thus, in the mechanism of pushing, the relation between the motion of the pushed object and the frictional forces between the object surface and the support forces plays a very dominant role. The direction and the magnitude of the frictional forces will determine the direction and magnitude of the velocity thats needs to be applied at the contact point to move the object in a desired trajectory. The velocity at the contact point is the control variable for the object motion and it is necessary to understand the properties of frictional forces before planning the pushing operation.

In this thesis, I am interested in translation of a regular object from one location to another by orientating the line of action of the pushing force to the desired direction. The desired translational motion of the object cannot be achieved if the

---

<sup>1</sup>The probe or pusher is always in contact with the micro-object during the pushing operation.

line of pushing at the contact point passes through the center of the mass of the micro-object. Due to the dominance of the frictional forces existing in between the micro-object and supporting surface, the inertial effect will be neglected and the motion will be dependent upon the motion and direction of the frictional forces. Thus, the resultant line of pushing needs to be directed to eliminate any moment caused by the frictional force so that orientation effect of the pushed object is rejected to ensure only translational motion. The frictional distribution in between the contact surface of the micro-object and supporting surface gives rise to centroid of the frictional distribution, center of friction<sup>2</sup> where all the distribution of friction can be lumped into a single point. Mason [23] showed that when the resultant pushing force vector applied on an object passes through the center of friction, the motion of the object is a pure translation. The result is obtained by assuming that the coefficient of friction of object with the substrate is constant over the time. Unfortunately, this is not a feasible solution in micro-world, where due to uncertain topography of the surfaces the frequency distribution changes with respect to time, giving rise to the unpredictable location of the center of friction which is not constant over time. Thus, the most important task lies in the online estimation of the center of friction using visual information.

In this section, the goal is to online estimate the center of friction and adapt the controller using visual feedback to generate the velocity to achieve the desired line of pushing. In the following subsections several issues related with stable pushing of micro-object to achieve translational motion will be presented such as:

- To prevent the sliding between the micro-object and the pusher at the contact point while the pushing operation is undergoing.
- To generate the desired line of pushing for known center of pushing such that the direction of line of pushing passes through the center of friction.
- Online estimation of the center of friction and center of instantaneous rotation while the object is in motion.

---

<sup>2</sup>Center of friction is defined as single point where the frictional distribution between the interface of object/substrate can be lumped.

### 6.0.5 Sliding of Micro-Objects

During the pushing operation of a regular object, the motion of an object being pushed through a single point of contact is often indeterminate. Despite this indeterminacy, it is sometimes possible to predict qualitative features of the motion, including whether the object will rotate and in which direction [9]. In order to understand pushing, it is necessary to introduce the following definitions:

- The *line of pushing*  $l_p$  passes through the contact point and is in the direction of the velocity of the pusher.
- The *line of motion*  $l_m$  passes through the contact point and is the direction of the velocity of the object.

The mechanism of orientation is described in Figure 6.3, depicting the line of pushing  $l_p$  and the line of motion  $l_m$ . The left and right edges of friction cone are denoted by  $l_L$  and  $l_R$ , respectively along with the line of pushing force  $l_F$ . To prevent sliding, the line of the pushing force needs to be within the friction cone. The value of this force can be altered depending upon the line of motion to achieve a desired trajectory.

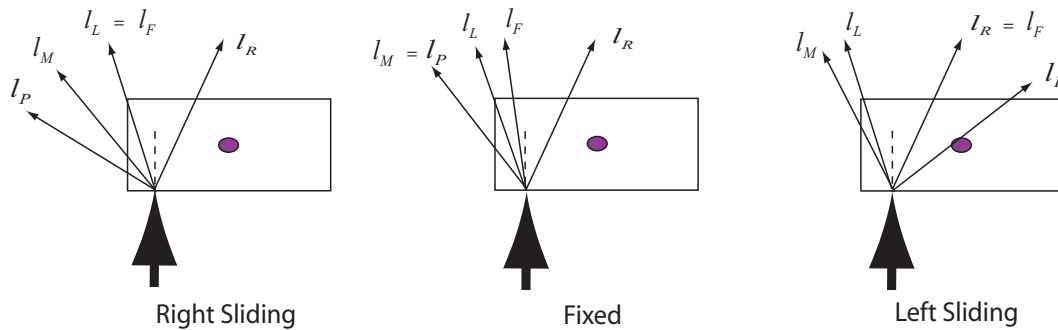


Figure 6.3: Sliding of micro-object [9]

Some constraints on the line of motion and line of action of pushing force can be stated for each contact mode as follows:

- *Separation.* The object remains in the same position. Line of action of pushing force and line of motion does not comes into affect.

- *Fixed.* The line of motion coincides with the line of action of pushing:  $l_P = l_M$ , and the line of action of pushing force comes in between the left and right edges of the friction cone.
- *Left Sliding.* The line of motion falls in left side with respect to the line of pushing, and the line of action of pushing force coincides with the right edge of the friction cone:  $l_F = l_R$ .
- *Right Sliding.* The line of motion falls to the right with respect to the line of pushing, and the line of action of force coincides with the left edge of the friction cone:  $l_F = l_L$ .

In order to prevent the sliding of the micro-object during the pushing operation, it is necessary that the the pusher falls within the friction cone<sup>3</sup> as denoted in Figure 6.4. Theoretical value of  $\mu$  between the silicon tip of the cantilever and micro-object is 0.25, thus the angle for friction cone can be calculated as  $28.07^\circ$ . Rotational manual base stages controlled by human operator can be set to proper rotational angle using visual display to ensure that the line of pushing lies within the friction cone for the desired translational motion.

### 6.0.6 Trajectory Control for Known Center of Friction

Figure 6.5 represents the scenario of pushing rectangular object using a point contact pushing to achieve pure translation motion. The rectangular micro-object has two points, namely COM (center of mass) and COF (center of friction). The contact point of the pusher is taken as the origin of the reference frame. The x-axis and y-axis of the frame is chosen to be parallel and perpendicular connecting to the edge of polygon. The velocity of the probe along x-axis ( $\vec{V}_x$ ) and y-axis ( $\vec{V}_y$ ) are controlled by visual feedback and human operator, respectively. The desired velocity vector  $\vec{V}_{des}$ , resultant of  $\vec{V}_x$  and  $\vec{V}_y$  needs to pass through COF, hence have an angle  $\theta_d$  to achieve a pure translation motion. The value of  $\vec{V}_y$  cannot be controlled to achieve

---

<sup>3</sup>friction cone is defined as to be the set of all wrenches satisfying Coulomb's law for an object at rest, i.e. all the wrenches satisfying:  $|f_t| \leq \mu|f_n|$

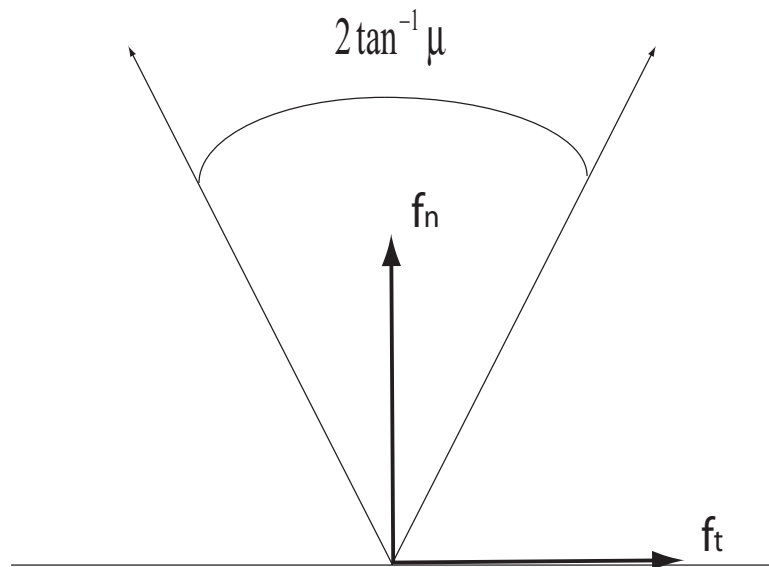


Figure 6.4: Calculation of friction cone

the desired velocity vector as it is administered by the human operator, rather it is only a measurable quantity. The variable  $\vec{V}_x$  can be calculated by taking into consideration the value of  $\vec{V}_y$  to achieve the desired velocity vector  $\vec{V}_{des}$  making an angle  $\theta_d$  as in the following equations.

The relationship between the  $\vec{V}_x$  and  $\vec{V}_{des}$  can be written as Eqn.(6.0.1) by analyzing Figure 6.5 and solving for  $\vec{V}_{des}$  yields Eqn.(6.0.2).

$$\vec{V}_{des} \cos \theta_d = \vec{V}_x \quad (6.0.1)$$

$$\vec{V}_{des} = \frac{\vec{V}_x}{\cos \theta_d} \quad (6.0.2)$$

Similarly, the relationship between the  $\vec{V}_y$  and  $\vec{V}_{des}$  can be written as Eqn.(6.0.3) and inserting the Eqn.(6.0.2) into Eqn.(6.0.3) will yield Eqn.(6.0.4)

$$\vec{V}_{des} \sin \theta_d = \vec{V}_y \quad (6.0.3)$$

$$\vec{V}_y = \vec{V}_x \tan \theta_d \quad (6.0.4)$$

The Eqn.(6.0.4) indicates that its possible to only control  $\vec{V}_y$  to achieve the resultant velocity vector  $\vec{V}_{des}$  to pass through COF. As its already discussed, the

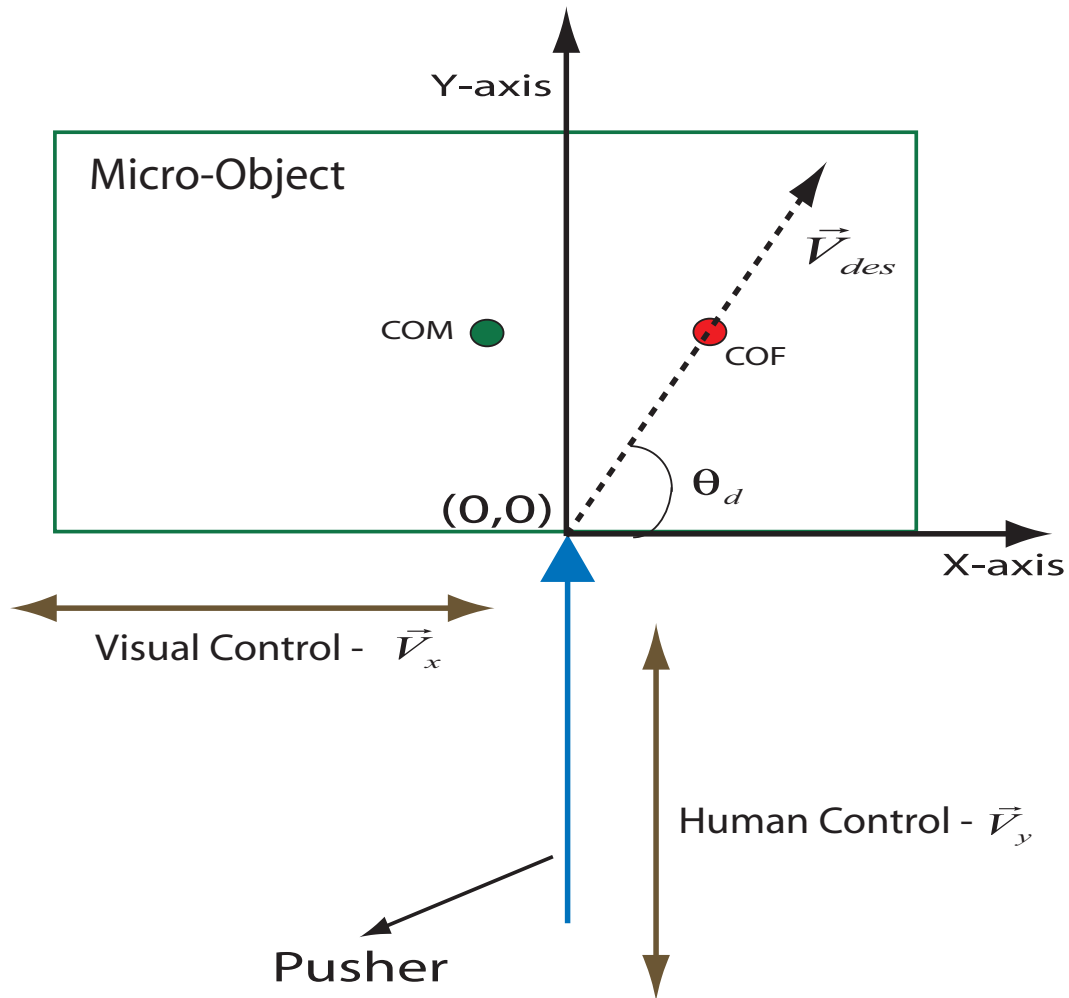


Figure 6.5: Calculation of velocity vector for known center of friction

location of the COF is not constant with respect to time, thus it is necessary to calculate the location of COF.

### 6.0.7 Center of Friction

In this subsection, I have focussed on the estimation of the center of friction of the rectangular micro-object lying on a support surface and pushed by the point contact probe using the technique proposed by Yoshikawa [74]. However, the concept is further extended by online estimation of COF for each visual data and necessary value of  $\theta_d$  is updated online.

Some of the assumption which needs to be considered are as follows:

1. The micro-object is rigid.

2. The micro-object is in contact with the supporting surface with  $n$  points, that is, the object is supported by  $n$  points. In this case  $n=4$ , as the four corners of the rectangle.
3. The position of the supporting points with respect to the object remains unchanged even when the micro-object is in motion.
4. Since the micro-object is pushed by point contact, the friction between the pusher and micro-object is assumed to be negligible due to the fact that contact area is very less.
5. The coefficient of friction between the object and the support surface may depend on the position of the supporting point, but is constant with respect to time.
6. The pushing force is applied horizontally to a point on the object near the support surface.
7. The velocity of the object is low enough that the inertia force can be ignored in comparison with the frictional force.

Figure 6.6 represents the micro-object lying on the supporting surface. A reference coordinate frame  $\sum_u(O_u - X_u Y_u Z_u)$  is attached to the supporting surface. An object coordinate frame  $\sum_o(O_o - X_o Y_o Z_o)$  is also fixed to the object with its  $X_o Y_o$  plane coinciding the base of the object. Some of the notations expressed in  $\sum_o$  are defined as follows:

- $p_i$  : Position of  $i^{th}$  supporting point.
- $v_i$  : Velocity of object relative to support surface at  $p_i$ .
- $a_i$  : Magnitude of frictional force at  $p_i$ .
- $f_i$  : Frictional force at  $p_i$ .
- $f$  : Frictional force vector.
- $m_i$  : Frictional moment at  $p_i$  with respect to  $\sum_o$ .

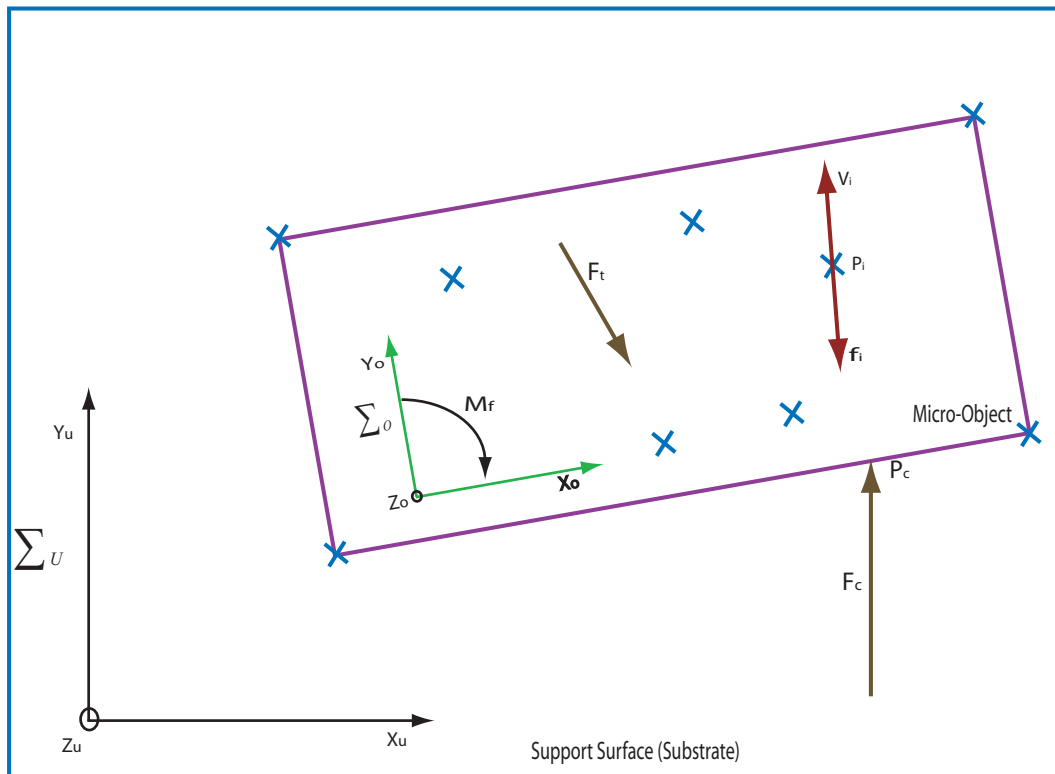


Figure 6.6: Reference frame and object frame

- $F_f$  : Total frictional force.
- $M_f$  : Total frictional moment with respect to  $\sum_0$ .
- $F_c$  : The pushing force applied by the probe.
- $p_c$  : The location of the contact point with the micro-object.
- $p_g$  : The location of the center of friction.

The frictional force  $f_i$  and the frictional moment  $m_i$  at the  $i^{th}$  supporting point are given by, Eqn.(6.0.5) and Eqn.(6.0.6), respectively:

$$f_i = -\frac{v_i}{\|v_i\|} a_i \quad (6.0.5)$$

$$m_i = p_i \times -\frac{v_i}{\|v_i\|} a_i \quad (6.0.6)$$



where  $\|\cdot\|$  and  $\times$  denote the Euclidean norm and the vector product. Thus, the total frictional  $F_f$  and total frictional moment  $M_f$  can be represented in Eqn.(6.0.7) and Eqn.(6.0.8), respectively:

$$F_i = \sum_{i=1}^n f_i = - \sum_{i=1}^n \frac{v_i}{\|v_i\|} a_i \quad (6.0.7)$$

$$M_f = \sum_{i=1}^n m_i = - \sum_{i=1}^n \left\{ p_i \times \frac{v_i}{\|v_i\|} a_i \right\} \quad (6.0.8)$$

If the micro-object rotates, then the position of instantaneous center of rotation of the motion  $p_r = [x_r, y_r, 0]^T$  can be deduced by using visual data. In Figure 6.7 the origin of the reference frame is placed at the lower left vertex of the rectangle. The edges PQ and P'Q' are the two edges of the rectangular micro-object before and after pushing by a probe using point contact. The midpoints of the line PP' and QQ' are found and a perpendicular line is formed from both the midpoints. The point where the two lines intersect meet is the instantaneous center of rotation referred as  $p_r$  whose location is denoted as  $[x_r, y_r, 0]^T$ .

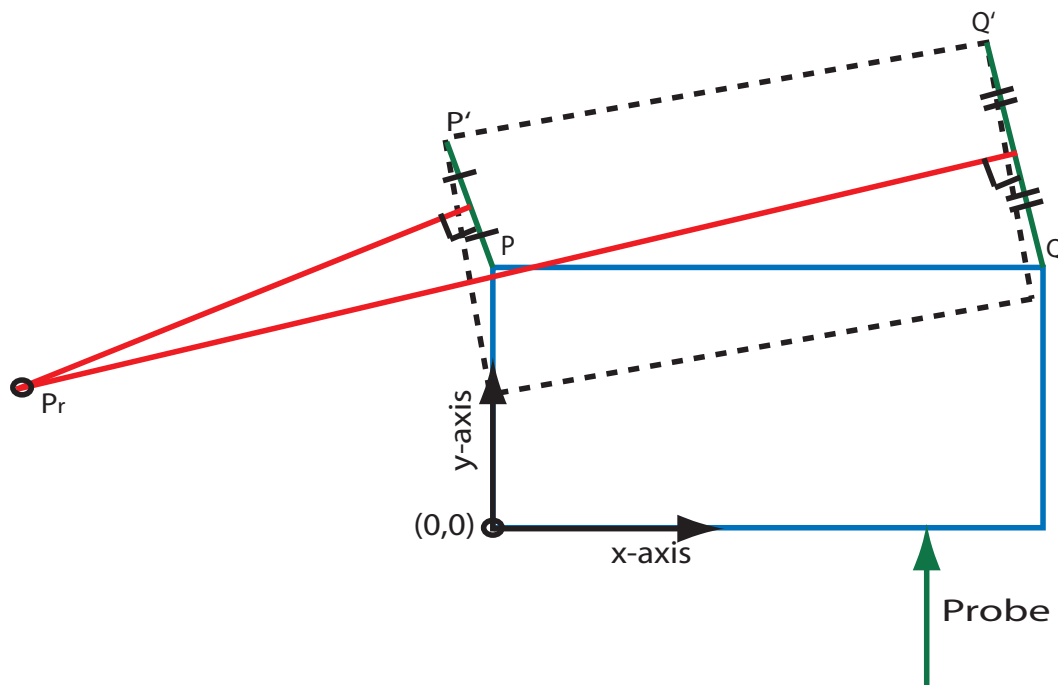


Figure 6.7: Instantaneous center of rotation

The unit vector which is along the direction of relative velocity at each supporting

point  $p_i = [x_i, y_i, 0]^T$  is denoted in Eqn.(6.0.9).

$$\frac{v_i}{\|v_i\|} = k \times \frac{p_i - p_r}{\|p_i - p_r\|} \quad (6.0.9)$$

where  $k$  is the unit vector that is along the direction of the rotation of the object. Let the rotational angle of frame  $\sum_0$  with respect to  $\sum_u$  be  $\theta$ . The unit vector  $k$  can be calculated as  $k$  is  $[0, 0, \text{sgn}(\dot{\theta})]^T$ . The value of  $k = [0, 0, -1]^T$  when the direction of rotation is counterclockwise and  $k = [0, 0, 1]^T$  when its object is rotating clockwise. The pushing force  $F_c$  at the contact point  $p_c = [x_c, y_c, 0]$  can be decomposed as  $F_c = [F_{cx}, F_{cy}, 0]^T$  and with assumption 7, one can state the following relations;

$$F_c = -F_f \quad (6.0.10)$$

$$M_c = -M_f = p_c \times F_c \quad (6.0.11)$$

where  $M_c = [0, 0, M_{cz}]^T$  denotes the moment due to  $F_c$ . Let the total friction force  $F_f$  be decomposed of  $F_f = [F_{fx}, F_{fy}, 0]^T$ ,  $M_f = [0, 0, M_{fz}]^T$ . From the Eqs.(6.0.7–6.0.11), one can obtain Eqs.(6.0.12–6.0.14).

$$\text{sgn}(\dot{\theta})F_{cx} = -\sum_{i=1}^n \frac{Y_i}{R_i} a_i \quad (6.0.12)$$

$$\text{sgn}(\dot{\theta})F_{cy} = \sum_{i=1}^n \frac{X_i}{R_i} a_i \quad (6.0.13)$$

$$\text{sgn}(\dot{\theta})M_{cz} = \sum_{i=1}^n \frac{x_i X_i + y_i Y_i}{R_i} a_i \quad (6.0.14)$$

Then, the value of  $X_i$ ,  $Y_i$  and  $R_i$  can be expressed as

$$X_i = x_i - x_r, Y_i = y_i - y_r, R_i = \sqrt{X_i^2 + Y_i^2} \quad (6.0.15)$$

Since  $a_i$  is the magnitude of the frictional force at the supporting point  $(x_i, y_i)$ , a frictional force vector can be formed as  $f = [a_1, a_2, \dots, a_n]^T$  for  $n$  supporting points. If the object moves without any rotation, the direction of the relative velocity  $\frac{v_i}{\|v_i\|}$  of all the supporting point are the same and can be written as

$$e_v = \frac{v_i}{\|v_i\|}, (i = 1, 2, \dots, n) \quad (6.0.16)$$

Rewriting the value of  $F_f$  and  $M_f$ , one can derive

$$F_f = -e_v \sum_{i=1}^n a_i \quad (6.0.17)$$

$$M_f = -\left\{ \sum_{i=1}^n p_i a_i \right\} \times e_v \quad (6.0.18)$$

Define a variable  $p_g$  and represented as if

$$p_g = \frac{\sum_{i=1}^n a_i p_i}{\sum_{i=1}^n a_i} \quad (6.0.19)$$

By the definition of  $p_g$ , Eqn.(6.0.18) can be written as

$$M_f = p_g \times F_f \quad (6.0.20)$$

Eqn.(6.0.20) indicates the total frictional force  $F_f$  to cause a frictional moment of  $M_f$  acts on the objects at point  $p_g$ , called as center of friction. From Eqn.(6.0.10) and Eqn.(6.0.17), the pushing force applied to the micro-object can be written as

$$F_c = e_v \sum_{i=1}^n a_i \quad (6.0.21)$$

$$\begin{aligned} M_c + M_f &= 0 \\ \vec{p}_c \times \vec{F}_c + \vec{p}_g \times \vec{F}_f &= 0 \\ (\vec{p}_c - \vec{p}_g) \times \vec{F}_c &= 0 \\ \vec{p}_g &= \vec{p}_c \end{aligned} \quad (6.0.22)$$

By analyzing Eqn.(6.0.21) and Eqn.(6.0.22), it can be concluded for a translational motion that the direction of  $F_c$  needs to be the same as the motion of the object and the line of action of  $F_c$  needs to pass through  $p_g$ . In other words, if one applies a external force  $F_c$  acting on the object such that the line of action  $F_c$  passes through the point  $p_g$ , then it is possible to push the object without any rotation.

### 6.0.8 Method for Online Estimation of the Center of Friction

As mentioned in the previous section, due to dominance of adhesion (surface) forces in the micro-world, the friction distribution between the micro-object and supporting surface alters giving rise to unpredictable changes of COF. The change in the location of the COF may be very fast due to unexpected changes in frictional distribution, thus online estimation of COF needs to be performed and the probe needs to align so that the line of action of the applied force  $F_c$  passes through the COF.

Visual information is utilized to determine the position and velocities of the four corners, the centroid of mass for the rectangular micro-object along with the position of the contact point  $p_c = (x_c, y_c)$  with the probe. The instantaneous center of rotation  $p_r$  and orientation angle  $\theta$  are calculated as discussed in above Section for each captured frame. The force  $F_c$  measured by the probe is coupled and can be decomposed into two dimension as  $F_{cx} = F_c \cos\theta$  and  $F_{cy} = F_c \sin\theta$ . The moment  $M_{cz}$  generated by the applied force be written as

$$M_{cz} = x_c F_{cy} - y_c F_{cx} \quad (6.0.23)$$

Once two consecutive visual frame are captured while pushing and from Eqn.(6.0.12–6.0.14), Eqn.(6.0.24), the relationship between the pushing force  $F_c$  and frictional force vector  $f$  can be written as

$$F_c = Gf \quad (6.0.24)$$

where  $F_c$  is calculated for each two consecutive frames captured using as

$$F_c = [sgn(\dot{\theta}_1)F_{cx1}, sgn(\dot{\theta}_1)F_{cy1}, sgn(\dot{\theta}_1)M_{cz1}, sgn(\dot{\theta}_2)F_{cx2}, sgn(\dot{\theta}_2)F_{cy2}, sgn(\dot{\theta}_2)M_{cz2}]^T \quad (6.0.25)$$

where  $F_{cx1}$ ,  $F_{cy1}$ ,  $M_{cz1}$  represents pushing force in x-axis for the first captured frame, pushing force in y-axis for the first captured frame and moment in the z-direction for the first captured frame respectively. Similarly  $F_{cx2}$ ,  $F_{cy2}$ ,  $M_{cz2}$  represents for the second captured frame. The value of  $G_{4 \times 6}$  matrix is calculated using two sets

of consecutive captured frame and four supporting points considering the vertices of the rectangle. The  $G_{4 \times 6}$  is written as

$$G = \begin{bmatrix} -\frac{Y_{11}}{R_{11}} & -\frac{Y_{21}}{R_{21}} & -\frac{Y_{31}}{R_{31}} & -\frac{Y_{41}}{R_{41}} \\ \frac{X_{11}}{R_{11}} & \frac{X_{21}}{R_{21}} & \frac{X_{31}}{R_{31}} & \frac{X_{41}}{R_{41}} \\ \frac{x_1 X_{11} + y_1 Y_{11}}{R_{11}} & \frac{x_2 X_{21} + y_2 Y_{21}}{R_{21}} & \frac{x_3 X_{31} + y_3 Y_{31}}{R_{31}} & \frac{x_4 X_{41} + y_4 Y_{41}}{R_{41}} \\ -\frac{Y_{12}}{R_{12}} & -\frac{Y_{22}}{R_{22}} & -\frac{Y_{32}}{R_{32}} & -\frac{Y_{42}}{R_{42}} \\ \frac{X_{12}}{R_{12}} & \frac{X_{22}}{R_{22}} & \frac{X_{32}}{R_{32}} & \frac{X_{42}}{R_{42}} \\ \frac{x_1 X_{12} + y_1 Y_{12}}{R_{12}} & \frac{x_2 X_{22} + y_2 Y_{22}}{R_{22}} & \frac{x_3 X_{32} + y_3 Y_{32}}{R_{32}} & \frac{x_4 X_{42} + y_4 Y_{42}}{R_{42}} \end{bmatrix} \quad (6.0.26)$$

From Eqn.(6.0.25), an estimate value of  $f(\hat{f})$  can be derived as

$$f = G^+ F \quad (6.0.27)$$

where  $G^+$  is the pseudo-inverse matrix of  $G$  matrix. From Eqn.(6.0.19), the estimated location of the center of friction  $\hat{p}_g$  can be obtained as

$$\hat{p}_g = \frac{X^T \hat{f}}{e_n^T \hat{f}} = \frac{X^T G^+ F}{e_n^T G^+ F} \quad (6.0.28)$$

where  $X^T$  represents the location of each vertices of the rectangle and can be written in matrix form as

$$X = \begin{bmatrix} x_1 & x_2 & x_3 & x_4 \\ y_1 & y_2 & y_3 & y_4 \\ 0 & 0 & 0 & 0 \end{bmatrix}^T \quad (6.0.29)$$

where  $e_n$  represents unity vector with four elements as

$$e_n = [1, 1, 1, 1]^T \quad (6.0.30)$$

### 6.0.9 Image Processing Procedures

Several image processing techniques are utilized to achieve the positions and velocities of the four vertices for the rectangular micro-object along with orientation angle. The image processing techniques are depicted as shown in Figure 6.8.

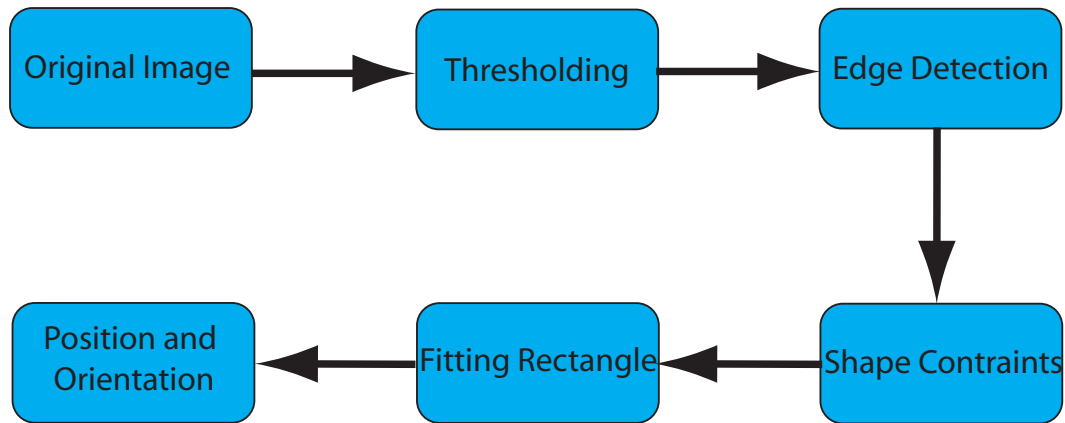


Figure 6.8: Image Processing Procedures

As the first step of image processing, gray scale images are captured with a rate of 30 frames per second using a commercial camera. Fast thresholding algorithm is performed for each frame to filter noise. After thresholding, edge detection algorithm is executed. Closed regions are detected using the rectangular shape and area of the object as the image invariants. This process is repeated for each frame, and the fitted rectangles are tracked during the course of pushing operation. The center, corners and contact point positions along with orientations of the fitted rectangles are calculated and numerically differentiated to estimate their velocities and angular velocities. The snapshot of tracking a polygonal object is demonstrated in Figure 6.9 along with the parameters of the rectangle such as center coordinates, length, width and orientation angle of the rectangle. The values are utilized to estimate the center of friction and align the micro-cantilever so that the line of action passes through the center of friction to achieve pure translation motion of the micro-object.

### 6.0.10 Pushing Algorithm

In order to push a rectangular micro-object to achieve pure translational motion, it necessary to get the friction distribution and location of the varying center of friction as discussed in above Subsection for online estimation of COF. The pushing operation is performed in several steps by considering the image frame as a reference frame. The steps are as follows:

- Step 1: Aligning the micro-cantilever such that the probe is in contact with

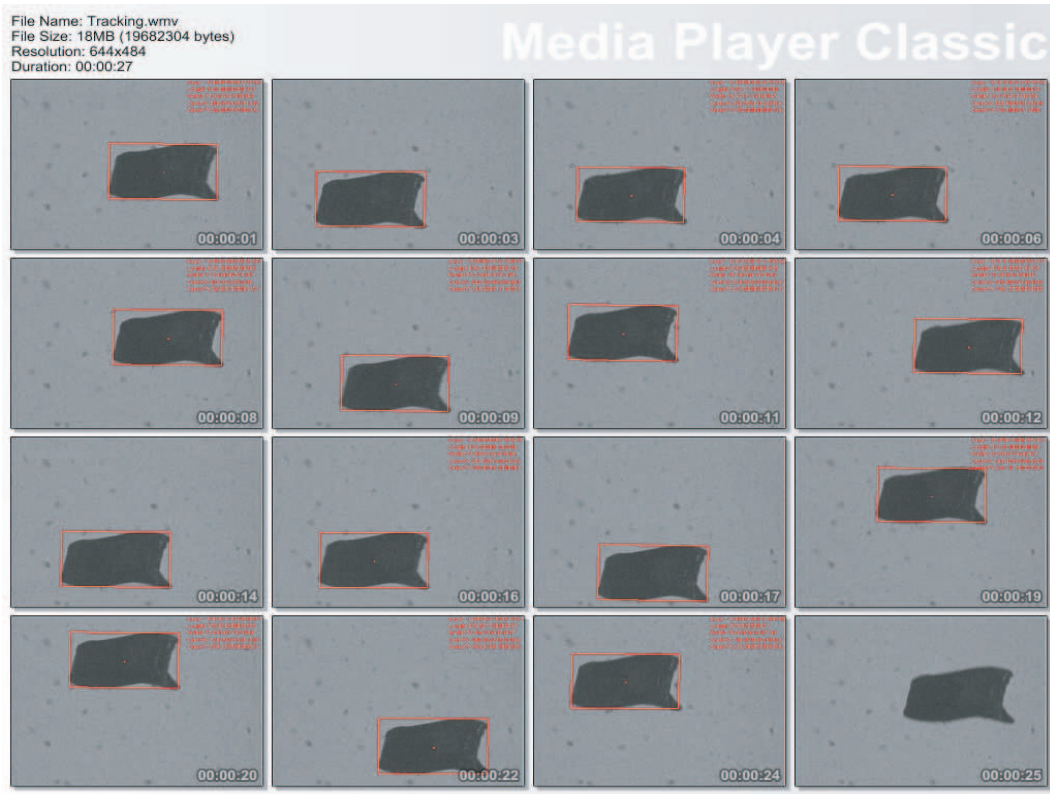


Figure 6.9: Snapshot of tracking polygonal micro-object

the rectangular micro-object at the midpoint of the length using the bilateral teleoperation as discussed in Section 5.3.

- Step 2: Human operator starts to push the object using bilateral teleoperation and monitors the behavior of the object using visual display. Concurrently, the visual processing starts as discussed in above subsection to generate the position and velocities of vertexes and contact point.
- Step 3: The data from visual processing is utilized to calculate the center of rotation  $p_r$  and concurrently the force exerted  $F_c$  by the probe is utilized to calculate  $F_{cx}$ ,  $F_{cy}$  and  $M_{cz}$  as discussed above.
- Step 4: The matrix  $F_c$  and  $G$  are formed using two successive visual and force data sets. The force data is downsampled and averaged to 30 Hz to matching the sampling rate of visual frame capturing.
- Step 5: The value of the center of friction  $p_g$  is estimated using the values

obtained in Step 4 and thereafter desired value of the velocity of the probe in x-direction  $\vec{V}_x$  is calculated as discussed in above subsection so that the vector of the resultant can be orientated to ensure that the lone of action passes through the estimated center of friction.

- Step 6:  $\vec{V}_x$  is set to the calculated value and kept constant until the arrival of new visual data.
- Step 7: The human operator continuously monitors any sliding of the micro-object at the contact point which may result if the probe comes out of the friction cone. When sliding occurs, the human operator reverts back and changes the location of the contact point after rotation stages is orientated to proper value.
- Step 8: Step 3 is repeated using the next visual data and the first three rows of  $G$  matrix are updated each time new data sets becomes available. Step 3 to Step 6 are repeated in a recursive manner to track the location of the center of friction.

Human operator is responsible for generating desired force for pushing of the micro-object by visualizing the motion of the micro-object and can pull the probe back if undesirable behavior in the motion of the micro-object is observed during any of the above mentioned steps. Since humans are very good at adapting to unexpected change in the forces, the force controlled pushing operation is administered by human operator.

### 6.0.11 Experimental Validation of Pushing Operation

In order validate the above mentioned pushing algorithm, several intermediate experiments were conducted by pushing a rectangular micro-object of size  $200 \mu m$  at the mid-point of the length of rectangle and the line of action passes through the center of mass. Figure 6.10 demonstrates the snapshot of the pushing operation and it can be clearly observed that after several steps the micro-object starts to rotate.



Thus, it is unmanageable to translate a micro-object by pushing through the center of mass.

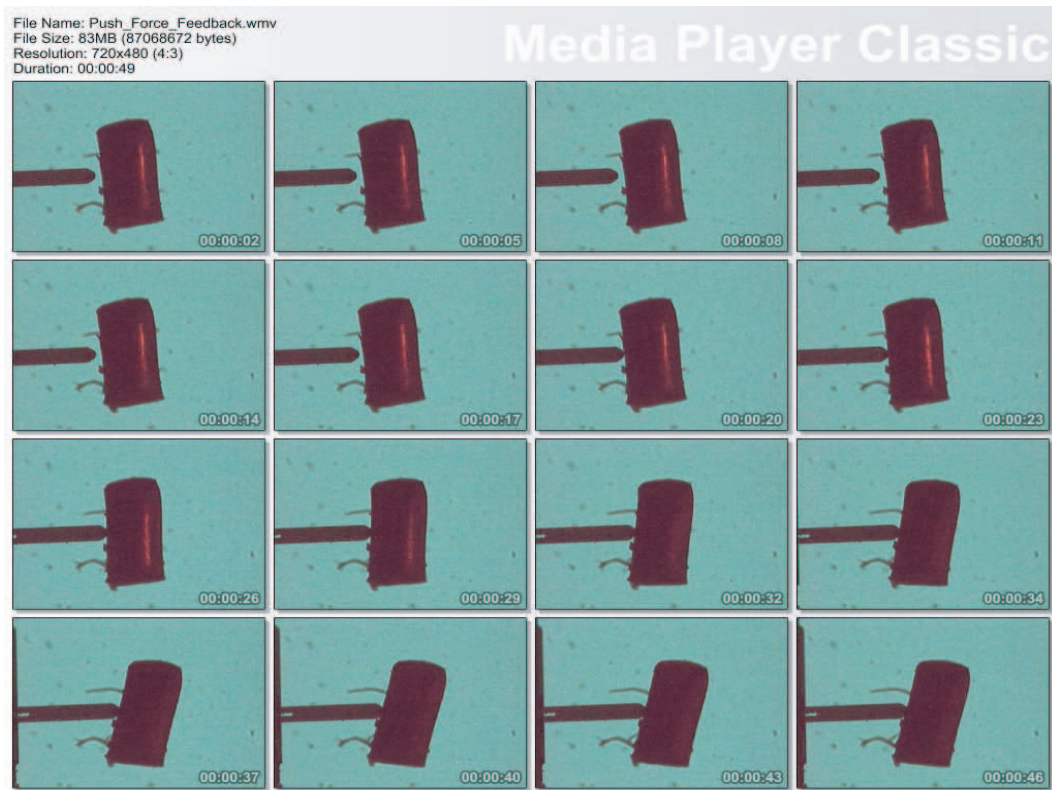


Figure 6.10: Snapshot of pushing rectangular object at the mid-point of the rectangle and line of action passes through center of mass of the object.

In another process, to compensate the orientation of the rectangle, the contact point was altered depending upon the sign of orientation angle with respect to the mid-point of length of the rectangle. Figure 6.11 demonstrates the pushing operation to achieve pure translation motion of micro-object by changing the contact point which depends upon the orientation angle. It can be clearly observed that it is not feasible solution to achieve pure translation motion because of the zigzag motion caused by the pushing process and moreover it is not desirable solution because the process of change from contact to non-contact may give rise to huge impact resulting damage to the probe or the micro-object.

The above mentioned discussion provides necessary arguments to conclude that to achieve pure translation motion it is necessary that the line of action passes through the center of friction to compensate the orientation angle. Figure 6.12

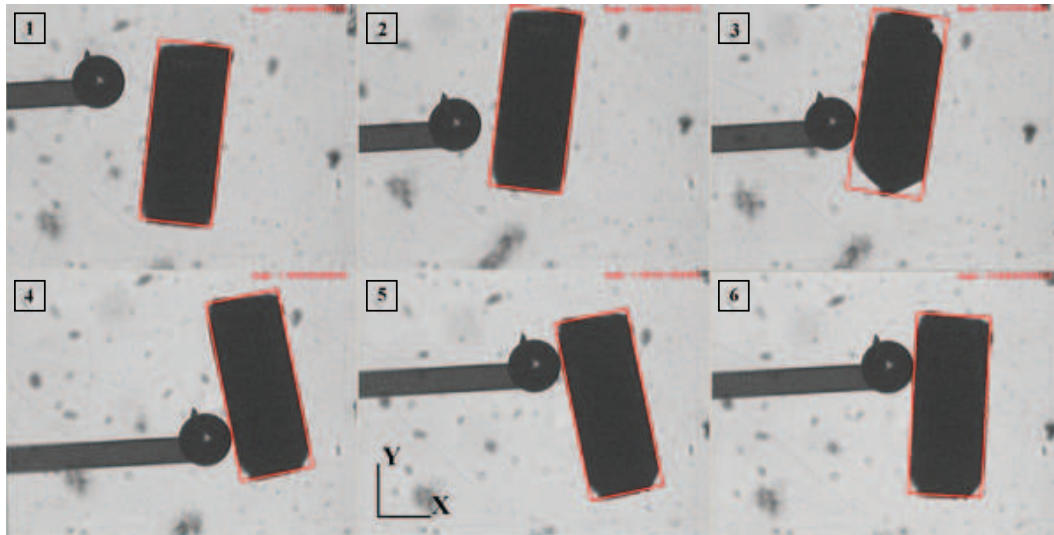


Figure 6.11: Snapshot of pushing rectangular object by changing the contact point depending upon the orientation angle

demonstrates the snapshot of pushing rectangular micro-object such that the line of action passes through the center of friction. It can be clearly seen that the proposed procedures was able to compensate the orientation effect to attain pure translational motion. Figure 6.13 shows the position of the probe in Y-axis, force sensed during the pushing operation and location of the center of rotation respectively.

## 6.1 Conclusion

In this chapter, a method for pushing polygonal micro-object using a hybrid force-position controller is proposed. The goal is to push the micro-object to achieve pure translation motion using semi-autonomous mechanism with the aid of human operator. The pushing operation is undertaken by the human operator using visual display which acts an impedance controller and can switch between velocity control to force control by adjusting the stiffness (muscle stiffness) depending upon the behavior of the motion of the micro-object. Visual module provides the information about the position and orientation of the micro-object to calculate the time-varying COF (center of friction) in recursive manner for each captured frame. The velocity at the contact point is altered using visual feedback procedures such that the resultant direction of velocity passes through the COF to achieve pure translational motion.

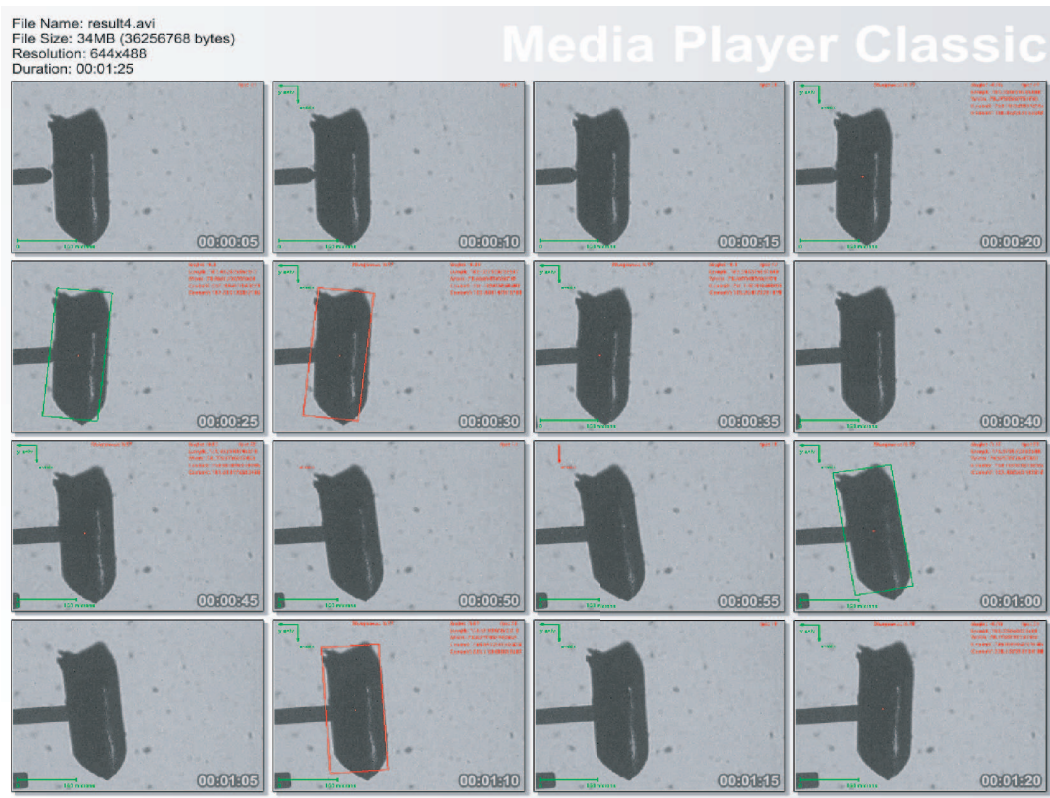


Figure 6.12: Snapshot of pushing rectangular object such that the line of action passes through the center of friction

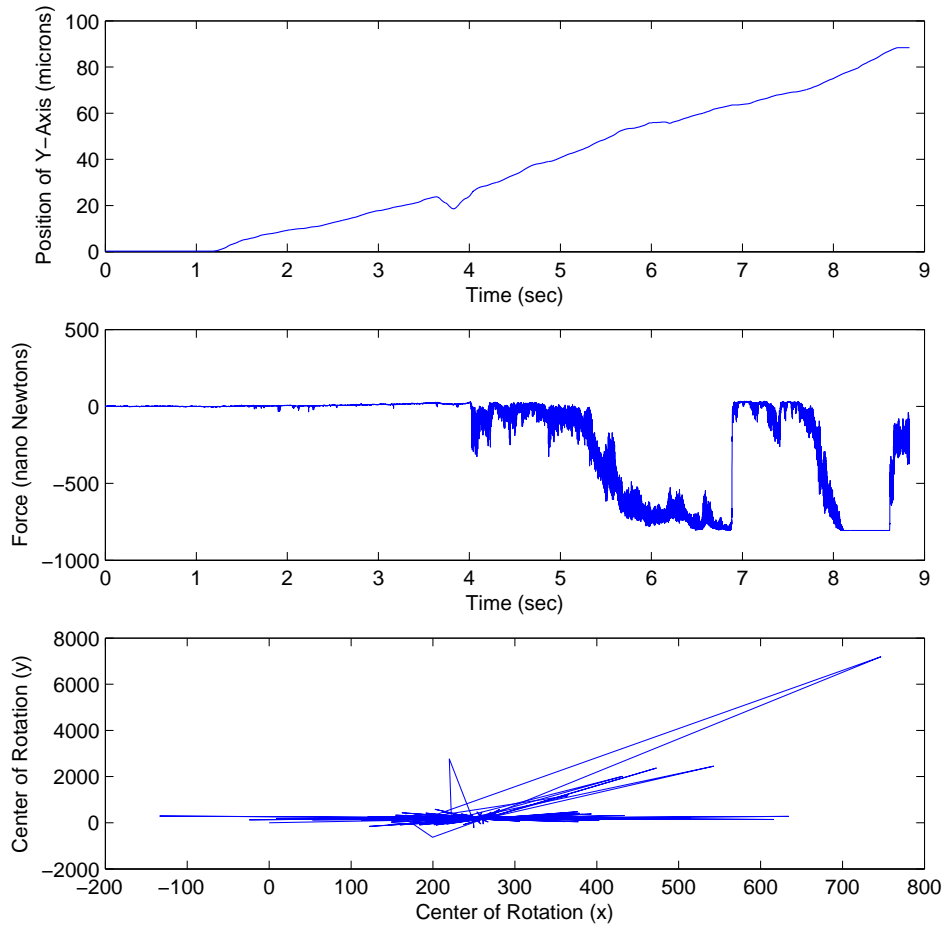


Figure 6.13: Snapshot of pushing rectangular object such that the line of action passes through the center of friction

# Chapter 7

## Conclusions

### 7.1 Summary of the Thesis

In this thesis, the effort is directed to push a polygonal micro-object in a semi-autonomous fashion, administered by human operator to achieve pure translational motion using a custom built tele-micromanipulation setup. Human operator utilizes the custom built tele-micromanipulation setup with force feedback to push the micro-object with a piezoresistive AFM probe. Moreover, the estimated center of friction is calculated online using recursive least square method utilization information received from image processing techniques and measured interaction forces. Visual feedback process align the micro-cantilever automatically so that the line of pushing passes through the center of friction of the micro-object, varying with time to attain pure translational motion.

A custom built tele-micromanipulation setup is employed to implement the above mentioned task. Discrete time sliding mode controller is implemented for high precision motion control using piezoelectric actuator. Force sensing with nano-Newton resolution is demonstrated with a commercial available piezoresistive cantilever which is utilized in scaled bilateral teleoperation with force feedback. Experimental verification concerning force/position tracking is provided to show the transparency between the master and the slave. Image processing procedures are developed to track polygonal micro-object to achieve the position/velocities of feature points along with the orientation angle.

## 7.2 Future Works

Some of the future works are as follows:

- Presently strain-gauge sensors are utilized for the position feedback in piezoelectric actuator which is not effective in nanometer range motion rather some other sensors should be utilized such as laser interferometer.
- The piezoelectric actuator takes voltage as an input which is provided by 16-bit DAC (Digital-to-Analog Converter) but in order to achieve sub-nanometer resolution it is indispensable to utilize DAC with much higher number of bits.
- Piezoresistive AFM cantilever is presently utilized to sense force with nanonewton range only in one dimension, for dexterous tele-micromanipulation its worth to investigate sensing the force in 2 and 3 dimensions.
- In the present context, position and force scaling is discussed in the context of scaled bilateral teleoperation, it will be worth to consider the frequency scaling from slave to master.
- Presently one probe is utilized to push the micro-object using point contact but the task may become simpler using more than one probe.
- Utilizing camera with faster frame capture rate may enhance the speed for pushing operation.
- The present discussion are limited to pushing of micro-objects but using a micro-gripper with force feedback is necessary for 3D manipulation of micro-objects.
- Accurate models are required to model the adhesion force between the micro-object and substrate, in order to move towards automatic pushing of micro-objects.

# Bibliography

- [1] J. Breguet, C. Schmitt, and R. Clavel, “Micro/nano factory: Concept and state of the art,” in *In Proc. of SPIE Conf. on Microrobotics and Micro Assembly II*, 2000.
- [2] M.Sitti, *Teleoperate 2-D Micro/Nanomanipulation Using Atomic Force Microscope*. PhD thesis, University of Tokyo, Intelligent Mechatronics Laboratory.
- [3] A.Menciassi, A.Eisinberg, I.Izzo, and P.Dario, “From ”macro” to ”micro” manipulation: models and experiments,” *IEEE/ASME Transactions on Mechatronics*.
- [4] G. A. V. Christiansson, “Introduction to haptic teleoperation,” in *Unpublished*, 2005.
- [5] D. A. Lawrence, “Stability and transparency in bilateral telemanipulation,” in *IEEE Transaction in Robotics and Automation*, vol. 9, pp. 624–637, 1993.
- [6] T. S. Low and W. Guo, “Modeling of a three-layer piezoelectric bimorph beam with hysteresis,” in *Journal of Microelectromechanical Systems*, vol. 4, pp. 230–237, 1995.
- [7] K. Abidi, “Sliding-mode control for high-precision motion control systems,” (MS Thesis,Sabancı University), 2004.
- [8] S. Khan, M. Elitas, E. D. Kunt, and A. Sabanovic, “Discrete sliding mode control of piezo actuator in nano-scale range,” in *IEEE/ICIT International Conference on Industrial Technology*, 2006.
- [9] M. T.Mason, *Mechanics of Robotics Manipulation*. MIT Press, 2001.

- [10] D. O. Popa and H. E. Stephanou, "Micro and meso scale robotic assembly," in *WTEC Workshop: Review of U.S. Research in Robotics*, 2004.
- [11] B. J. Nelson, "Microassembly and its applications," in *In Proceedings of Symposium of Mechatronics and Microsystems*, p. 59, TUDelft, The Netherlands, 2003.
- [12] K. F. Bohringer, K. Y. Goldberg, M. Cohn, R. Howe, and A. Pisano, "Parallel microassembly with electrostatic force fields," in *In Proc. of IEEE Int. Conf. on Intelligent Robotics and Automation, ICRA*, (New York), p. 1204, 1998.
- [13] M. Weck and B. Petersen, "High precision positioning stage for micro assembly purposes," in *In Symposium on Design, Test, and Microfabrication of MEMS and MOEMS, SPIE*, pp. 734–739, 1999.
- [14] B. Nelson and B. Vikramaditya, "Visually guided microassembly using optical microscope and active vision techniques," in *In Proc. IEEE Int. Conf. on Robotics and Automation (ICRA)*, (Albuquerque), 1997.
- [15] J. T. Feddema and R. W. Simon, "Cad-driven microassembly and visual servoing," in *In Proceedings on IEEE-ICRA*, pp. 1212–1219, 1998.
- [16] P. Cantilever. Applied nanostructures; <http://www.appnano.com/>.
- [17] <http://www.mw.com/dictionary/bilateral>. Merriam Webster Online Dictionary.
- [18] C. D. Onal, "Bilateral control - a sliding mode control approach," (MS Thesis, Sabanci University), 2005.
- [19] Y. Yokokohji and T. Yoshikawa, "Bilateral control of master-slave manipulators for ideal kinesthetic coupling," in *IEEE Transaction in Robotics and Automation*, vol. 10, pp. 605–620, 1994.
- [20] S. Katsura, Y. Matsumoto, and K. Ohnishi, "Realization of "law of action and reaction" by multilateral control," in *IEEE Transaction in Industrial Electronics*, vol. 52 of 5, pp. 1196 – 1205, 2005.



- [21] D. J. Lee and M. W. Spong, "Bilateral teleoperation of multiple cooperative robots over delayed communication networks," in *IEEE Transactions on Robotics*, 2004.
- [22] D.G.Gersema, "Kinesthetic feedback and enhanced sensitivity in robotic endoscopic telesurgery," in *Ph.D. Dissertation*, Katholieke Universiteit Leuven, 2005.
- [23] M.T.Mason, "Mechanics and planning of manipulator pushing operations," in *International Journal of Robotics Research*, vol. 5 of 3, pp. 53–71, 1986.
- [24] K. M. Lynch and M. T. Mason, "Stable pushing: Mechanics, controllability, and planning," *The International Journal of Robotics Research*, vol. 15, no. 6, pp. 533–556, 1996.
- [25] C. Keller and R.T.Howe, "Hexil tweezers for teleoperated micro-assembly," in *In Proc. IEEE Workshop on MEMS*, (Nagoya,Japan), pp. 72–77, 1997.
- [26] M. Sitti and H. Hashimoto, "Two-dimensional fine particle positioning under optical microscope using a piezoresistive cantilever as a manipulator," in *Journal of Micromechatronics*, vol. 1 of 1, pp. 25–48, 2000.
- [27] G. Dedkov, "Friction on the nanoscale: New physical mechanisms," in *Materials Letters*, vol. 38, pp. 360–366, 1999.
- [28] G. Dedkov, "Experimental and theoretical aspects of the modern nanotribology," in *Physics State Solids*, vol. 179 of 3, pp. 3–35, 2000.
- [29] J.Prescott, "Mechanics of particles and rigid bodies," in *London: Longmans, Green, and Co*, 1923.
- [30] W. D.MacMillan, "Dynamics of rigid bodies," in *New York: Dover*, 1936.
- [31] R.C.Brost, "Dynamic analysis of planar manipulation tasks," in *In Proc. of IEEE Int. Conf. Robotics and Automation*, pp. 2247–2254, 1992.

- [32] M. A.Peshkin and A. C.Sanderson, “The motion of a pushed, sliding work-piece,” in *IEEE Journal of Robotics and Automation*, vol. 4 of 6, pp. 569–598, 1988.
- [33] S.Goyal, A.Ruina, and J.Papadopoulos, “Planar sliding with dry friction. part 1: Limit surface and momentum function,” in *Wear*, vol. 143 of 2, pp. 307–330, 1991.
- [34] J.C.Alexander and J. H.Maddocks, “Bounds on the friction-dominated motion of a pushed object,” in *International Journal of Robotics Research*, vol. 12 of 3, pp. 231–248, 1993.
- [35] M.Mani and W.Wilson, “A programmable orienting system for flat parts,” in *North American Manufacturing Research Institute Conference XIII*, 1985.
- [36] Z.Balorda, “Automatic planning of robot pushing operations,” in *In Proc. of IEEE Int. Conf. Robotics and Automation*, vol. 1, pp. 732–737, 1993.
- [37] M. T.Mason, “Compliant sliding of a block along a wall,” in *In Proc. of Int. Symp. Experimental Robotics*, pp. 568–578, 1989.
- [38] H.Mayeda and Y.Wakatsuki, “Strategies for pushing a 3d block along a wall,” in *In Proc. of IEEE/RSJ Int.Conf. Intelligent Robots and Systems*, pp. 461–466, 1991.
- [39] M. Kurisu and T. Yoshiwaka, “Tracking control for an object in pushing operation,” in *IEEE International Conference of Intelligent Robots and Systems*, pp. 729–736, 2006.
- [40] M. Goldfarb and N. Celanovic, “Modeling piezoelectric stack actuators for control of micromanipulation,” in *IEEE Control Systems Magazine*, vol. 17, pp. 69–79, 1997.
- [41] H.Adriaens, W. L. de Koning, and R.Banning, “Modeling piezoelectric actuators,” in *Journal of Mechatronics*, vol. 5, pp. 331–341, 2000.

- [42] Y.Stepanenko and C.Y.Su, “Intelligent control of piezoelectric actuators,” in *In Proceedings of the 37th IEEE Conference on Decision and Control*, vol. 4, pp. 4234–4239, 1998.
- [43] D.Song and C.J.Li, “Modeling of piezo actuator’s nonlinear and frequency dependent dynamics,” in *Journal of Mechatronics*, vol. 4, pp. 391–410, 1999.
- [44] K. Kuhnen and H. Janocha, “Real-time compensation of hysteresis and creep in piezoelectric actuators,” in *Journal of Sensors and Actuators*, vol. 7 of 9, pp. 83–89, 2000.
- [45] B. J. Lazan, “Damping of materials and members in structural mechanics,” in *Pergamon*, 1968.
- [46] Y.K.Wen, “Method for random vibration of hysteretic systems,” in *Journal of Engineering and Mechanics*, vol. 102, pp. 249–263, 1976.
- [47] M.C.Constantinou and I.G.Tadjbakhsh, “Hysteretic dampers in base isolation: Random approach,” in *Journal of Structural Engineering*, pp. 705–721, 1998.
- [48] A. Smyth and et.al, “Development of adaptive modeling techniques for non-linear hysteretic systems,” in *International Journal of Non-Linear Mechanics*, vol. 37, (1435-1451).
- [49] C.P.Heine, “Simulated response of degrading hysteretic joints with slack behavior,” in *Ph.D. dissertation*, Virginia Polytechnic Institute and State University, 2001.
- [50] B.F.Spencer, “Reliability of randomly excited hysteretic structures,” in *Springer-Heidelberg*, (New York).
- [51] B. Zhang and Z. Zhu, “Developing a linear piezomotor with nanometer resolution and high stiffness,” in *IEEE/ASME Transactions on Mechatronics*, vol. 2 of 1, pp. 22–29, 1997.

- [52] R. Banning, W. L. de Koning, and J. M. T. A. Adriaens, "Modeling piezoelectric actuators," in *IEEE/ASME Transactions on Mechatronics*, vol. 5 of 4, pp. 331–341, 2000.
- [53] B. M. Chen, T. H. Lee, C.-C. Hang, Y. Guo, and S. Weerasooriya, "An infinity almost disturbance decoupling robust controller design for a piezoelectric bimorph actuator with hysteresis," in *IEEE Transactions on Control Systems Technology*, vol. 7 of 2, pp. 160–174, 1999.
- [54] K. K. Tan, T. H. Lee, and H. X. Zhou, "Micro-positioning of linear-piezoelectric motors based on a learning nonlinear pid controller," in *IEEE/ASME Transactions on Mechatronics*, vol. 6 of 4, pp. 428–436, 2001.
- [55] S. B. Chang, S. H. Wu, and Y. C. Hu, "Submicrometer overshoot control of rapid and precise positioning," in *Journal of American Society of Precision Engineering*, vol. 20, pp. 161–170, 1997.
- [56] S. V. Drakunov and V. Utkin, "A semigroup approach to discrete-time sliding modes," in *Proceedings of the American Control Conference*, 1995.
- [57] S. Yang and M. Tomizuka, "Adaptive pulse width control for precise positioning under the influence of stiction and coulomb friction," in *Journal of Dynamics, Systems, Measurement and Control*, 1998.
- [58] E. D. Tung, G. Anwar, and M. Tomizuka, "Low-velocity friction compensation and feed-forward solution based on repetitive control," in *Journal of Dynamics, Systems, Measurement and Control*, 1993.
- [59] P. I. Rao, W. Shim, and S. Jeong, "Robust friction compensation for submicrometer positioning and tracking for a ball-screw-driven slide system," in *Journal of Precision Engineering*, 2000.
- [60] Y. C. Pan, "Investigation of static friction and high precision positioning control," in *PhD Thesis*, Department of Aeronautical and Astronautical Engineering, Cheng Kung University, Tainan Taiwan, 2000.

- [61] C.Hsieh and Y.C.Pan, “Dynamic behavior and modeling of the pre-sliding static friction,” in *Journal of Wear*, vol. 242, pp. 1–17, 2000.
- [62] I.T.Teeter, M.W.Chow, and J.J.Brickley, “A novel fuzzy friction compensation approach to improve the performance of a dc motor control system,” in *IEEE Transaction in Industrial Electronics*, vol. 43 of 1, pp. 113–120, 1996.
- [63] S.Cetinkunt and A.Donmez, “Cmac learning controller for servo control of high-precision machine tools,” in *In Proceedings of the American Control Conference*, 1993.
- [64] C. C. de Wit and H. Olsson, “A new model for control of systems with friction,” in *IEEE Transaction On Automatic Control*, vol. 4 of 3, 1995.
- [65] V. Utkin and S. Drakunov, “On discrete-time sliding mode control,” in *In Proceedings of IFAC Symposium on Nonlinear Control Systems*, (Capri, Italy), pp. 484–489, 1987.
- [66] J. Hutter and J. Bechhoefer, “Calibration of atomic-force microscope tips,” in *Review of Scientific Instruments*, vol. 64, pp. 1868–1873, 1993.
- [67] S. Khan, A. O. Nergiz, A. Sabanovic, and V. Patoglu, “Development of a micromanipulation system with force sensing,” in *IEEE/IROS International Conference on Intelligent Robots and Systems*, 2007.
- [68] S.Khan, A.Sabanovic, and A.O.Nergiz, “Scaled bilateral teleoperation using discrete-time sliding mode controller,” in *IEEE Transaction in Industrial Electronics*, p. In Review, 2007.
- [69] K. L. Johnson, *A continuum mechanics model of adhesion and friction in a single asperity contact:In Micro-nanotribology and its applications*. Kluwer Academic Publishers, 1997.
- [70] D. Maugis, “Adhesion of spheres : the jkr-dmt transition model using a dugdale model,” in *Journal of Colloid and Interface Science*, vol. 150, pp. 243–269, 1992.

- [71] M. Sitti and R. Fearing, “Synthetic gecko foot-hair micro-nanostructures as dry adhesives,” in *Journal of Adhesion Science Technology*, vol. 17 of 8, pp. 1055–1073, 2003.
- [72] P. Rougeot, S. Regnier, and N. Chaillet, “Force analysis for micromanipulation,” in *IEEE CIRA*, pp. 105–110, 2005.
- [73] S. Khan, A. O. Nergiz, M. Elitas, V. Patoglu, and A. Sabanovic, “A hybrid force-position controller based man-machine interface for manipulation of micro objects,” in *IEEE/MHS International Conference on Micro-Nano Mechatronics*, 2007.
- [74] T. Yoshikawa and M. Kurisu, “Identification of the center of friction from pushing an object by a mobile robot,” in *IEEE/RSJ International Workshop on Intelligent Robots and Systems - IROS*, 1991.

# Appendix A

## Bilateral Control

### Micromanipulation

#### A.1 PI P-854 PiezoMike: Piezoelectric Micrometer Drive

Table A.1 explains the technical specification of the open-loop piezoelectric micro-motor drive.

Table A.1: PI P-854 PiezoMike: Piezoelectric Micrometer Drive Technical Data

Property	Value	Units
<i>Travel range (micrometer drive)</i>	18	mm
<i>Piezo fine travel range (@ 0 to 100 V)</i>	25	$\mu\text{m} \pm 20\%$
<i>Min. incremental motion (piezo drive)</i>	<1	nm
<i>Micrometer sensitivity</i>	1	$\mu\text{m}$
<i>Max. axial push/pull force</i>	20 / 5	N
<i>Micrometer drive</i>	M-626.10	
<i>Micrometer pitch</i>	0.5	mm/rev.
<i>Stiffness</i>	1.5	N/ $\mu\text{m}$
<i>Electrical capacitance (piezo)</i>	1.5	$\mu\text{F}$
<i>Electrical connection</i>	LEMO Cable: coaxial, FFA.00.250, male. RG 178, Teflon coated, 1 m	
<i>Weight</i>	0.1	kg
<i>Body material</i>	N -S	
<i>Recommended piezo driver</i>	A, C, G	

## A.2 PI P-611 NanoCube XYZ Piezo Nanopositioning Systems

Table A.2 provides the technical specification of the P-611 Nanocube.

Table A.2: PI P-611 3-S NanoCube XYZ Piezo Nanopositioning System Technical Data

Property	Value	Units
Active axes	X, Y, Z	
Open-loop travel @ 0 to 100 V	100 / axis	$\mu\text{m} \pm 20\%$
Closed-loop travel	100 / axis	$\mu\text{m}$
Integrated feedback sensor	SGS	
* Closed- / open-loop resolution	2 / 1	nm
Repeatability	25	nm
Stiffness	0.3	$\text{N}/\mu\text{m} \pm 20\%$
Max. normal load	+15/-5	N
Electrical capacitance	1.5 / axis	$\mu\text{F} \pm 20\%$
Dynamic operating current coefficient (DOCC)	1.7 / axis	$\mu\text{A}/(\text{Hz} \times \mu\text{m})$
Unloaded resonant frequency (X/Y/Z)	350/220/250	$\text{Hz} \pm 20\%$
Operating temperature range	-20 to 80	$^{\circ}\text{C}$
*** Voltage connection	D	
*** Sensor connection	D	
Weight (w/o cables)	250	$\text{g} \pm 5\%$
Body material	S/Al	
Recommended amplifier/controller	N, D, H	

## A.3 PI E664 NanoCube Piezo Controller

Table A.3 provides the technical specification of E-664 Nanocube Controller.

## A.4 Maxon RE-40 DC Servo Motor

Table A.4 provides the technical details of the RE-40 DC Servo motor utilized as master device.



Table A.3: PI E664 NanoCube Piezo Controller Technical Data

Property	Value
Function	Power amplifier sensor/position servo-control of P-611 NanoCube NanoPositioning systems
Channels	3
Amplifier	
Maximum output power	14 W / channel
Average output power	6 W / channel
Peak output current <5 ms	140 mA / channel
Average output current >5 ms	60 mA / channel
Current limitation	Short-circuit proof
Voltage gain	10 ±0.1
Polarity	Positive
Control input voltage	-2 to +12 V
Output voltage	-20 to 120 V
DC offset setting	0 to 100 V with 10-turn pot.
Input impedance	100 kΩ
Display	3 x 3 <sup>1/2</sup> -digit, LED
Control input sockets:	3 x BNC (rear)
PZT voltage output socket	25 pin sub-D on rear
Dimensions	236 x 88 x 273 mm + handles
Weight	3.0 kg
Operating voltage	90-120 / 220-240 VAC, 50-60 Hz (linear P/S)
Position Servo-Control	
Sensor type	Strain Gauge
Servo characteristics	P-I (analog) + notch filter
Sensor socket	25 pin sub-D on rear (same as PZT voltage)
Sensor monitor output socket	3 x BNC on rear
Additional I/O	14 pin connector on rear for On-Target and Overflow status and control in and sensor monitor out

## A.5 Maxon 4-Q-DC Servoamplifier ADS in Module Housing

Table A.5 provides the technical specification of Maxon 4-Q-DC Servoamplifier utilized as driver for Master device.

Table A.4: Maxon RE 40 DC Motor Data

Nominal voltage	48 V
No load speed	7580 rpm
No load current	68.6 mA
Nominal speed	7000 rpm
Nominal torque (max. continuous torque)	184 mNm
Nominal current (max. continuous current)	3.12 A
Stall torque	2500 mNm
Starting current	41.4 A
Max. efficiency	92 %
Terminal resistance	1.16 $\Omega$
Terminal inductance	0.329 mH
Torque constant	60.3 mNm / A
Speed constant	158 rpm / V
Speed / torque gradient	3.04 rpm / mNm
Mechanical time constant	4.39 ms
Rotor inertia	138 gcm <sup>2</sup>

Table A.5: Maxon 4-Q-DC Servoamplifier Data

Supply voltage $V_{CC}$	12 - 50 VDC
Max. output current $I_{max}$	10 A
No load current	mA
Continuous output current $I_{cont}$	5 A
Switching frequency of power stage	50 kHz
Efficiency	95 %
Band width current controller	2.5 kHz
Built-in motor choke	160 $\mu$ H / 5 A
<b>Input</b>	
Set value	-10 ... +10 V
Enable	+4 ... +50 V
Input voltage DC tachometer	2 VDC - 50 VDC
Encoder signals	max. 100 kHz, TTL
<b>Output</b>	
Current monitor "Monitor I"	-10 VDC ... +10 VDC
Speed monitor "Monitor n"	-10 VDC ... +10 VDC
Status reading "READY"	max. 30 VDC
<b>Voltage output</b>	
Aux. voltage, short circuit protected	+12 VDC, -12 VDC, max. 12 mA
Encoder supply voltage	+5 VDC, max. 80 mA

## Publications

- Referred Journals
  - **S. Khan**, A. Sabanovic and A. O. Nergiz, “Scaled Bilateral Teleoperation Using Discrete-Time Sliding Mode Controller” 2006 IEEE Transaction on Industrial Electronics. (In Review)
  - “Semi-Automated Pushing of Micro-Object using scaled bilateral teleoperation”. (In Preparation)
- Referred Conference Proceedings (Year Wise)
  - M. Elitas, **S. Khan**, A. O. Nergiz and A. Sabanovic, “Function Based control for Bilateral Systems in Tele-Micromanipulation”, IEEE Advanced Motion Control (AMC-08) (Accepted)
  - **S. Khan**, A. O. Nergiz, M. Elitas, V. Patoglu and A. Sabanovic, “A Hybrid Force-Position Controller based Man-Machine Interface For Manipulation of Micro Objects”, IEEE International Symposium on Micro-NanoMechatronics and Human Science (MHS-2007).
  - **S. Khan**, A. O. Nergiz, A. Sabanovic and V. Patoglu, “Development of a micromanipulation System with Force Sensing”, IEEE IROS-2007 (IEEE International Conference on Robotics and Automation Systems).
  - **S. Khan**, A. O. Nergiz, A. Sabanovic and V. Patoglu, “Hysteresis Compensation for Open Loop Piezoelectric Linear Drives”, TOK-07 (Turkish Automatic Control). (In Turkish).
  - A. Sabanovic, **S. Khan**, M. Elitas and K. Jajernik “Sliding Mode Adaptive controller for PZT Actuator”, Nov 8-10 IEEE IECON-2006, (IEEE International Conference on Industrial Electronics) Paris.
  - **S. Khan**, M. Elitas and A. Sabanovic “Discrete Sliding Mode Control of Piezo Actuator in Nano-Scale Range”, Dec 15-17 IEEE ICIT-2006, (IEEE International Conference on Industrial Technology) Mumbai, India.

- **S. Khan** and A. Sabanovic, “Discrete Time Sliding Mode control of High precision linear Drive using Frictional Model”, IEEE AMC-06 (IEEE International Workshop on Advanced Motion Control) Istanbul March 2006.
- **S. Khan** and A. Sabanovic, “Sliding Mode Control for Linear drive and Disturbance Compensation for Micro-Motion Applications”, IEEE IICAI-05 (IEEE Indian International Conference in Artificial Intelligence), Pune December 2005.
- C. Onal, S. Kabadayi and **S. Khan**, “A Cascaded Sliding Mode Hybrid Force/Position Controller”, IEEE (Co-Sponsored) TOK-05 (Turkish Automatic Control), ITU Istanbul 2-3 June 2005. (In Turkish)
- A. Sabanovic, **S. Khan** and A. Onat, “Generalized Motion Control- A SMC perspective”, EDPE 2005 (International Conference on Electrical Drives and Power Electronics) Dubrovnik Croatia.
- A. Sabanovic, **S. Khan**, C. Onal, “Hybrid Motion Control SMC Point of View”, IEEE ISIE-2005 (International Symposium on Industrial Electronics) Dubrovnik Croatia 12-15 June 2005.